Fall 2017

Design and performance of cost-effective ultra high performance concrete for bridge deck overlays

Mahdi Valipour

Department: Civil, Architectural and Environmental Engineering

DESIGN AND PERFORMANCE OF COST-EFFECTIVE ULTRA HIGH PERFORMANCE CONCRETE FOR BRIDGE DECK OVERLAYS

by

MAHDI VALIPOUR

A DISSERTATION

Presented to the Faculty of the Graduate School of the

MISSOURI UNIVERSITY OF SCIENCE AND TECHNOLOGY

In Partial Fulfillment of the Requirements for the Degree

DOCTOR OF PHILOSOPHY

in

CIVIL ENGINEERING

2017

Approved by

Dr. Kamal H. Khayat, Advisor
Dr. Genda Chen
Dr. Mohamed A. Elgawady
Dr. Hongyan Ma
Dr. K. Chandrashekhara

ABSTRACT

The main objective of this research is to develop a cost-effective ultra-high performance concrete (UHPC) for bonded bridge deck overlays. The high durability and mechanical properties of such repair material can offer shorter traffic closures and prolong the service life of the pavement. The UHPC was optimized using supplementary cementitious materials (SCMs), proper combinations of sands, and adequate selection of fiber types and contents. Packing density studies included paste, sand, and fiber combinations. The robustness of optimized UHPC mixtures to variations of mixing and curing temperatures was examined. The efficiency of various shrinkage mitigation approaches in reducing autogenous and drying shrinkage of optimized UHPC mixtures was evaluated. This included the use of CaO-based and MgO-based expansive agents, shrinkage-reducing admixture, and pre-saturated lightweight sand. Optimized UHPC mixtures were cast as thin bonded overlays of 25, 38, and 50 mm in thickness over pavement sections measuring 1 × 2.5 m^2. Early-age and long-term deformation caused by concrete, humidity and temperature gradients, as well as cracking and delamination were monitored over time. Test results indicate that the designed UHPC mixtures exhibited relatively low autogenous shrinkage and drying shrinkage. The G50 mixture had the lowest autogenous and drying shrinkage of 255 μm/m at 28 days and 55 μm/m at 98 days, respectively. All tested UHPC mixtures exhibited a high mechanical properties and excellent frost durability. The use of 60% lightweight sand led to significantly reduction in autogenous shrinkage from 530 to 35 μm/m. Test results indicate that there was no surface cracking or delamination in UHPC overlays after 100 days of casting.

ACKNOWLEDGMENTS

My advisor, Dr. Kamal H. Khayat, is an outstanding professor and excellent researcher. Words cannot express how grateful I am to have such an amazing advisor. He is higher than every standard you can consider for a teacher or researcher. I thank him for all that he taught me and undoubtedly, he is one of my best friends.

I would like to thank my advisory committee members, Dr. Genda Chen, Dr. Mohamed A. Elgawady, Dr. Hongyan Ma, Dr. K. Chandrashekhara, and my advisor, Dr. Kamal H. Khayat, for their time to review my dissertation and for their constructive comments.

I would like to offer my special thanks to my wonderful colleagues Weina Meng, Seyedhamed Sadati, Iman Mehdipour, Matthew S. Hopkins, Ahmed T. Abdelrazik, Zemei Wu. I would like to sincerely thank the staff of the Center for Infrastructure Engineering Studies (CIES); Ms. Abigayle Sherman, Ms. Gayle Spitzmiller, Mr. Jason Cox, and Dr. Soo Duck Hwang for their great help and support. I would like to thank John Bullock, Brian Swift, Gary Abbott, and Michael Lusher for their technical assistance.

I would like to acknowledge the financial support provided by Missouri Department of Transportation (MoDOT), the RE-CAST (REsearch on Concrete Applications for Sustainable Transportation) Tier-1 University Transportation Center (UTC) at Missouri University of Science and Technology (Missouri S&T), and the Center for Infrastructure Engineering Studies (CIES).

Last but not least, I would like to express my deepest appreciation and everlasting love to my parents, brother, and sister for their love, encouragement, and support.

TABLE OF CONTENTS

LIST OF ILLUSTRATIONS

LIST OF TABLES

1. INTRODUCTION

1.1. NEED FOR RESEARCH

Pavements usually consist of a base and sub-base layers which last 20-40 years or more, covered with a wearing coarse material having a much shorter service life. The maintenance work for these surface layers induces high external cost (De Larrard, 2011). Intensive effort is devoted to introduce new generations of materials to enhance the performance of such surface layers to prolong the service life of concrete pavement. Given their superior mechanical properties and durability, overlay cast using ultra-high performance concrete (UHPC) can provide significant improvement in durability and service life of the overlay pavement. In addition, the absence of mechanical consolidation due to the high fluid nature of the UHPC materials can reduce construction time for new overlay and/or rehabilitation of the pavement.

Degradation of concrete bridge decks can be in the form of spalling, delamination, scaling due to poor material design, freeze-thaw damage, and/or corrosion of reinforcing steel due to infiltration of chloride ions and moisture or inadequate clear cover (Shann, 2012; Krauss et al., 2009). Overlays are often applied to bridge decks to protect the superstructure from these mechanisms (Knight et al., 2004; Griffin et al., 2006). However, traditional overlays have several limitations; for instance they have relatively short service life (typically between 5 and 25 years), which results in continuous maintenance, repair, and replacement of the system. Furthermore, several typical overlays require experienced contractors and specialized equipment for proper implementation, which significantly increase dead load. They also often have compatibility issues associated with differences in time-dependent properties between materials (Shann, 2012; Krauss et al., 2009).

It is important to note that due to the time, cost, and environmental considerations, the thickness of overlay materials for the pavement is required to be minimized. In general, the shallow overlays are more prone to have high risk of shrinkage cracking. Therefore, the incorporation of proper type of steel and/or synthetic fibers is needed to minimize the risk of cracking as well as delamination over time. In addition, the use of fibers can reduce the depth of pavement overlay, thus reducing the overall costs and

speeding up the construction process (Shann, 2012). This research aims at developing an ultra-high strength fiber-reinforced concrete overlay on concrete pavements and/or bridge decks.

1.2. OBJECTIVE AND SCOPE OF WORK

The main objective of this research is to develop a cost-effective UHPC materials for thin bonded overlays targeted for bridge deck applications to enhance the service life.

A comprehensive investigation involving laboratory material performance evaluation was conducted to develop the mixture design methodology and validate the material performance. The specific objectives of the proposed research are summarized as follows:

- A systematic mix design procedure is developed and implemented, incorporating preliminary testing and mathematical models. The mix design aims at achieving a densely-compacted cementitious matrix for UHPC with enhanced fresh and mechanical properties and relatively low cost. A number of cost-effective UHPC mixtures, which have high-volume SCMs, conventional concrete sand, and relatively low fiber content, are proposed and evaluated in terms of key workability, shrinkage, and durability characteristics.
- Ensuring high robustness of UHPC to temperature variations is key to successful production of UHPC. The objective of this investigation is to evaluate the robustness of UHPC made with silica fume, Class C fly ash, and ground granulated blast-furnace slag that at different casting and curing temperatures of 10, 23, and 30 ºC. The investigated properties included rheology, workability, setting time, mechanical properties as well as autogenous and drying shrinkage.
- Given the critical effect of autogenous and drying shrinkage on the performance of thin overlays made with UHPC, a study is carried out to evaluate the benefits of using combined addition of shrinkage mitigating admixtures in the presence of lightweight sand in UHPC. The effect of initial moist curing of the UHPC on shrinkage and compressive strength is also of special interest.
- Feasibility of performance of optimized UHPC mixtures for thin-bonded overlay application is verified on concrete pavement sections as substrate. Emphasis is placed to evaluate the shrinkage deformation, relative humidity and temperature

variations through different overlay thicknesses of optimized UHPC. The demonstration projects provide insights into the applicability of the developed UHPC mixtures for practical purposes.

- Bond performance between UHPC and substrate concrete is assessed. The complications related to use of conventional test methods are addressed. As a solution, a modified test method is proposed to evaluate the interface bond behavior properly over time.

1.3. DISSERTATION OUTLINE

This dissertation includes seven sections and one appendices. Section 1 provides a brief introduction to the subject area and explains the need for the current research study. The first section also presents the objective and scope of work. Section 2 reviews the current state-of-the-art on the relevant topics to establish the state-of-the-art on the proposed topic. Section 3 presents a mix design method for UHPC prepared with high-volume supplementary cementitious materials and conventional concrete sand. Section 4 explores the effect of mixing and curing temperature variations on key properties of UHPC. Section 5 investigates the efficiency of various shrinkage mitigation approaches in reducing autogenous and drying shrinkage of UHPC. Section 6 discusses the validation of performance of optimized UHPC as bonded concrete bridge deck overlay on pavement sections. Section 7 finally summarizes the outcomes and findings of the present dissertation, and proposes the perspectives for future studies.

Appendix B develops a delamination detection system for smart UHPC overlays using a fully distributed fiber optic sensor.

2. LITERATURE REVIEW

2.1. NEED FOR CONCRETE OVERLAYS

A large percentage of bridges in the United States will reach their design service life in the upcoming decades and more than 11% are currently listed as structurally deficient and over 12% is rated as functionally obsolete (Shann, 2012; Krauss et al., 2009). Concrete bridge decks can be one of the main factors to cause the degradation of an entire bridge system, due to their directly exposure to de-icing salts (Knight et al., 2004). This degradation can be problematic for the entire bridge because the deck provides not only the riding surface, but also as acts as a barrier exposed to de-icing agents, environmental conditions, and vehicle traffic, which can lead to bridge deck's degradation (Krauss et al., 2009; Krstulovic-Opara et al., 1995).

The main purpose of constructing concrete overlays is to optimize and/or extend the use of the remaining life of the existing pavement by placing an additional layer of concrete above it. The benefits of concrete overlay include expedited construction, reduced cost, increased structural integrity, improved riding quality, and protection of the structure against deleterious environmental effects.

Concrete overlays on pavements or bridge decks can strengthen the structure against further deterioration due to fatigue cracking and can also be an effective means to enhance pavement sustainability by improving surface reflectance, increasing structural longevity, and enhancing surface profile stability. The overlays can serve as complete preventive maintenance or rehabilitation solutions or can be used in conjunction with spot repairs of isolated distresses. In addition, concrete overlays can provide cost-effective solutions for pavement and bridge deck repairs. In concrete overlays, the existing pavement does not need to be removed. It needs few or no pre-overlay repairs. Concrete overlays can be placed using conventional concrete pavement practices. One of the best benefits of concrete overlay is that the pavement or bridge can be opened to traffic within a day of placement as well as accelerated construction practices can be used throughout the normal construction season (Shann, 2012).

Concrete overlays are categorized into two types: bonded type concrete overlay and unbonded type concrete overlay. In bonded type concrete overlays, there are ultra-

thin and thin whitetoppings and bonded concrete overlay. These concrete overlays require bonding between the concrete overlay and the existing pavement. In unbonded type concrete overlays, there are conventional whitetopping, and unbonded depending on their thickness (Shann, 2012).

2.2. BONDED AND UNBONDED CONCRETE OVERLAYS

A bonded concrete overlay is a relatively thin concrete that is used to resurface an existing concrete pavement. This type of overlay is typically 50 to 100 mm. thick and its performance depends on the bond strength of the overlay to the existing pavement. The purpose of bonded concrete overlay is to rehabilitate deteriorating concrete pavement to increase load capacity and ride quality. Bonded concrete overlay is recommended when the existing pavement is considered to be in fair or better condition with minor surface distresses and less than a few punch-outs per lane mile (Kim, 2011).

The effectiveness of bond is necessary in the case of bonded concrete overlay. Proper bond will provide monolithic behavior, ensuring that the stiffness of the rehabilitated pavement will carry the traffic load as one structure. Since bonded concrete overlays rely on the existing pavement to assist in carrying the traffic load; the condition of the existing pavement affects the performance of the rehabilitated pavement. Proper repairs or upgrades should be made to provide adequate support as required by design. In addition, if joints are made, well designed joint spacing helps to reduce curling and bending stresses due to traffic and environmental loads. It is crucial that the transverse joints in the bonded concrete overlays match those in the existing pavement to promote monolithic behavior.

In bonded concrete overlay, different modes of failure can occur, and the loss of bond is one of the critical issues. The bond between the overlay and the existing pavement can be lost due to lack of quality control in surface preparation or placement during construction. Another failure mode is delamination due to differences in coefficient of thermal expansion (CTE): if bonded concrete overlay have a CTE that is greater than the CTE of the existing pavement, then the overlay will expand or contract more than the existing pavement. These results in shear stresses at the bond, and the induced stresses can cause the cracking and delamination of the overlay. These stresses in

general, are greater at the edges of the overlay section and along cracks compared to the bonded areas in the middle of the section. This is due to curling and warping at the top of the overlay as temperatures and moisture conditions change more rapidly at the top surface than the rest of the slab depth (Kim, 2011).

On the other hand, unbonded concrete overlay is categorized as relatively thick concrete overlays that are used to resurface the existing concrete pavement. This type of overlay is typically 130 to 280 mm thick and is designed to perform without bonding to the existing pavement. Unbonded concrete overlay is used when the existing pavement is severely deteriorated with major surface distresses. A separation layer is used to maintain separation between concrete overlay and existing pavement (Kim, 2011).

Several factors determine the performance of unbonded concrete overlays. The effectiveness of the separation layer is critical. An effective separation layer should act as a shear plane that prevents migrating cracks from the existing pavement into the overlay. In addition, the separation layer prevents bonding between the new and the old layer allowing them to move independently. Also, a well-constructed drainage system can prevent the building up of pore pressure from the traffic loads. The system serves to prolong the life of the overlay by reducing pumping, asphalt stripping of the separation layer, faulting, and cracking.

Different failure modes can take place in the unbonded concrete overlay. Failure at-grade and overhead structures is one of them. The elevation of the pavement after an unbonded concrete overlay placement will significantly increase. Therefore, at-grade and overhead structures should be raised, or existing pavement should be removed and replaced near these structures. Other failure mode is due to inadequate separation layer. The separation layer prevents reflective cracks. If the new overlay is not structurally separated from the deteriorated existing pavement, the movement of the two structures will affect each other, which will induce heavy reflective stress to the overlay. In addition, poor drainage can be considered as another failure mode. The higher elevation of the pavement necessitates a change in the drainage grade lines. Additional right-of-way may be required to provide the proper slopes for the ditches (Kim, 2011).

Various overlay materials are compared in Table 2-1. Each overlay material has pros and cons, and therefore, care should be taken to select proper type of overlay

materials, depending on the type of repair/rehabilitation. In the case of bonded overly for the pavements and bridge decks, high-performance concrete (HPC) with low overlay thickness can be an effective method to ensure long average life span compared to the other types of overlay materials given the low permeability, high mechanical properties, and good durability.

The use of properly designed UHPC materials that have significantly greater mechanical properties and durability can be even more cost-effective solution since the thickness of the overlay can be reduced further compared to the case of HPC and other overlay materials.

2.3. CHARACTERISTICS OF UHPC AND GOVERNING FEATURES

UHPC is categorized as a relatively new class of concretes with extremely high durability and mechanical properties. UHPC can be considered as part of the family of engineered cementitious composites (Habel et al., 15). It can be defined as a cement-based concrete having compressive strength equal to or greater than 150 MPa (Naaman and Wille, 2012; Resplendino, 2012). In addition, this novel material is characterized as a concrete which has an extremely low water-to-cement ratio (w/c), high binder content, and optimum packing density to eliminate capillary pores and provide an extremely dense matrix, and direct tensile mortar strength higher than 7 MPa (Naaman and Wille, 2012; Resplendino, 2012). In most cases, UHPC contains steel micro fibers which enhance the materials' ductility and mechanical properties. Aïtcin (2000) described how UHPC can achieve such a high strength as follows: "We know how to make 150 MPa concrete on an industrial basis. Because at such a level of strength it is the coarse aggregate which becomes the weakest link in concrete, it is only necessary to take out coarse aggregate, to be able to increase concrete compressive strength and make reactive powder concrete having a compressive strength of 200 MPa; it is only necessary to confine this reactive powder concrete in thin-walled stainless steel tubes to see the compressive strength increased to 375 MPa; and when the sand is replaced by a metallic powder, the compressive strength of concrete increases to 800 MPa"

Table 2-1 Comparisons of different overlays (Shann, 2012)

Overlay type	Latex-modified concrete (LMC)	Silica fume modified concrete (SFMC)	Low slump dense concrete (LSDC)	Fiber-reinforced concrete
Cost ($)/S.F.	18-39	More expensive than LMC	13-19	1.4-2.6
Alternative names or types	Latex-modified mortar2 and high strength LMC4	Microsilica modified concrete (MMC), Silica fume concrete (SFC).		
Avg. thickness	1.25”, 1.25-3”, 1.5”, 2.25”	1.25”, 2”, 2.25”	2-3”, 2”	1”, 2.75”
Service-fife	14-29 yrs	5-10 yrs	16-32 yrs	
Mix components	Portland cement, latex (typically styrene-butadiene), water, coarse and fine aggregates, and antifoamer. Steel or synthetic fibers are often used.	Silica fume, Portland cement, water, coarse and fine aggregates, high-range water reducer, and air-entraining admixture. Steel or synthetic fibers are often used.		Steel, glass, synthetic, plastic fibers, or blends are used with Portland cement, water, and coarse and fine aggregates. High-range water reducer and air-entraining admixture are often needed. Fly ash or microsilica can be added. Steel or synthetic fibers have been used.
w/b	0.35, 0.37, 0.4	0.35-0.4		0.4
MOE	3.8 ksi	4.1 ksi		4.9 ksi
Compressive strength	High early age and 28 day compressive strength	High early age and 28 day compressive strength	5,000 psi at 7 days is required	High early age compressive strength, but low 28 and 90 days
Tensile strength	710 psi at 28 days for splitting tensile strength	680 psi at 28 days for splitting tensile strength		825 psi at 28 days for splitting tensile strength
Resistance to Cl ion penetration	ASTM Rating "Low"	ASTM Rating "Very low"		ASTM Rating "Moderate"
Chloride permeability specification	1000 Coulombs at 90 days	1000 coulombs at 90 days		

Due to the large difference in elastic moduli between aggregate and cement paste, conventional concrete and even HPC have a mismatch in the properties of their constituent materials. This is significantly reduced in the case of UHPC by selecting constituent materials with similar elastic moduli (Gao et al., 2005). Another problem in conventional and HPC is a weak transition zone in the interface between the aggregate and cement paste compared to UHPC.

Table 2-1Comparisons of different overlays (Cont'd)

Overlay type	Latex-modified concrete (LMC)	Silica fume modified concrete (SFMC)	Low slump dense concrete (LSDC)	Fiber-reinforced concrete
Construction notes	Substrate should be wetted before application of bonding agent, requires special mixing equipment and contractor experience, and is sensitive to weather conditions. Burlap and/or plastic are used during curing, very limited widow for finishing (15-30 min), but typical concrete finishing machines can be used	Fog sprays are used to control water evaporation. Wet burlap sacks and polyethylene sheets should be placed quickly to avoid plastic shrinkage. Overlay should be continuously wet and the area should be well drained. Bull float trowel are often used after screeding. Can be tined, broomed, burlap, or turfed finish early	Requires experienced contractors. Bonding agents should be applied to a dry substrate. Wind fences are commonly used. Mechanical tamping is used in some cases to obtain proper densification, but care must be taken as it is not difficult to overwork the surface. Overlay must be screed and finished immediately	
State use	WV, DE, IL, IN, KS, KY, MA, MI, MO, NC, OK, PA, RI, SD, TN, WA, Ontario	WV, NY, Oregon, OH, RI	KY, MN, NY, ND, Iowa, KS, MI, MO, ND, SD, Puerto Rico	
Overall pros	High bond strength, good durability, high abrasion and skid resistance, low permeability, low cracking. Short cure time, quick installation, and long estimated service-life	Low permeability, high early and ultimate strength, good bond strength, high abrasion and skid resistance, high electrical resistance (suppresses the corrosion reaction in concrete)	Low permeability, good durability and long estimated service-life, increased structural capacity	Post cracking tensile capacity. High early strength. High ductility due to fibers. Many possibilities of specialization within mix design
Overall cons	High cost, placement difficulties and need for experienced contractors. If improperly constructed, cracking and/or debonding are often major issues. Wear has been noted in wheel paths. Some have experienced long curing times. A few mix designs (primarily older designs) have issues odor, toxicity, and flammability	Premature cracking, spalling and delamination due to surface shrinkage and strength failure at interfaces have been experienced	Difficulties of placement and consolidation, long cure times, higher dead loads. Susceptible to cracking. Vulnerable to weather conditions	Additional dead load, not as high compressive strength long-term as some high strength alternatives. Chloride resistance is not superior to other overlay types

Figure 2-1 illustrates a representation of the force transfer through normal concrete compared to UHPC materials. In the case of conventional concrete, the force or load is transferred through only aggregates. In UHPC, all the material constituents, including cement paste and aggregates, take part in the force transfer, which can result in a significant improvement in the mechanical properties of the novel construction materials.

Table 2-1Comparisons of different overlays (Cont.)

Overlay type	**Hot-mix asphalt (HMA) single or multi-layer**	**Polymer-concrete (PC)**	**High-performance concrete overlay (HPC)**	**Portland cement concrete overlay (PCC) standard concrete and reinforced concrete overlay.**
Cost ($) /S.F.	3.1-7.6	10-17	17-25	22-36
Alternative names or types	Layered overlays are also called sandwich seal overlays.			Structural bridge deck overlays (SBDO).
Avg. thickness	2-3.25"	0.5-1.4"	1.6-3.5"	3-3.8"
Avg. lifespan	10-15 yrs	9-18 yrs	16-29 yrs	15-24 yrs
Mix design - Mix components	Can be made with one asphalt layer or as a multiple, sandwich layer. Asphalt and bridge deck sealant (rubber, fiberglass, bitumen, polyester membrane). Layered Overlay includes a tack coat	Aggregate and binder. Binder can be epoxy, polyester styrene, or methacrylate. No Portland cement or water is used		Type I Portland cement, water, and coarse and fine aggregate. High early strength Portland cement is also used
Comparison		Often used as a preventative measure on newer deck. Lower dead load		Used in deck rehabilitation more than other overlays
Curing and construction duration	Total construction time is around 3 days	Total construction can take less than 24 hrs	Total construction time can take over 7 days	1-2 day moist curing
Construction notes	Substrate repairs must be made before overlay placement. Typical asphalt paving equipment and procedures are used. Sealant is placed between bridge deck and first asphalt layer.	Substrate roughening is vital to this overlay's success. Must follow temperature and humidity tolerances. Usually two-component systems: one component contains resin and the second contains the curing agent or initiator. Uniformly graded aggregates are used with slurry and premixed overlays. Gap graded aggregates are used with multiple-layer overlays and are broadcast on the top of slurry and some premix overlays.	Typically contains low w/c ratio. Admixtures may be added for improved workability	Substrate surface preparation is typically achieved through hydro demolition
State use	CO, CT, IL, KY, NE, NY, RI, SD, TN, UT, VT, Alberta, Ontario, Quebec	AK, CA, CO, GA, ID, IL, KS, MA, ME, MO, NM, NV, NY, OK, OR, TN, UT, BT, WY, VA	AK, AZ, ID, IL, KS, MI, MO, NE, NY, OK, OR, WV, WY, Alberta	No agencies reported using PCC overlays for new construction, though half of the agencies surveyed used PCC for over 25years
Overall pros	Low cost, ease and speed of installation, improves ride-ability, effective	High early compressive strength, high bond strength, good durability and skid resistance, low permeability, low dead load. Does not require modification of approaches or existing expansion joints.	Low permeability, good durability, high strength. High cost-effective performance	Long life, familiar and quick installation, good record. Good alternative to repair and replacement.
Overall cons	The layered asphalt overlay can trap moisture in the deck, which can damage bond and/or reinforcement. Short service-life and timely maintenance is required. Some have found difficulty of removal. Effectiveness of membrane is unknown. Poor performance has been found on curved. Does not contribute structurally to the superstructure.	Installation difficulties. Some have found low durability. Higher cost. Cannot be used as a replacement for bridge deck concrete.	Installation difficulties. Cracking has been found during curing. Long cure times. Higher cost.	Long construction time and high cost. Low bond strength. Not conductive to decks containing slag.

Some of principles that are used in UHPC to achieve high mechanical properties and durability include the enhancement of homogeneity by elimination of coarse aggregate and packing density by optimization of the granular skeleton of the mixture through a wide distribution of powder size classes. The addition of SCMs, such as silica fume and the use of low water-to-binder ratio (w/b) can result in significant improvement in the mechanical properties and durability of the cement matrix of the UHPC materials. The enhancement of the microstructure by employing post-set heat-treatment and the improvement of ductility, tensile strength, and crack resistance by the incorporation of small fibers, such as steel fibers are the main keys for the proper design of the novel construction materials (Richard and Cheyrezy, 1995).

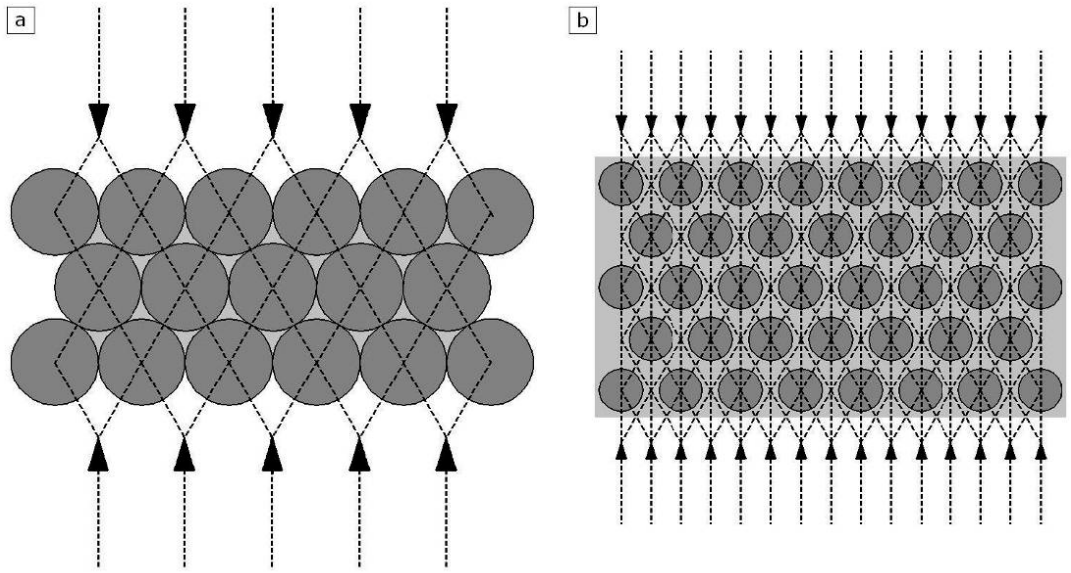

Figure 2-1 Depiction of force transfer through: (a) normal concrete; (b) UHPC (Walraven, 2002; Voort et al., 2008)

UHPCs have high packing density which can be achieved by optimizing the proportioning of different components (Richard and Cheyrezy, 1995). The particles should be selected to fill up the voids between large particles with smaller particles, leading to a smaller volume of gaps within the aggregate skeleton. The concept of packing density, i.e. the ratio of the volume of solids to a given volume, is introduced to

evaluate the arrangement of granular mixtures. Figure 2-2 illustrates how the concept of packing density can be applied with three granular systems, i.e. single-, binary-, and ternary- systems (Stovall et al., 1986). The single-sized aggregate can be packed together to occupy only a limited space, i.e. it can achieve only a relatively low packing density. However, the multi-sized aggregates can be packed together much more effectively to achieve higher packing density, i.e. binary and ternary mixtures. For a given volume of cement paste, the increase in packing density of the aggregates can increase the workability of concrete at the same w/b, or increase the strength of concrete by reducing the w/b at a given workability. Key engineering properties of conventional concrete, HPC, and UHPC are compared in Table 2-2.

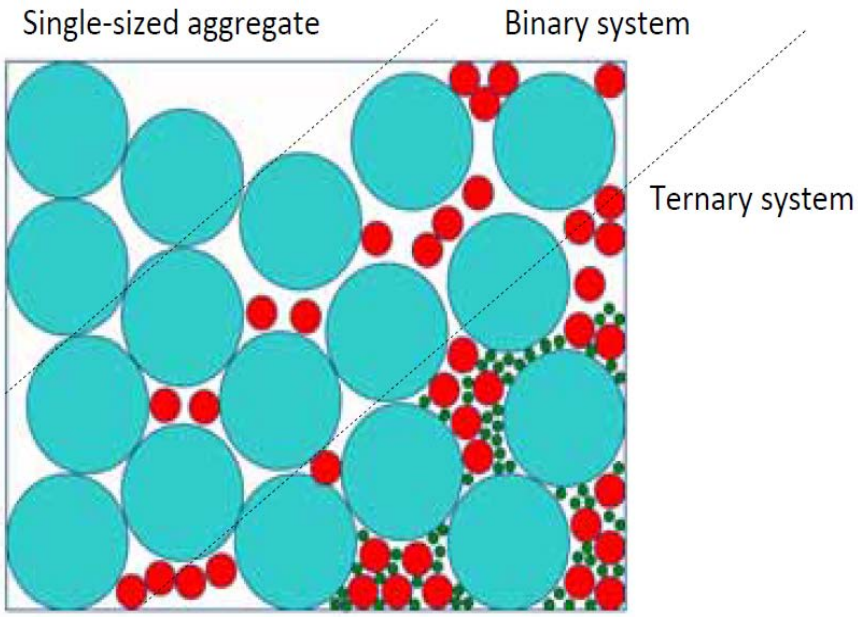

Figure 2-2 Typical packing arrangements of binary and ternary mixtures (Stovall et al., 1986)

It is important to review different components and the microstructural properties of typical UHPC mixtures. Sand, cement, silica fume, crushed quartz, fibers, high-range water reducer (HRWR) or superplasticizer (SP), as well as water, are the main components of a UHPC, as presented in Table 2-3.

Table 2-2 Comparison of UHPC material properties to other concrete classifications (Ahlborn et al., 2008)

Material characteristics	Conventional concrete	HPC	UHPC
Maximum aggregate size, (in.)	0.75-1.00	0.38-0.50	0.016-0.024
w/cm	0.40-0.70	0.24-0.35	0.14-0.27
Mechanical properties			
Compression strength, (ksi)	3.0-6.0	6.0-14.0	25.0-33.0
Split cylinder tensile strength, (ksi)	0.36-0.45	-	1.0-3.5
Poisson's ratio	0.11-0.21	-	0.19-0.24
Creep coefficient, Cu	2.35	1.6-1.9	0.2-0.8
Porosity (%)	20-25	10-15	2-6
Fracture energy, (k-in/in^2)	0.00057-0.00086	-	0.057-0.228
Young's modulus, (ksi)	2000-6000	4500-8000	8000-9000
Modulus of rupture 1st crack, (ksi)	0.4-0.6	0.8-1.2	2.4-3.2
Flexure strength - ultimate, (ksi)	-	-	3.0-9.0
Shrinkage	-	Post cure 40-80×10^{-5}	Post cure <1×10^{-5}, No autogenous shrinkage after cure
Coefficient of thermal expansion (/°F)	4.1-7.3×10^{-6}	-	7.5-8.6 ×10^{-6}
Ductility	-	-	250 Times > NSC
Durability			
Freeze/thaw resistance	10%	90%	100%
Chloride penetration (Coulomb)	> 2000	500-2000	< 100
Air permeability (k) at 24 hrs and 40°C, (in^2)	4.65×10^{-14}	0	0
Water absorption at 225 hr (lb/in^2)	4×10^{-3}	5×10^{-4}	7.1×10^{-5}
Chloride ion diffusion coefficient (by steady state diffusion), (in^2/s)	1.55×10^{-9}	7.75×10^{-10}	3.1×10^{-11}
Penetration of carbon / sulfates	-	-	None
Mass of scaled off (lb/ft^2)	> 0.205	0.016	< 0.002

2.4. CASE STUDIES: USE OF UHPC IN BRIDGE STRUCTURAL ELEMENTS

2.4.1. SAMARIS (Sustainable and Advanced Materials for Road Infrastructures).

UHPFRC, CEMTEC$_{multiscale®}$ family, was applied for rehabilitation and widening purpose on a bridge over the river La Morge in Switzerland in 2004, as a part of European project, SAMARIS. The bridge was damaged as a result of chloride ingress. Rehabilitation process was conducted in three phases. First, the bridge was widened using

prefabricated UHPFRC edge beam on a new reinforced concrete beam. Second, the upper surface of the bridge deck contaminated by chloride ingress was replaced by UHPFRC which had 3 cm thickness. Finally, the concrete surface of the upstream kerb was rehabilitated with 3 cm of UHPFRC. The details of this bridge was shown in Figure 2-3. UHPFRC used in this project has the Microsilica/Cement and Water/Binder ratio were 0.26 and 0.125, respectively, containing cement (1430 kg/m^3), microsilica, fine quartz sand with a maximum grain size of 0.5 mm. Total fiber dosage of 706 kg/m3 (9 vol.%) including microfibers, steel wool of 2 to 3 mm length, in combination with macrofibers with 10 mm length and an aspect ratio of 50, was used as reinforcement. The average values of 182 MPa and 47 GPa were reported for 28-day compressive strength and modulus of elasticity of UHPFRC, respectively. Construction cost analysis of the project indicated that the cost of rehabilitation with UHPFRC was about 10% higher than using conventional option using repair mortar with waterproofing membrane (Bruhwiler and Denarie, 2008).

Table 2-3 Range of UHPC mixture components (Dugat et al., 1996; Castellote et al., 2003; Droll, 2004)

Components	Typical range (kg/m^3)	Mass ratio/cement	Volume fraction (%)
Sand	490 – 1390	1.43	38.8
Cement	610 – 1080	1.00	22.7
Silica fume	50 – 334	0.32	10.6
Crushed quartz	0 – 410	0.30	8.1
Fibers	40 – 250	0.21	2.0
Superplasticizer	9 – 71	0.02	1.4
Water	126 – 261	0.23	16.5

*Superplasticizer is expressed as the weight of the solid fraction; the liquid fraction is included in the water weight.

2.4.2. Application of UHPFRC on Barrier Walls as Protection Layers. Concrete crash barrier wall of a highway bridge severely suffered severely from de-icing salts ingress such as de-icing salts was rehabilitated using UHPFRC in 2006, as shown in Figure 2-4. A 3 cm layer of UHPFRC with w/c of 0.17, containing 1100 kg/m³ cement, 26% silica fume related to the cement content, quartz-sand, 6% steel fibers by volume was applied on the barrier wall. UHPFRC mixture was prepared in a concrete ready mix

plant and hauled to job site of the project by conventional truck in order to cast in 120 cm height wide formworks. After 4 months of rehabilitation, no crack was observed (Bruhwiler and Denarie, 2008).

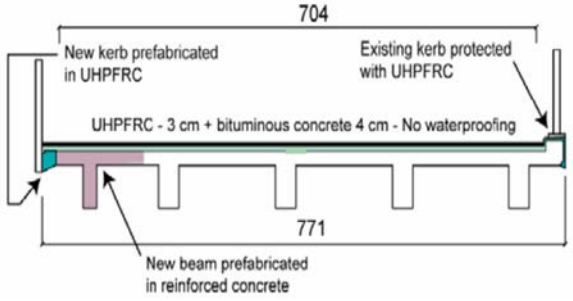

Figure 2-3 Bridge cross section after rehabilitation with UHPC – (dimensions in cm) (Bruhwiler and Denarie, 2008)

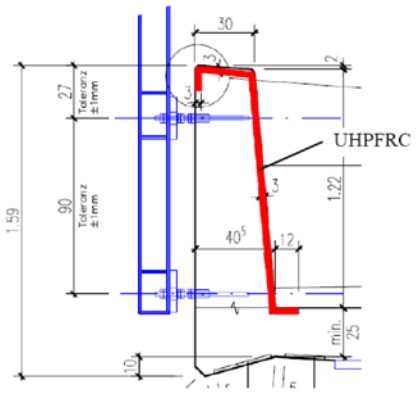

Figure 2-4 Typical cross section of the crash barrier wall and view after rehabilitation (Bruhwiler and Denarie, 2008)

2.4.3. Rehabilitation of a Bridge Pier Using Prefabricated UHPFRC Shell Elements. As shown in Figure 2-5, an existing 40 years old reinforced concrete bridge pier subjected to severe environmental exposure of de-icing slats splashes was protected by 4 cm prefabricated UHPFRC elements in 2007. Before UHPFRC installations, chloride-contaminated concrete, about 10 cm thickness, was removed. In the mix design of UHPFRC which had 0.155 w/c, 1300 kg/m³ of cement, silica fume, quartz-sand, steel fibers, and superplasticizer was used (Bruhwiler and Denarie, 2008).

Figure 2-5 Strengthening of an industrial floor (Bruhwiler and Denarie, 2008)

2.4.4. Strengthening of an Industrial Floors. In this project, load bearing capacity of a 50 years old reinforced concrete slab in area of 720 m^2 was enhanced by applying 4 cm UHPFRC overlay. 1300 kg/m^3 cement, associated with silica fume, quartz-sand, steel fibers, and superplasticizer were incorporated in UHPFRC mix deign with 0.155 w/c (Bruhwiler and Denarie, 2008). Details are presented in Figure 2-6.

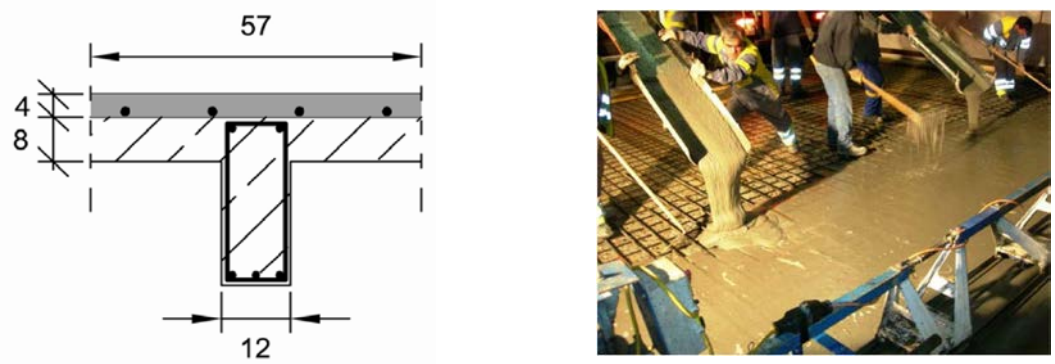

Figure 2-6 Cross section (dimensions in cm) with UHPFRC layer (in grey) and view of UHPFRC casting performed (Bruhwiler and Denarie, 2008)

2.4.5. LOG ČEZOŠKI Bridge, Slovenia. As shown in Figure 2-7, UHPFRC was used to rehabilitate a bridge deck, with 65m in length and 5% longitudinal slope, over Šoka River in Slovenia in 2009. The continuous UHPFRC was applied to protect the full upper face of the bridge deck, footpath and external faces of the kerbs. In this project the UHPFRC thickness was varied between 2.5 cm to 3 cm. UHPFRC mix design included 763 kg/m^3 cement,763 kg/m^3 Limestone filler, 153 kg/m^3 microsilica fume, with

W/(C+LF+SF) ratio of 0.155. A mix of micro-steel wool with 1 mm length and macrofibers, lf=10 mm, aspect ratio: 50, with a total dosage of 706 kg/m^3 (9% vol.) was incorporated. The average mixing time of UHPFRC for this project was reported 12 minutes. UHPFRC moist-cured for 7 days after casting (Bruhwiler and Denarie, 2008).

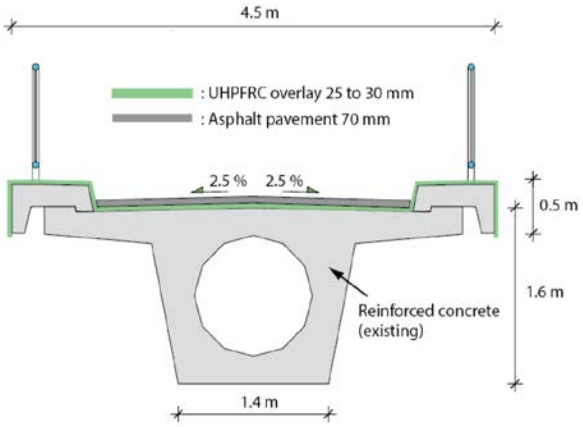

Figure 2-7 Cross section of the bridge with concept of rehabilitation (Bruhwiler and Denarie, 2008)

2.4.6. Pinel Bridge, France. The Pinel Bridge (Figure 2-8 and Figure 2-9) was constructed using conventional concrete in 1996 in France. The bridge had two lanes with a filler beam deck with two span lengths of 1220 and 1480 m. In 2007, it was decided to extend the lanes from two to five using prefabricated UHPFRC in order to increase traffic volume capacity over bridge. The depth of each seventeen UHPFRC beams was 620 mm. UHPFRC was produced using 2360 kg of premix, 45 kg of superplasticizer, 195 kg of water, and 195 kg of steel fibers, yielding 28-day compressive strength of 165 MPa (Matteis et al., 2008).

2.4.7. Experimental Validation of a Ribbed UHPFRC Bridge Deck in France. An experimental validation of ribbed UHPFRC bridge deck made of two segments assembled by post-tensioning were conducted as part of MIKTI French R&D national project focusing on steel-concrete composite applications, as shown in Figure 2-10 and Figure 2-11. One of the segments was made of Ductal®-FM and the other of BSI®. The UHPFRC ribbed slab was supported by two longitudinal steel beams. This designed for a 3 span bridge having two lanes with each 3.5 meters wide. The total depth of ribbed slab

had 0.38 m depth with 0.05 m slab only. In order to provide sufficient strength the ribbed slab was post-tensioned (Toutlemonde et al., 2007).

Figure 2-8 General view of the existing bridge (Matteis et al., 2008)

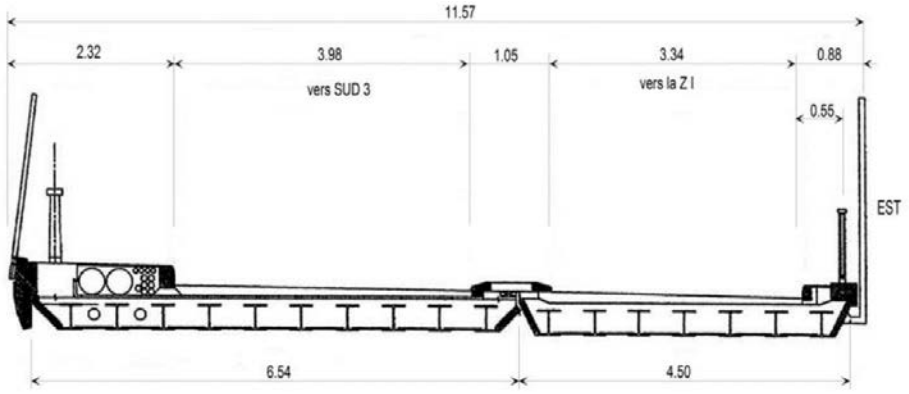

Figure 2-9 Deck Cross section of the existing bridge (Matteis et al., 2008)

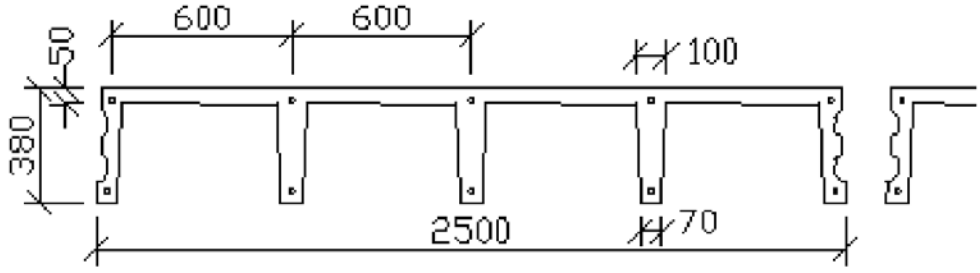

Figure 2-10 Longitudinal cross-section of precast segments. Longitudinal ribs are 50 mm-wide only at bottom. Lengths in mm (Toutlemonde et al., 2007).

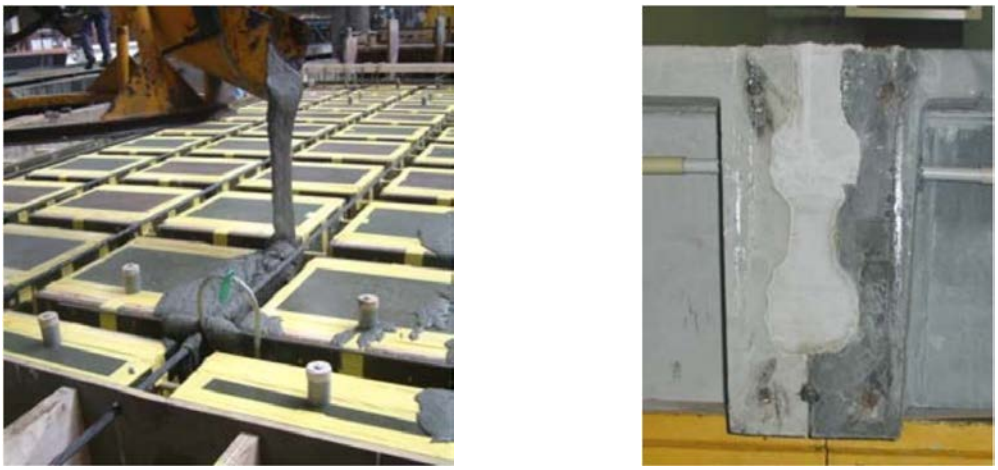

(a) (b)

Figure 2-11 Model ribbed slab for validation tests. a) Casting - b) Cold joint (Toutlemonde et al., 2007)

2.4.8. Sherbrooke Pedestrian Bridge, Canada. A new pedestrian bridge was constructed over Magog River in Canada in 1997 (Figure 2-12) using Ductal, a commercial UHPC premix. The bridge had single lane with 60m in length precasted in 6 segments (10 m long and 3 m height) with a space truss. Using UHPFRC allowed the top deck slab to be as low as 30 mm, using no passive reinforcement in the bridge (Russell and Graybeal, 2013).

Figure 2-12 Sherbrooke Pedestrian Bridge (Russell and Graybeal, 2013).

2.4.9. Glenmore/Legsby Pedestrian Bridge. As shown in Figure 2-13, Glenmore/Legsby Pedestrian Bridge was another case constructed using Ductal over an

8-lane highway in Canada. This bridge was a single span, 53 m long. Post-tensioned girders held bridge deck which had 3.6 m wide at the mid-span. The girders were T-shaped with 11m in depth 33.6 m long. Passive GFRP, glass fiber-reinforced plastic, was used. A high shear mixer was employed to deliver proper and sufficient mixture for this application which required 40 m^3 UHPFRC. The prepared Ductal was hauled to the job site from batch plant using conventional concrete trucks while UHPFRC was maintained agitated at a low revolution (Russell and Graybeal, 2013).

Figure 2-13 Glenmore/Legsby pedestrian bridge, Calgary, Alberta, Canada (Russell and Graybeal, 2013)

2.4.10. Mars Hill Bridge. Mars Hill bridge (Figure 2-14), located in Wapello county Iowa, is the first bridge in the united states made of UHPC in 2006 (Russell and Graybeal, 2013). Three prestressed bulb-tee girders of this bridge were fabricated using Ductal UHPC. The girders had 33.5 m long and 1.14 m depth with a cast-in-place concrete bridge deck. Other bridge parts were constructed using conventional concrete materials. Ductal UHPC consists of fine sand, cement, silica fume and quartz flour were incorporated in UHPC mixture in low w/cm between 0.15 and 0.19. Achieved average 28-day compressive strengths ranged from 125-207 MPa depending on the mixing and curing process. To improve ductility, steel or polyvinyl alcohol (PVA) fibers in amount of 2% by volume were included in order to improve ductility.

Figure 2-14 Mars Hill Bridge, Wapello County, IA, USA (Russell and Graybeal, 2013)

2.5. UHPC AS BONDED OVERLAY

UHPC has extremely high impermeability, negligible dry shrinkage if properly cured, and excellent post-cracking tensile capacity. UHPC also exhibits high compressive strength, between 125-230 MPa, at 28 days depending on the cure regime, which is required for the rehabilitation of bridge decks when added load capacity and load transfer is desired (Graybeal, 2006; Misson, 2008). Furthermore, UHPC develops high early strength, which could reduce traffic closure time and increase the rate of precast bed turnover. In order to fully benefit from the superior properties of UHPC, the bond integrity of the novel material to the conventional concrete deck systems has to be evaluated. The thickness of the UHPC overlay should be optimized to reduce the dead load while maintaining the integrity of the bond interface.

In spite of the aforementioned benefits of UHPC over conventional overlay materials, its high initial cost can limit its broader use. Bonneau et al. (1996) reported the UHPC's price as $\$1400/m^3$ in 1996 in Europe which decreased to $\$750/m^3$ in 2000 with more common use (Blais and Couture, 1999). The cost estimation of the UHPC was $\$2620/m^3$ in North America in 2007 (Suleiman et al., 2008). More recently, a 30-mm thick UHPFRC was used as an overlay to repair a short span of a heavy traffic road bridge (Bruhwiler and Denarie, 2008; Denarie et al., 2005). Two alternatives were suggested in this overlay project, which were the rehabilitation using UHPFRC without water proofing membrane and typical repair mortar with water proofing membrane. Cost analysis for the two alternatives indicated that the UHPFRC overlay would have 12% higher material

cost than the mortar overlay. However, the typical mortar overlay necessitates longer traffic closure time due to the drying process before applying the water proofing membrane compared to the UHPFRC overlay which reduces the traffic disruption and can provide superior mechanical properties and durability (Denarie et al., 2005).

The flexural behavior of UHPC overlay was investigated by Yuguang et al. (2008) using a multilayer model. This research was done by varying the numbers of rebars and fiber volumes; the fiber volume was set to 0%, 0.8%, and 1.6%. The results indicated that a 30.5-mm thick UHPC overlay made without any rebars could endure the maximum traffic load. Lee and Wang (2005) evaluated compressive strength, bond strength, and steel pull out capacity. The results indicated that the use of a 10-mm thick reactive powder concrete (RPC) or UHPC bonding layer increases compressive and flexural strength between 150% and 200% over conventional concrete overlay. In addition, abrasion resistance of RPC overlay was approximately eight times greater than that of conventional concrete overlay. Bernardi et al. (2016) reported successful use of UHPC in thin overlay of 45 mm in thickness reinforced with UHPC made with 3.25% steel fibers for bridge deck rehabilitation in Switzerland in 2014. The details of this application are shown in Figure 2-15 and Figure 2-16. The overlay repair included reinforcing rebar and UHPC to strengthen the existing deck that was damaged from alkali silica reactivity. Similarly, a successful use of UHPC measuring 38 mm in thickness applied on a 30-m long bridge was also reported in Iowa, USA.

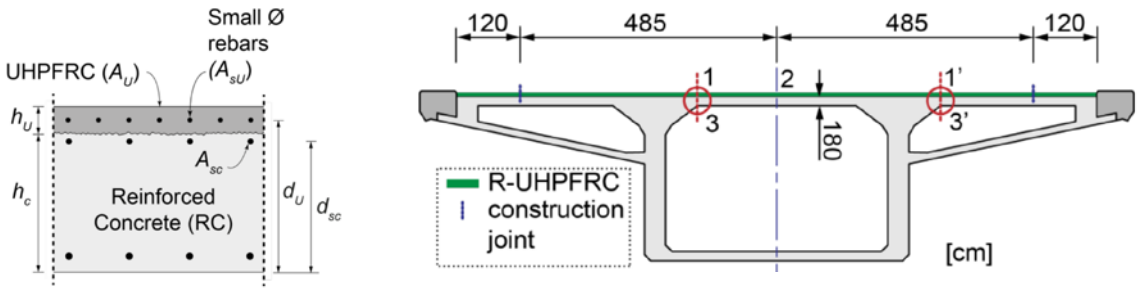

(a) (b)

Figure 2-15 Cross section details of the project (a) Typical composite cross section (b) Geometry of the box girders cross-section

Figure 2-16 Implementation details of UHPC overlay application

2.6. STRESS AND STRAIN IN BONDED CONCRETE OVERLAYS

This section presents the status of stress distribution in a system of composite overlay due to moisture variations. Figure 2-17 illustrates the variation of normal stress (σ_{xx}) over the width section at 10 days, including restrained shrinkage stress, the total stresses and the relaxation because of restrained creep. The shrinkage stresses reduced gradually because of creep relief at the critical point of the center line (Lange and Shin, 2001; Beushausen and Alexander, 2007; Tran et al., 2007; Rahman et al., 2000).

Figure 2-18 illustrates the variation of tensile stresses (σ_{yy}) over the width section of composite system at the interface. As shown, peeling stresses govern at the edge of the system (Lange and Shin, 2001; Beushausen and Alexander, 2007; Tran et al., 2007; Rahman et al., 2000). At a short distance (20 mm) from the edge, the peeling stresses drop in magnitude and alter from tensile to compressive. Unbalanced moment that σ_{xx} stress make through the overlay depth results in σ_{yy} stress field at the interface. Figure 2-19 presents the shear stress (τ_{xy}) variation at the interface over the width section. As shown, considerable value of shear stress concentrating at the overlay edges, moderately decrease towards the center and become zero when it reaches to the center. Thus, the combination of biaxial tensile and shear state of stress at the interface can most likely make a zone to initiate the interface failure (Lange and Shin, 2001; Beushausen and Alexander, 2007; Tran et al., 2007; Rahman et al., 2000).

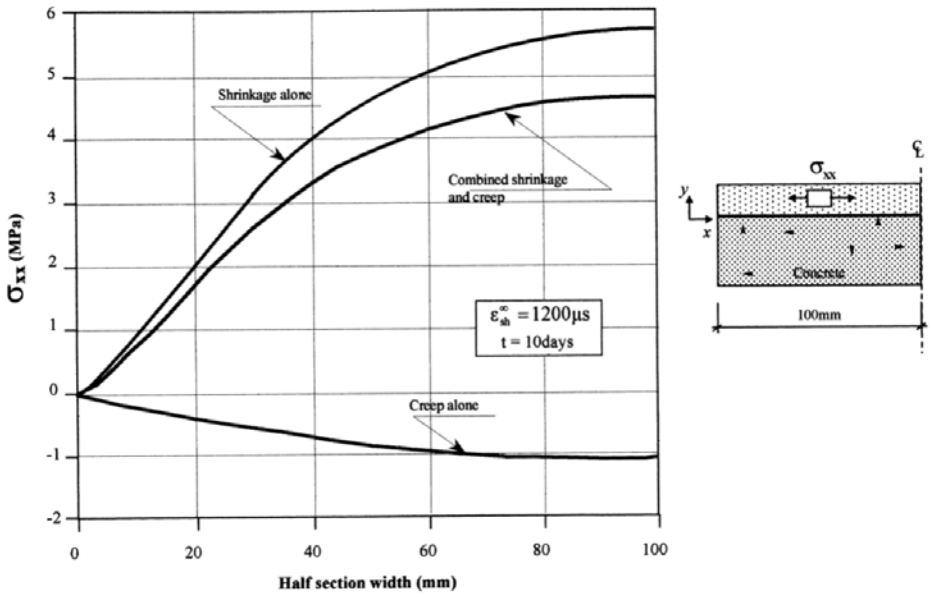

Figure 2-17 Variation of stress σ_{xx} across the width at top at (10 days) (Rahman et al., 2000)

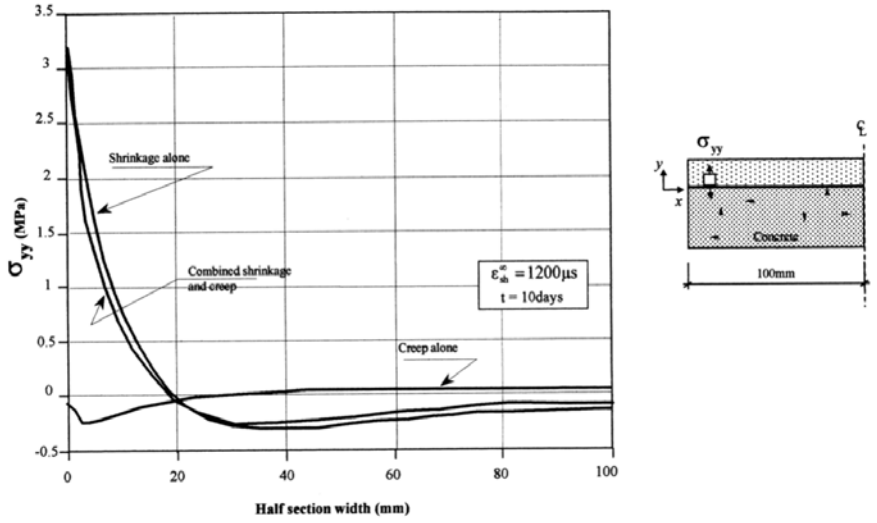

Figure 2-18 Variation of stress σ_{yy} across the width at top at (10 days) (Rahman et al., 2000)

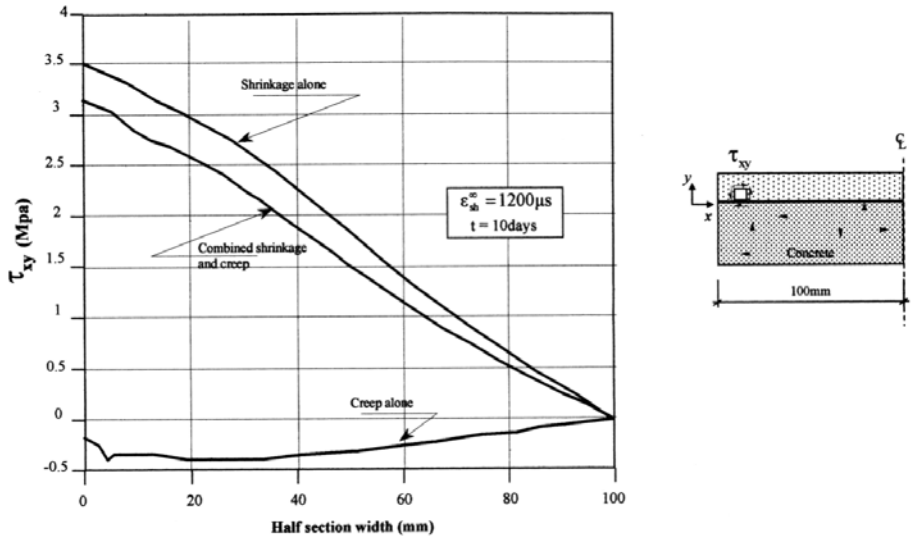

Figure 2-19 Variation of shear stress (Rahman et al., 2000)

2.7. SUMMARY

Based on the aforementioned literature, the specific objectives that this dissertation aims to elucidate are as follows:

- A systematic mix design procedure is developed and implemented, incorporating preliminary testing and mathematical models. The mix design aims at achieving a densely-compacted cementitious matrix for UHPC with enhanced fresh and mechanical properties and relatively low cost. A number of cost-effective UHPC mixtures, which have high-volume SCMs, conventional concrete sand, and relatively low fiber content, are proposed and evaluated in terms of key workability, shrinkage, and durability characteristics.
- Ensuring high robustness of UHPC to temperature variations is key to successful production of UHPC. The objective of this investigation is to evaluate the robustness of UHPC made with silica fume, Class C fly ash, and ground granulated blast-furnace slag that at different casting and curing temperatures of 10, 23, and 30 ºC. The investigated properties included rheology, workability, setting time, mechanical properties as well as autogenous and drying shrinkage.
- Given the critical effect of autogenous and drying shrinkage on the performance of thin overlays made with UHPC, a study is carried out to evaluate the benefits

of using combined addition of shrinkage mitigating admixtures in the presence of lightweight sand in UHPC. The effect of initial moist curing of the UHPC on shrinkage and compressive strength is also of special interest.

- Feasibility of performance of optimized UHPC mixtures for thin-bonded overlay application is verified on concrete pavement sections as substrate. Emphasis is placed to evaluate the shrinkage deformation, relative humidity and temperature variations through different overlay thicknesses of optimized UHPC. The demonstration projects provide insights into the applicability of the developed UHPC mixtures for practical purposes.
- Bond performance between UHPC and substrate concrete is assessed. The complications related to use of conventional test methods are addressed. As a solution, a modified test method is proposed to evaluate the interface bond behavior properly over time.

3. OPTIMIZATION AND PERFORMANCE OF COST-EFFECTIVE UHPC

This chapter [Meng et al., 2017] presents a mix design method for UHPC prepared with high-volume supplementary cementitious materials and conventional concrete sand. The method involves the optimization of binder combinations to enhance packing density, compressive strength, and rheological properties. The water-to-cementitious materials ratio is then determined for pastes prepared with the selected binders. The sand gradation is optimized using the modified Andreasen and Andersen packing model to achieve maximum packing density. The binder-to-sand volume ratio is then determined based on the void content, required lubrication paste volume, and compressive strength. The optimum fiber volume is selected based on flowability and flexural performance. The high-range water reducer dosage and w/cm are then adjusted according to the targeted mini-slump flow and compressive strength. Finally, the optimized UHPC mix designs are evaluated to determine key properties that are relevant to the intended application. This mix design approach was applied to develop cost-effective UHPC materials. The results indicate that the optimized UHPC can develop 28-days compressive strength of 125 MPa under standard curing condition and 168-178 MPa by heat curing for 1 days. Such mixtures have unit cost per compressive strength at 28 days of 4.1-4.5 $\$/m^3/MPa$ under standard curing.

With appropriate combination of cementitious materials, adequate sand gradation, and incorporation of fiber reinforcement and high-range water reducer (HRWR), UHPC can be produced to deliver high flowability (self-consolidating), mechanical properties, and durability (De Larrard et al. 1994; Richard et al. 1995). However, high material cost is restricting UHPC's wider acceptance worldwide (Bruhwiler et al. 2008; Habert et al. 2013; Yu et al. 2014). Development of cost-effective UHPC is crucial for greater acceptance of this novel construction material.

High-volume replacement of cement with sustainable SCMs, such as fly ash, ground granulated blast furnace slag (GGBS), and silica fume (SF), can be performed to reduce cement content without significantly sacrificing the mechanical strengths (Yu et al. 2014; El-Dieb et al. 2009; Hassan et al. 2012; Wang et al. 2012). Mixtures containing 20-35% (vol.%) GGBS, 10-30% Class C fly ash (FAC), and 15-30% SF have been used

in proportioning UHPC (Yu et al. 2014; El-Dieb et al. 2009; Hassan et al. 2012; Wang et al. 2012). However, the substitution ratios were relatively low. A high-volume substitution of SCMs in proportioning UHPC need to be further investigated to reduce material costs.

Ground quartz sands (0-0.6 mm) are typically used for producing UHPC (Wille et al. 2011a; Wille et al. 2011b). Conventional concrete sand was used to replace quartz sand and reduce the initial unit cost. (Yang et al. 2009) used two types of locally natural sand to replace finely ground quartz sand. Experimental results indicated that the use of natural sand led to reduction in compressive strength and fracture energy of about 15% lower than those of UHPC made with quartz sand. (Wang et al. 2012) reported that the 91-days compressive strength could achieve 150 MPa or higher strength when conventional concrete sand was used. However, high-volume SF (25%, by volume) was used. Besides, reducing the binder content can decrease unit cost of UHPC. The binder content can be reduced by optimizing the sand gradation to achieve a higher packing density (Le et al. 2015). Appropriate binder contents need to be investigated in order to strike a balance between mechanical properties and unit cost of UHPC.

Reducing the steel fiber content is also vital in reducing unit cost of UHPC (Wille et al. 2011). While steel fibers greatly enhance tensile properties of UHPC, they import an adverse effect on flowability. An optimum content of steel fibers should be adopted to balance the workability, and mechanical performance (Wille et al. 2011; Graybeal 2011). An effective mix design method is of great importance for UHPC proportioning. The mix design should involve combining optimum proportions of all mixture constituents to fulfill the requirements of fresh and hardened concrete for a particular application (Khayat et al. 2007). In general, two methodologies exist for UHPC mix design. The first approach seeks to reduce porosity by decreasing the w/cm, by mass (Richard et al. 1995; Richard et al. 1994), and applying high temperature/pressure curing or vacuum mixing (Dils et al. 2015). However, the reduction in w/cm may lead to a high amount of entrapped air, negatively affecting mechanical properties (Wille et al. 2011). High temperature/pressure curing or vacuum mixing may not be practical for cast-in-place applications. The second approach for UHPC mix design involves the increase in packing density (De Larrard et al. 1994; Yu et al. 2014). A modified Andreasen and Andersen

model was employed to optimize UHPC mix design (Funk et al. 1994). The binder combinations and sand gradations were adjusted to achieve the best fit to the target particle size distribution proposed by the modified Andreasen and Andersen model using a least square method (Yu et al. 2014; Yu et al. 2015). However, the significant effects of water and chemical admixture on packing density of fine particles (<100 lm) were not considered and only the solid materials were taken into account. The packing density of cementitious materials is strongly dependent on the water addition and dispersion imported by the use of HRWR (Li et al. 2014). Since the interparticle cohesive forces, especially electrostatic and Van der Waals forces, far exceed the gravitational forces, flocculation can form and compromise the packing (Iveson et al. 2001). A slight increase in free moisture content around fine particles can enhance packing. Water on particle surfaces can lead to lubrication and act as electrical conductor to relieve interparticle forces (Tomas 2004). Considering the presence of water, the packing density should be determined under wet conditions (Li et al. 2014). However, packing models are still applicable for sand since sand particles are relatively large, and the gravitational forces far exceed the cohesive forces. Therefore, the packing densities of cementitious materials and sand should be analyzed separately.

A systematic mix design procedure was developed and implemented, incorporating preliminary testing and mathematical models. The mix design aims at achieving a densely-compacted cementitious matrix for UHPC with enhanced fresh and mechanical properties and relatively low cost. A number of cost-effective UHPC mixtures, which have high-volume SCMs, conventional concrete sand, and relatively low fiber content, are proposed and evaluated in terms of key workability, shrinkage, and durability characteristics.

3.1. MATERIALS, MIXERS, AND SPECIMEN PREPARATIONS

In this study, the cementitious materials included FAC, GGBS, SF, and Type III Portland cement. The characteristics of the investigated raw materials are listed in Table 3-1. Fine SF with particles smaller than 1 μm in diameter was used; the mean diameter of the SF is about 0.15 μm, and the specific surface area determined using the Brunauer, Emmet, and Teller (BET) method is 18,500 m^2/kg. Missouri River sand (0-4.75 mm) and

masonry sand (0-2.00 mm) were used under saturated surface dry (SSD) condition. The water absorptions of the river sand and masonry sands are 0.14 and 0.06%, respectively. A polycarboxylate HRWR was used to enhance the workability. The HRWR has a solid mass content of 23% and a specific gravity of 1.05. Straight steel fibers with 0.2-mm diameter and 13-mm length were used to enhance mechanical properties. The tensile strength and elastic modulus of the steel fiber are 1.9 and 203 GPa, respectively.

All mixtures were prepared and tested at room temperature (23 ± 2 °C). Two mixers were used which were a 12-L Hobart mixer and a 150-L EIRICH mixer. The Hobart mixer was used for optimizing the individual components for UHPC, and the EIRICH mixer was employed for finalizing the UHPC mixtures. A specific mixing procedure was employed for each mixer. When the Hobart mixer was used, the mixing procedure was composed of three steps: (1) dry cementitious materials or/and sand were mixed for 2 min at 1 rps; (2) 90% of the mixing water and 90% of the HRWR were added and the mixture was mixed for 3 min at 2 rps; (3) the rest of water and HRWR were added and the mixture was mixed for 9 min at 2 rps. When the EIRICH mixer was used, the mixing procedure was composed of five steps: (1) the mixer was pre-wetted; (2) the sand and cementitious materials were added into the mixer and mixed for 2 min at 1 rps; (3) 90% of the total liquid (water + HRWR), by volume, was added and mixed for 2 min at 6 rps; (4) the rest of the liquid was introduced, and the materials were mixed for 4 min at 6 rps; (5) the fibers were added gradually over a period of 1 min; (6) the materials were mixed for 2 min at 10 rps. While mixing, the pan speed of the mixer was fixed at 2 rps.

For each mixture, specimens were cast in one lift without mechanical consolidation. The molds were immediately covered after casting with wet burlaps and plastic sheets. They were demolded after 1 days, and then cured in lime-saturated water at 23 ± 1 °C until the time of testing (standard curing). To investigate the effects of curing on compressive strength, two sets of UHPC specimens were prepared and tested, one set with standard curing and the other set with heat curing. Heat curing was performed at a maximum temperature of 90 °C for 24 h. The specimens were then cured in lime-saturated water for 7 days, followed by air-curing at room temperature.

Table 3-1 Characteristics of raw materials

	Type III Portland cement	Class C fly ash	Silica fume	GGBS	Missouri river sand	Masonry sand
SiO_2 (%)	19.72	36.5	95.5	36.8	80.3	86.5
Al_2O_3 (%)	5.10	24.8	0.7	9.2	10.5	0.39
Fe_2O_3 (%)	2.76	5.2	0.3	0.76	3.43	1.47
CaO (%)	64.50	28.1	0.4	37.1	1.72	9.42
MgO (%)	2.30	5	0.5	9.5	1.70	0
SO_3 (%)	3.25	2.5	0	0.06	1.07	0
Na_2O eq. (%)	0.33	0	0.4	0.34	–	0
C_3S (%)	65.23	–	–	–	–	–
C_2S (%)	7.33	–	–	–	–	–
C_3A (%)	8.85	–	–	–	–	–
C_4AF (%)	8.40	–	–	–	–	–
Loss of ignition (%)	2.6	0.3	2.6	5.1	1.28	0.24
Blaine surface area (m^2/kg)	562	465	–	589	–	–
B.E.T. (m^2/kg)	–	–	18,200	–	–	–
Specific gravity	3.15	2.70	2.20	2.90	2.65	2.64

3.2. PROPOSED MIX DESIGN PROCEDURE AND EXPERIMENTAL PROGRAM

The proposed UHPC mix design method consists of six main steps, as illustrated in Figure 3-1: (1) determine binder candidates; (2) preliminarily select a w/cm; (3) determine the sand combination; (4) assess the binder to-sand volume ratio (V_b/V_s); (5) optimize the fiber content; and (6) evaluate and adjust the UHPC mixture. Step 1 is composed of three sub-steps: (1a) select binder combination candidates based on flow characteristics; (1b) narrow down the binder candidates according to the combined effects of minimum water content (MWC), relative water demand (RWD), and HRWR demand, as well as 1- and 28-days compressive strengths; (1c) finalize the binder combinations based on the rheological properties.

3.2.1. Step 1: Optimize Binder Combinations for Paste. With the initially-selected binder combinations, which aim at using high-volume SCMs in proportioning UHPC, flow tests are conducted to evaluate the MWC and RWD of binders under wet conditions in order to screen candidates for binders. The paste mixtures with lower MWC are advantageous in terms of the packing density, and thus, the corresponding binders are selected for further optimization. To further narrow down the candidates of the optimum

binder combinations, the HRWR demand and compressive strength of the binders selected based on flow characteristics are then evaluated. For a given sand and fiber content, any change in the rheological characteristics are directly related to the changes of the paste matrix (Wu et al. 2014). Therefore, final binder selection is based rheological properties of the successful binder systems. The three sub-steps are elaborated as follows.

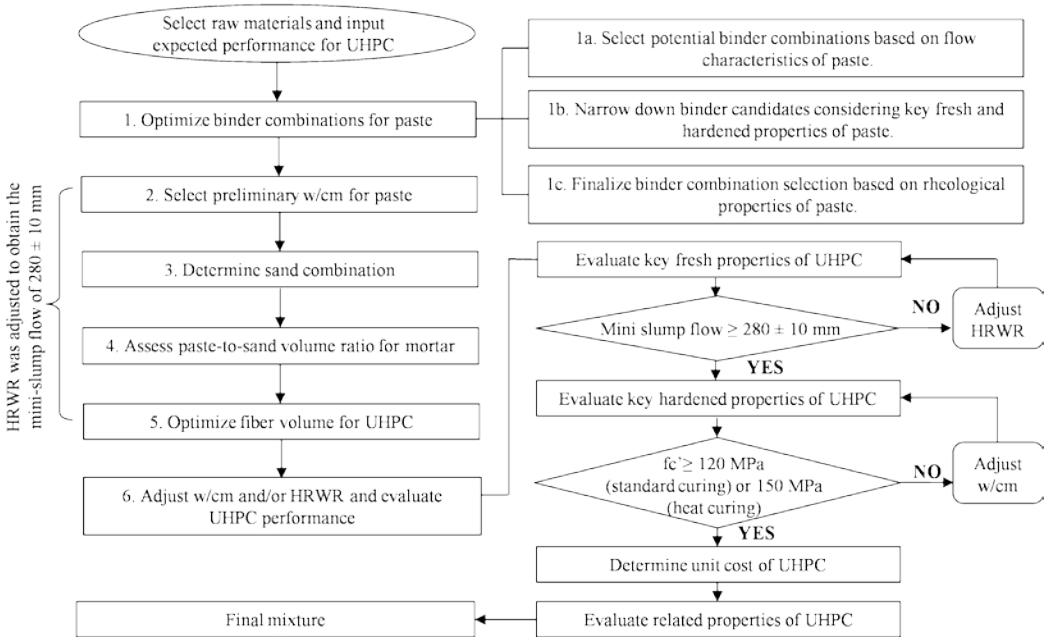

Figure 3-1 Procedure of mix design methodology for UHPC

3.2.1.1 Sub-step 1a: Select binder candidates based on flow characteristics. A mini-slump test is conducted in accordance with ASTM C 230/C 230 M. For each of the test binders, seven mixtures are prepared with various w/b, by volume, values ranging from 0.4 to 1.0. This is carried out to establish a relationship between fluidity and w/b for each binder combination, as illustrated in Figure 3-2. The intercept on the vertical axis represents the MWC required to initiate flow, and the slope of the relationship represents the RWD. Assuming there is no air entrapped in the paste, the volume occupied by the water content can be taken as the minimum void content. Therefore, a low MWC represents a high packing density of the binder (Hwang et al. 2006). A high RWD indicates that a given increase in w/b can result in small impact on the flowability. Thus,

mixtures with high RWD are more robust to variations in water content (Hwang et al. 2006). Therefore, binder combinations with low MWC and high RWD are desirable for designing UHPC.

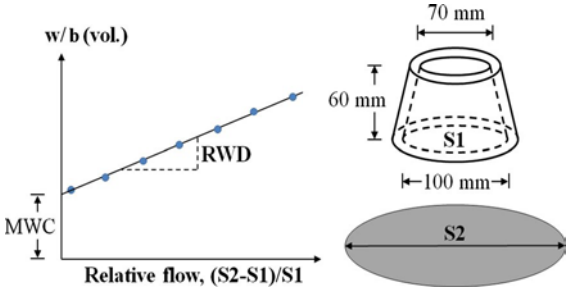

Figure 3-2 MWC and RWD in the mini-slump flow test

3.2.1.2 Sub-step 1b: Narrow down binder candidates. To further narrow down the binder combinations, key fresh and hardened properties of the selected binder combinations are evaluated. The 1- and 28-days compressive strengths are measured in accordance with ASTM C 109. The HRWR dosage is adjusted to obtain a mini-slump flow of 280 ± 10 mm, which is commonly adopted to ensure good flowability and low air entrapment (Dudziak et al. 2008). The flow time is measured using a mini-V funnel in accordance with the (EFNARC 2002). The mixtures with higher compressive strength and lower HRWR demand are preferred.

A radar chart is employed to display multivariate criteria for the selection of binder (Khayat et al. 2014). The criteria include the MWC, RWD, HRWR demand, and 1- and 28-days compressive strengths. The plot consists of a sequence of equi-angular spokes (radii), and each spoke represents one variable (see Fig. 5, Sect. 4.1). The length of each spoke is proportional to the magnitude of the corresponding variable. Each variable is assigned with a specific weight factor. The data points of each spoke are sequentially connected and formed a specific area. A larger area indicates a better performance of the mixture (Khayat et al. 2014).

3.2.1.3 Sub-step 1c: Finalize the binder selection. The rheological properties of paste mixtures with the selected binders in Sub-step 1b are tested using a coaxial rheometer (Anton Paar MCR 302) at different ages, up to 60 min. The w/b is fixed at

0.63, which corresponds to a w/cm of 0.20, for mixture made with 100% Portland cement. The mini-slump spread value is fixed at 280 ± 10 mm by adjusting the HRWR dosage.

The plastic viscosity (μ_p) is measured at 20, 40 and 60 min after water addition. The paste in the rheometer undergoes a 60-s pre-shearing period at a shear rate of 100 s^{-1}. This operation could minimize the structural build-up of paste at rest. Then, the shear rate is reduced by 10 s^{-1} for every 5 s until zero. The dynamic yield stress (τ_0) and μ_p are calculated using the Bingham fluid model (Tattersall et al. 1983), as shown in Eq. 3.1:

$$\tau = \tau_0 + \mu_p \dot{\gamma} \tag{3.1}$$

where γ denotes the shear rate. A relatively low value of μ_p is more desirable to ensure the proper filling capacity.

3.2.2. Step 2: Preliminarily Select a w/cm for Paste. The w/cm of UHPC is typically in the range of 0.15-0.25 (Willeet al. 2011). Paste mixtures of the selected binder combinations were proportioned with w/cm ranging between 0.18 and 0.23. The selection of the appropriate w/cm is based on HRWR demand and 28-days compressive strength under standard curing. The selected w/cm is applied in the later investigations to determine the optimum sand and fiber content (see Steps 3 and 4). The preliminary w/cm may be slightly adjusted in the final UHPC mixtures to achieve good balance between flowability and strength which is elaborated in Step 6.

3.2.3. Step 3: Determine Sand Gradation. The modified Andreasen and Andersen model acts as a targeted function for the optimization of sand gradation, as shown in Eq. 3.2 (Funk and Dinger, 1994):

$$P(D) = \frac{D^q - D_{\min}^q}{D_{\max}^q - D_{\min}^q} \tag{3.2}$$

where P(D) represents the weight percentage of sand passing the sieve with size D, D_{max} is the maximum particle size (μm), D_{min} is the minimum particle size (μm), and q is the distribution modulus which is related to the sand particle size. For fine particles, q can be set at 0.23 (q<0.25) (Yu et al. 2014). The sand proportions are adjusted until the best fit is achieved between the composed gradation and the targeted curve, using an optimization algorithm based on the least square method. When the discrepancy between the targeted

curve and the composed sand gradation is minimized, the sand combination can be considered as optimum.

According to the excess thickness theory (Li et al. 2011), the fluid paste volume should be high enough to fill voids between sand particles and provide a lubrication layer that envelops the particles to achieve a high flowability (Koehler et al. 2007). The bulk density of the compacted sand blend can be determined using a Gyrator compactor testing machine. A sand sample can be compacted by a continuous kneading action consisting of axial pressure and shear. The applied overhead air pressure is set at 4 ± 10^5 Pa. The gyrator angle and cycle number are fixed at 2° and 200, respectively. The working speed is 1 rps. The void content (α) of the compacted sand blend can be then be calculated as:

$$\alpha = (1 - \gamma_{RM} / \rho_{RM}) \times 100 \tag{3.3}$$

$$\rho_{RM} = \rho_{Ri} \times \sum_{i-1}^{n} (V_{Ri} / V_{RM}) \tag{3.4}$$

where γ_{RM} is the bulk density of dry sand blend, V_{Ri} and V_{RM} are absolute volumes of river sand and sand blend, respectively, and ρ_{Ri} and ρ_{RM} are the densities of river sand and sand blend, respectively.

3.2.4. Step 4: Determine V_b/V_s of Mortar. The primary paste volume, denoted by V_b, takes into account the paste volume that is necessary to fill the void content of the sand and lubricate the sand particles. The primary paste can be calculated using the approach proposed by (Koehler et al. 2007):

$$V_b = V_{\exp} + V_{void} \tag{3.5}$$

$$V_{\exp} = 8 + (16 - 8) / 2(R_{S,A} - 1) \tag{3.6}$$

$$V_{void} = \alpha(100 - V_{\exp}) / 100 \tag{3.7}$$

$$V_S = (V_{\exp} + V_{void}) / (100 - V_{\exp} - V_{void}) \tag{3.8}$$

where V_S expresses as the sand volume, V_{exp} denotes excess paste volume (vol.%), V_{void} is void content in mortar (vol.%), and $R_{S,A}$ is a coefficient related to the shape and the angularity of sand in the range of 1-5 (Koehler et al. 2007).

The minimum V_b/V_S value can provide the necessary paste for filling ability. However, the minimum value is not necessarily appropriate for a specific requirement of

strength. Therefore, additional experiments need to be carried out to validate the optimum value of V_b/V_S using mortar mixtures. The 28-days compressive strength of each mortar mixture with a V_b/V_S value can be evaluated. The HRWR dosage is adjusted to obtain a mini slump flow of 280 ± 10 mm.

3.2.5. Step 5: Determine Fiber Content of UHPC. The fiber content of UHPC commonly ranges from 2 to 5% (Park et al. 2012). The optimum fiber content is determined based on key fresh and mechanical properties of UHPC mixtures made with different fiber contents. The mini-V-funnel and mini-slump tests are used to express workability. The HRWR dosage is adjusted to obtain a mini-slump flow of 280 ± 10 mm. Flexural load-deflection relationships are determined in accordance with ASTM C 1609 to evaluate the first cracking strength and load capacity. Beam specimens (304.8 x 76.2 x 76.2 mm^3) are tested after 28-days standard curing.

3.2.6. Step 6: Adjust w/cm and/or HRWR and Evaluate Performance of UHPC. In this step, trial batches are prepared to verify compliance of selected mixtures with mini-slump flow of 280 ± 10 mm and 28-days compressive strength C120 MPa under standard curing and/or C150 MPa under heat curing. If the mixture does not achieve the targeted performance, either the HRWR dosage or w/cm can be adjusted. For the selected mixture(s), key properties of the UHPC should be determined, as elaborated below.

3.2.6.1 Fresh properties. The HRWR dosage is adjusted to secure an initial mini-slump flow of 280 ± 10 mm. The unit weight and air content are measured in accordance with ASTM C 138 and ASTM C 231, respectively. The initial and final setting times are tested in accordance with ASTM A403. A ConTech 5 viscometer can be employed to determine τ_0 and μ_p of the UHPC. Typically, the measurements begin at 10 min after water addition with samples subjected to pre-shear at a rotational velocity of 0.50 rps during 25 s, followed by a stepwise reduction in rotational velocity. The τ_0 and μ_p are then calculated using the Bingham fluid model (Tattersall et al. 1983), as shown in Eq. 1.

3.2.6.2 Mechanical properties. Compressive strength and flexural properties can be tested at different ages. The elastic modulus can be determined in accordance with ASTM C 469. The splitting tensile strength can be measured in accordance with ASTM C 496. Three samples are replicated in each test.

3.2.6.3 Autogenous and drying shrinkage. The autogenous shrinkage can be evaluated in accordance with ASTM C 1698 using samples in corrugated plastic tubes and stored immediately after casting at 20 ± 0.5 °C and 50 ± 2% RH. The first measurement is taken as final setting. The second measurement is taken at 12 h after final setting. Other measurements are carried out daily within the 1st week, and then, weekly until 28 days after final setting. Drying shrinkage can be evaluated using prism specimens in accordance with ASTM 596, until 91 days after 7-days moist curing.

3.2.6.4 Durability. If deemed necessary, some durability characteristics of the optimized UHPC mixture can be investigated. For example, electrical resistivity can be measured in accordance with ASTM C 1760, and frost durability can be determined in accordance with the ASTM C 666, Procedure A.

3.3. EXPERIMENTAL VALIDATIONS

As stated earlier, the study aimed at using high volume SCMs and locally available conventional concrete sand in proportioning UHPC to reduce the material's unit cost. An example of using the mix design method in detail is presented as follows.

3.3.1. Optimize Binder Combinations for Paste. Optimized binder combinations for paste are discussed as followings.

3.3.1.1 Select binder candidates based on flow characteristics of paste. The initial binder combinations contained SF ≤25%, vol.%, and FAC or/and GGBS C30%, vol.%, as listed in Table 3-2. In total, 27 binder systems were investigated, which consisted of the reference, 14 binary, nine ternary, and three quaternary binders. The binary binders were categorized into three groups: (i) four GGBS systems, (ii) four FAC systems, and (iii) six SF systems. The ternary binders included four FAC-SF systems and five GGBS-SF systems. Three quaternary binders were prepared with FAC-SFGGBS.

Figure 3-3 compares the MWC and RWD results of the 27 binder combinations, which are listed in Table 3-2. For the binary systems, the FAC and GGBS systems exhibited lower MWC values than that of the reference made with 100% cement. The MWC value decreased with the increase of FAC's content due to the lubrication effects of FAC (Termkhajornkit et al. 2001). However, GGBS had an optimum amount that allowed the lowest MWC, due to its higher Blaine fineness than that of the cement, which

improves the grain size distribution of the powder component and reduces the water demand (Parka et al. 2005). However, GGBS has irregular shapes and large specific areas that may result in increase of the MWC. The MWC values of the SF binary systems were close to that of the reference mixture. The small and spherical SF particles can fill the voids between cement particles, which reduce the water demand. However, the fine SF particles are highly chemically reactive and can adsorb HRWR, which is adverse for the MWC (Otsubo et al. 1980).

Figure 3-3 indicates that the use of SCMs could increase the RWD and lead to a greater robustness. For the binary systems, the FAC60 mixture provided the smallest MWC, and the largest RWD. For the GGBS binary system, the G50 mixture had the best performance (smallest MWC and largest RWD). For the SF binary system, the SF5 mixture gave the best performance. For the GGBS-SF ternary systems, the use of 5% SF slightly reduced the MWC and increased the RWD, compared with the corresponding GGBS binary systems. The fine SF particles filled the voids between the bigger cement and GGBS particles and formed gel that reduced the friction between the particles (Parka et al. 2005), thus reducing the MWC. However, using 5 or 8% SF in the FAC-SF ternary systems did not demonstrate significant improvement for the corresponding FAC binary systems. Particularly, the use of 5% SF led to a notable increase in MWC and reduction in RWD when 60% FAC was used. In summary, the G50SF5 mixture provided the highest packing density (smallest MWC) and robustness (largest RWD). All three quaternary systems offered relatively low MWC and high RWD, as indicated inFigure 3-3.

Out of the 27 binder combinations shown in Figure 3-3, 18 binders that have relatively low MWC (high packing density) were selected. Aside from Group 1, two combinations having the lowest MWC were selected in each group. For Groups 2, 4, 5, 6, and 7, three mixtures were selected since the second and third mixtures have similar performance.

Table 3-2 Codification of initial investigated binders (vol.%)

Group	Code	Cement	GGBS	FAC	SF
1	Ref	100	–	–	–
2	G40	60	40	–	–
	G50	50	50	–	–
	G60	40	60	–	–
	G70	30	70	–	–
3	FAC30	70	–	30	–
	FAC40	60	–	40	–
	FAC50	50	–	50	–
	FAC60	30	–	60	–
4	SF5	95	–	–	5
	SF8	92	–	–	8
	SF11	89	–	–	11
	SF14	86	–	–	14
	SF20	80	–	–	20
	SF25	75	–	–	25
5	FAC40SF5	55	–	40	5
	FAC50SF5	45	–	50	5
	FAC50SF8	42	–	50	8
	FAC60SF5	35	–	60	5
6	G40SF5	55	40	–	5
	G50SF5	45	50	–	5
	G60SF5	35	60	–	5
	G50SF8	42	50	–	8
	G50SF11	39	50	–	11
7	F40S5G10	45	10	40	5
	F40S5G20	35	20	40	5
	F40S5G30	25	30	40	5

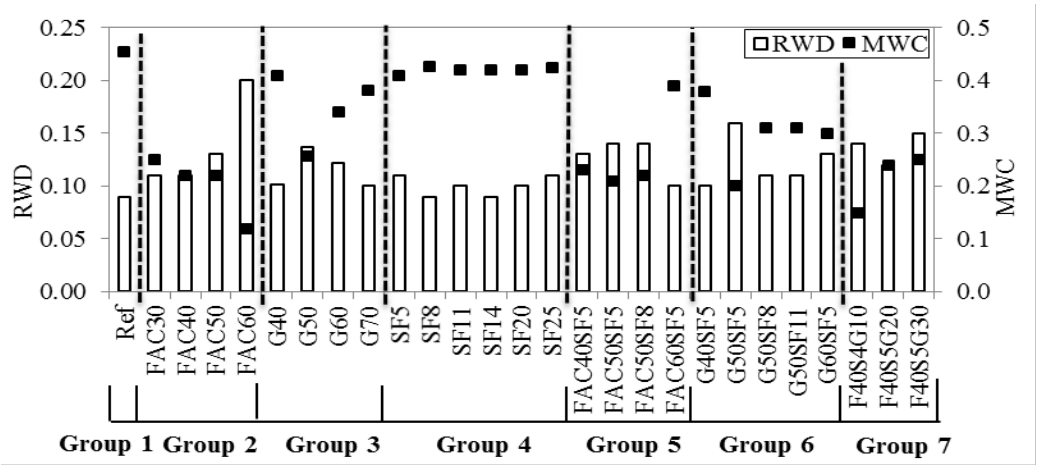

Figure 3-3 Effect of binder type on minimum water content and relative water demand

3.3.1.2 Narrow down binder combinations. In this step, the w/cm was fixed at 0.20. Figure 3-4 shows the results of HRWR demand (active solid material in HRWR divided by binder, wt.%), and 1- and 28-days compressive strengths of paste mixtures. Under standard curing, the FAC binary systems, except for the FAC60 mixture, achieved higher 1-days compressive strengths but lower 28-days compressive strengths than those of the GGBS binary systems. Using high-volume GGBS or FAC could lead to 75% lower HRWR demand compared with the reference mixture. The use of SF did not influence the HRWR demand and 28-days compressive strength significantly but increased considerably the 1-days compressive strength. For example, the use of 5% SF resulted in 95.8 MPa of the 1-days compressive strength which is more than twice that of the reference mixture (45.8 MPa). The SF binary systems demonstrated the highest 1-days compressive strength compared to other binary systems but also the highest HRWR demand. Except for the FAC40SF5G10 mixture, the 28-days compressive strength of the 17 binder combinations was in the range of 125-158 MPa. The HRWR demand of the binders with high-volume SCMs combinations was about one-third of those of the reference and the SF binary systems.

In this study, the weighted factors that were used in radar chart analysis were selected to secure high performance of UHPC intended for precast application. The factors for the 1-days compressive strength, 28-days compressive strength, MWC, flow time, RWD, and HRWR demand were 2, 4, 3, 3, 2 and 3, respectively. Figure 3-5 shows the area obtained from the radar charts. The FAC60 had the largest area, followed by G50SF5, G50, FAC40SF5, FAC40, and G50SF11 mixtures. The top six binder combinations were selected for evaluating the rheological properties.

3.3.1.3 Finalize binders based on rheological properties for paste. Seven binder combinations, including the reference (Ref) and six candidates selected from the previous steps, were further evaluated in terms of the rheological properties. Since the w/b and initial mini-slump flow were fixed for all mixtures, spreads of μ_p at 20 min between the mixtures were mainly due to their differences in packing densities and water film thicknesses that depend on the HRWR dosage and binder in use (Ferraris et al. 2001). Figure 3-6 shows the variation in μ_p from 20 to 60 min after water addition. At 20 min, the G50SF5 mixture achieved the lowest μ_p, whereas the reference paste had the

highest μ_p. A lower μ_p of binders indicated more additional water amount, thicker water film, and lower friction between particles (Wong et al. 2008). Between 20 and 60 min, the μ_p values did not change significantly and had similar rates of increase in μ_p.

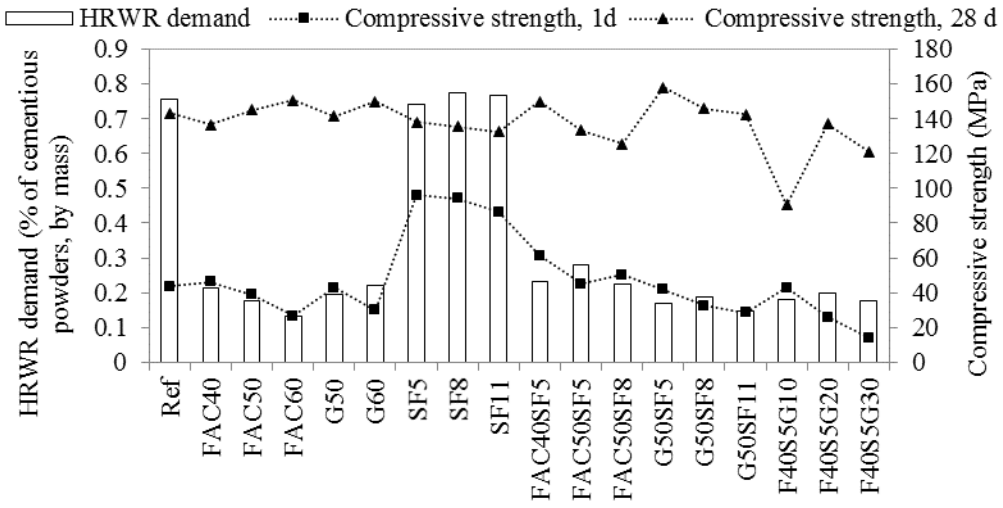

Figure 3-4 HRWR demand and 1- and 28-d compressive strength of paste

Low μ_p is desirable to achieve good filling capacity (Mechtcherine et al. 2015). Relatively low μ_p can also help fibers get evenly distributed in the matrix and improve the flexural performance. Mixtures that are highly viscous can entrap air, and, thus have reduced strength. Therefore, based on the results presented in Fig. 6, the G50SF5, FAC40SF5, G50, and FAC60 mixtures were select for further evaluation.

3.3.2. Preliminarily Select a w/cm for Paste. A w/cm in the range of 0.18-0.23 was investigated for the four optimum binders. As indicated in Figure 3-7, when the w/cm was increased from 0.18 to 0.23, the 28-days compressive strengths under standard curing did not decrease significantly (<10%), but the HRWR demand was reduced by about 40-60%. When the w/cm was increased from 0.20 to 0.23, the HRWR demand did not change significantly. Therefore, a w/cm of 0.2 was preliminarily selected, which allowed high compressive strength and flowability and relatively small temperature change.

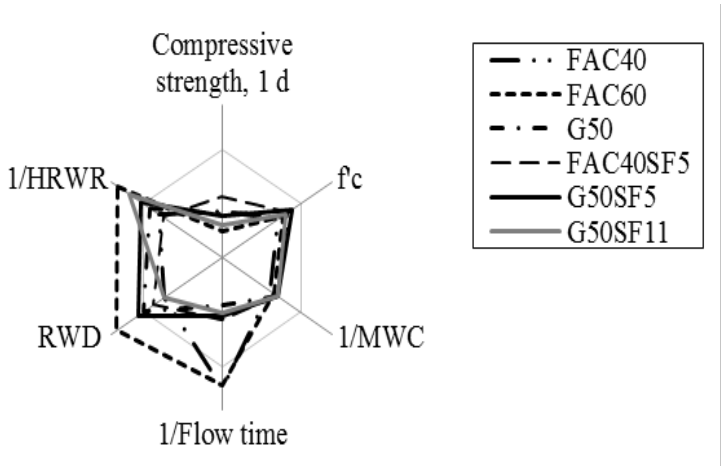

(a)

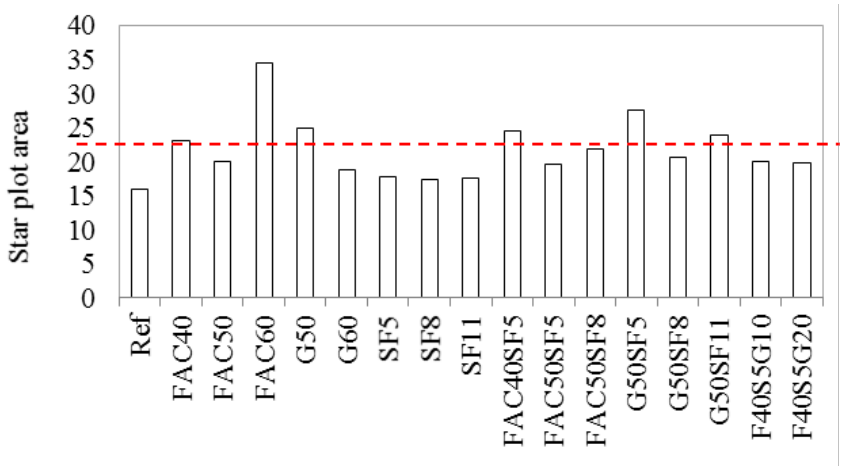

(b)

Figure 3-5 Multi-variable analysis: (a) radar chart and (b) areas in radar chart

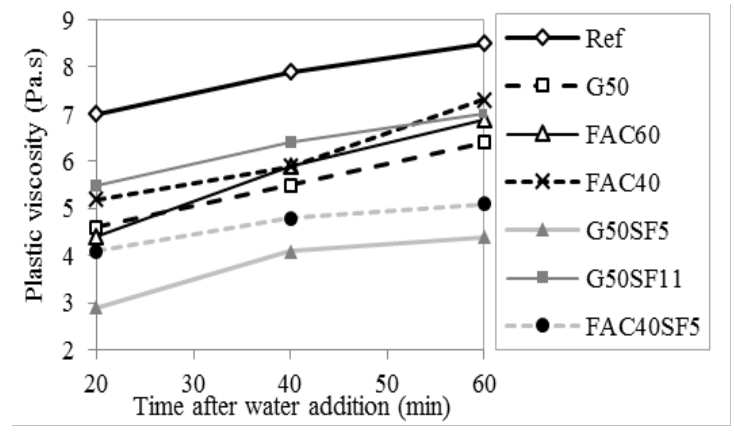

Figure 3-6 Time versus plastic viscosity of paste mixtures

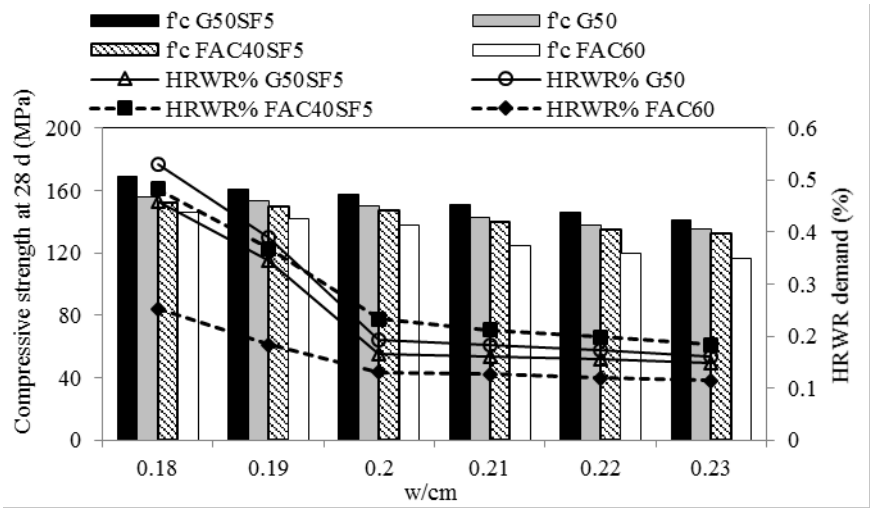

Figure 3-7 HRWR demand and compressive strength at 28 day for different w/cm

3.3.3. Determine Sand Combination. The D_{max} and D_{min} values were determined by the sieve sizes of 4.75 and 0.15 mm, respectively. The optimized sand combination can result in an optimized gradation curve that could be achieved with the minimum deviation from the target gradation curve, as shown in Figure 3-8. For the river sand and masonry sand employed in this study, the optimized sand combination to meet the targeted particle size distribution consisted of 70% of river sand and 30% of masonry, by mass.

In order to validate the suitability of the optimized sand to achieve high packing density, the densities of different sand combinations were measured using a gyrator compaction testing procedure. The combination with 70% river sand and 30% masonry indeed resulted in the highest bulk packing density (1870 kg/m^3) compared to the density of other sand blends.

By applying the Eqs. 3 and 4, the void content (a) can be determined as: $\alpha = (1 - 1870/ 2640)\ 9\ 100 = 30$. This value is required for evaluating the binder-to-sand volume ratio (V_b/V_S).

3.3.4. Determine V_b/V_s. The minimum V_b/V_S is determined to be 0.6 according to Eqs. 5-8, where $R_{S,A}$ equals 2 (Koehler et al. 2007). The flow properties and compressive strength for mortars with V_b/V_S values of 0.6, 0.7, 0.8, 0.9, 1.0 and 1.3 were tested, as shown in Table 3-3. The mixtures were prepared with the same binder made with 50% GGBS, 5% SF, and 45% cement. The w/cm was set to 0.2. As V_b/V_S value was

increased from 0.6 to 1.3, the HRWR demand and flow time were increased from 0.12 to 0.30% and from 46 to 129 s, respectively. The corresponding 1-days compressive strength was increased from 40 to 42 MPa, respectively, and the 7- and 28-days compressive strengths were increased from 75 to 90 MPa and from 100 to 124 MPa, respectively. Therefore, as V_b/V_S value increased from 1.0 to 1.3, the compressive strength results did not change considerably, but the HRWR demand and flow time were significantly increased. The V_b/V_S value was determined to be 1.0, which resulted in optimized mixture with relatively low HRWR demand and viscosity, low paste content, and high compressive strength.

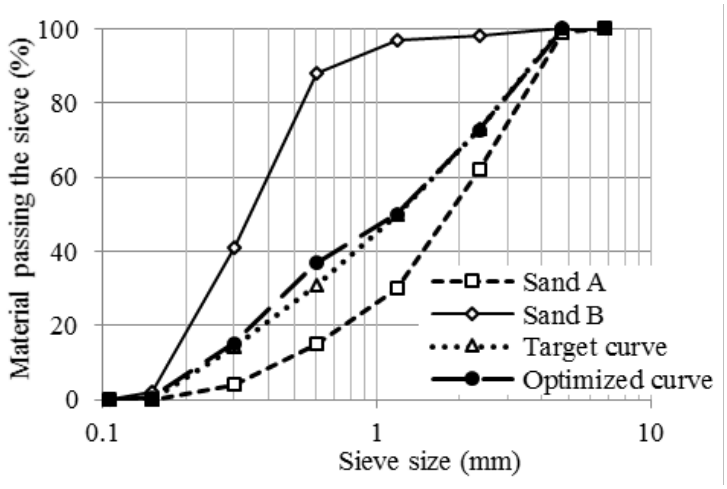

Figure 3-8 Sand gradation

3.3.5. Determine Fiber Content. Short steel fibers were used to enhance the post cracking performance. As the fiber content was increased from 0 to 2.5% with a step size of 0.5 %, as shown in Table 3-4, the HRWR demand, which was required to ensure the slump flow of 280 ± 10 mm was increased from 0.28 to 0.69%, and the flow time was increased from 12 to 35 s. Particularly, when the fiber volume percentage, denoted by V_f, was increased from 2 to 2.5%, the HRWR dosage and flow time were increased by 72 and 94%, respectively.

For the flexural properties, the first cracking load is expressed as f_1, which corresponds to the load at the appearance of the first crack, as shown in Table 3-3. The peak load is denoted by f_p. The mid-span deflections corresponding to f_1 and f_p are denoted by and d_1 and d_p, respectively. The area under load versus deflection curve

between deflection values of 0 to L/150 (L = 202 mm) is referred to as T_{150}, which represents the toughness and is an indicator of energy dissipation. As the fiber content increased from 0 to 2%, the f_1 and f_p increased by 20 and 48%, respectively. However, as the fiber content was further increased from 2 to 2.5%, without significantly change in f_p and T_{150}. A drop in f_1 was observed. The highest f_p and T_{150} were secured by the use of 2% steel fibers which is considered as the optimum fiber content.

Table 3-3 Compressive strengths of different binder-to-sand ratio (V_b/V_S)

V_b/V_s	HRWR demand (%)	Flow time	Compressive strength		
			1 day	7 days	28 days
0.6	0.12	46	40	75	100
0.7	0.18	64	41	80	106
0.8	0.21	79	43	83	111
0.9	0.25	92	42	85	115
1.0	0.28	104	42	88	123
1.3	0.30	129	42	90	124

Table 3-4 Performance of UHPC made with different fiber contents

Code	Vf (%)	HRWR demand (%)	Slump flow (mm)	Flow time (s)	28-days compressive strength (MPa)	f1 (MPa)	d1 (mm)	fp (MPa)	dp (mm)	T150 (J)
Ref.-no fiber	0.0	0.28	29.0	12	123	13.7	0.10	13.7	0.10	1.0
Steel-0.5%	0.5	0.28	29.0	20	124	14.9	0.10	14.9	0.10	24.5
Steel-1.0%	1.0	0.28	28.5	22	124	15.9	0.07	16.5	0.61	38.4
Steel-1.5%	1.5	0.29	28.0	24	125	16.2	0.11	19.6	0.77	41.3
Steel-2.0%	2.0	0.40	28.0	18	125	16.5	0.08	20.3	1.05	50.2
Steel-2.5%	2.5	0.69	28.0	35	126	12.7	0.07	19.7	1.65	49.7

3.3.6. Evaluate and Adjust Designed UHPC Mixtures. Based on the above investigations, four mixtures were selected for further evaluation. Table 3-5 lists the four mixtures and a proprietary UHPC mixture taken as the reference mixture. These mixtures were prepared using the EIRICH mixer. The UHPC mixtures were designed to have a mini-slump flow diameter of 280 ± 10 mm, by adjusting the HRWR dosage, without consolidation. The w/cm was not changed since all the mixtures achieved 28-days compressive strengths higher than 120 MPa under standard curing.

3.3.6.1 Fresh and physical properties. Table 3-6 summarizes the results of fresh properties. All the mixtures were self-consolidating and stable. The mini V-funnel flow times and plastic viscosities of the mixtures ranged from 12 s to 46 s and 23-50 Pa, respectively. The reference mixture exhibited the lowest flow time and plastic viscosity, which were 12 s and 23 Pa.s, respectively. The highest flow time and plastic viscosity, which were 46 s and 50 Pa.s, respectively, were obtained by the G50 mixture. The HRWR demands of all the mixtures were in the range of 0.5-1.4%. The HRWR demand was the lowest for the FAC60 mixture and the highest for the G50SF5 mixture. The FAC40SF5 mixture demonstrated the longest initial setting time of 10 h and final setting time of 15 h. The G50SF5 had the shortest initial and final setting time of 2 h and 6 h, respectively.

Table 3-5 Proportioning of the designed UHPC mixtures (unit: kg/m^3)

Code	Cement	SF	FAC	GGBS	Quartz sand	Fine sand	Sand A	Sand B	HRWR	Total water	Steel fibers
Ref.	712	231	–	–	1020	211	–	–	6.5	164	156
G50SF5	548	42	–	535	–	–	694	304	16.0	167	156
G50	593	–	–	546	–	–	698	295	12.5	182	156
FAC40SF5	663	42	367	–	–	–	703	308	12.0	171	156
FAC60	486	–	556	–	–	–	715	304	5.5	188	156

3.3.6.2 Compressive strengths. Compressive strengths of the selected mixtures at 28 days under standard and heat curing methods were compared, as listed in Table 3-6. The 28-days compressive strength of the reference mixture was 135 MPa and that of the designed mixtures was up to 125 MPa, under standard curing. The designed mixtures had slightly lower compressive strengths than that of the reference mixture. This may be due to the low silica fume content of the designed UHPC mixtures compared with the reference mixture. The designed UHPC mixtures achieved 28-days compressive strength up to 178 MPa under heat curing, which was 12% lower than that of the reference UHPC (202 MPa). The FAC60 mixture had 136 MPa under initial heat curing, which is under the target value of 150 MPa.

3.3.6.3 Unit cost per compressive strength under standard curing. The unit cost per strength, defined as the ratio of the unit cost ($/m^3) normalized by the 28-days compressive strength under standard curing conditions, as shown in Table 3-6. The unit

cost includes the costs of all ingredients necessary for producing the UHPC mixtures in exception of transportation cost. The unit cost of the selected cement, SF, FAC, GGBS, local river sand, masonry sand, quartz sand, HRWR, and steel fiber are 0.2, 0.66, 0.03 0.05, 0.014, 0.007, 2.2, 3.8 and 1.0 $/kg, respectively. These costs apply to St. Louis, MO, in 2016. The FAC and GGBS have 75% lower unit cost than the cement. The local river sand has about 99.5% lower unit cost than the special finely-ground quartz sand. Thus, the use of high volume SCMs and local river sand could significantly reduce the unit cost of the UHPC. The unit cost per strength was 14.8 $/m^3/MPa for the reference mixture, and 3.5, 4.2, 4.3 and 4.7 $/m^3/MPa for the designed FAC 60, G50, FAC40SF5, and G50SF5 mixtures, respectively. This corresponds to 68-76% reduction in unit cost per unit compressive strength.

3.3.6.4 Other mechanical properties. Table 3-6 summarizes the test results of the splitting tensile strength, Young's modulus, and flexural properties of the investigated UHPC mixtures under standard curing. The G50SF5 and FAC60 mixtures offered the highest and the lowest splitting tensile strengths of 14.3 and 10.3 MPa, respectively. The FAC40SF5 and FAC60 gave the highest and the lowest elastic moduli of 51.6 and 45.8 GPa, respectively. For the flexural properties, the flexural strengths of the five mixtures were close and ranged from 19.7 to 22.8 MPa. The G50 mixture had the highest first cracking and peak loads and toughness. The reference mixture had the lowest flexural strength and T_{150}.

3.3.6.5 Shrinkage. Autogenous shrinkage, which is caused by volume reduction due to chemical reactions during hydration and self-desiccation, contributes mostly to the total shrinkage in UHPC (Bao et al. 2015). Table 3-6 shows the results of 28-days autogenous shrinkage measured since the final setting. The reference mixture had the highest 28-days autogenous shrinkage, which was 730 μm/m, due to the high silica fume content. The lowest autogenous shrinkage of 250 μm/m was obtained by the G50 mixture. The G50SF5, FAC60 and FAC40SF5 mixtures had 28-days autogenous shrinkage values of 600, 595 and 545 μm/m, respectively.

The drying shrinkage values measured after 7 days of moist curing. The end of the moist curing was chosen as "time zero" (t=0). The reference mixture reached a total drying shrinkage of 600 μm/m, which was the highest value compared with the other

designed mixtures. The G50 mixture displayed the minimum drying shrinkage, which was only 55 μm/m. The total shrinkage of the UHPC can be considered as the initial autogenous shrinkage after 7 days, when autogenous shrinkage was stabilized, plus the drying shrinkage determined following 7 days of moist curing. The G50 mixture had the lowest total shrinkage of 310 μm/m. The reference mixture obtained the highest total shrinkage, which was 1330 μm/m.

Table 3-6 Mechanical properties and durability of the UHPC mixtures

Code		Ref.	G50SF5	G50	FAC40SF5	FAC60
Flow time (s)		12	30	37	39	46
HRWR demand (%)		0.69	1.38	1.06	1.01	0.51
Mini slump flow (mm)		275	280	285	285	285
Yield stress (Pa)		39	35	37	34	30
Plastic viscosity (Pa·s)		23	39	50	44	29
Air content (%)		4	5	5	4	3.5
Specific gravity		2.47	2.45	2.43	2.44	2.41
Initial setting (h)		5	2	6	10	6
Final setting (h)		10	6	12	15	12
1 d – Standard curing (MPa)		53	52	64	65	69
28 d - Standard curing (MPa)		135	125	124	124	120
Splitting tensile strength (MPa)		12	14	12	12	10
Unit costs normalize by compressive strength ($/m^3/MPa)		14.8	4.7	4.2	4.3	3.5
Modus of elasticity (GPa)		53	50	50	52	46
Flexural performance	First cracking load (kN)	22	21	24	21	20
	Peak load (kN)	21	29	33	31	28
	δ_1 (mm)	0.092	0.085	0.080	0.093	0.089
	δ_p (mm)	0.701	0.690	0.653	0.820	0.635
	Peak strength (MPa)	19.7	20.2	22.8	21.3	20.1
	T150 (J)	40.4	48.8	51.5	51.1	49.4
Surface conductivity (kΩ·cm)		45	30	28	38	34
Durability factor (%)		99.8	99.8	99.8	99.7	99.7
Autogenous shrinkage at 28 d (μm/m)		731	602	253	545	593
Drying shrinkage at 98 d (μm/m)		600	430	56	466	500

3.3.6.6 Electrical resistivity. The electrical resistivity affects the corrosion resistance of the material. Test results of surface resistivity, which is an indicator of electrical resistivity, of the five UHPC mixtures determined at 28 days, are shown in

Table 3-6 Mixtures with a surface conductivity greater than 20 kΩ cm can be considered to have a low risk of corrosion rate (Broomfield 2011). Hence, all the mixtures that had surface conductivities of 30-38 kΩ cm can be considered to exhibited a low risk of corrosion rate. The reference mixture with high silica fume content had the highest electrical resistivity. The G50 mixtures had the lowest electrical resistivity.

3.3.6.7 Freezing and thawing. The variations in durability factor of the UHPC mixtures after 300 freeze-thaw cycles are shown in Table 3-6. All the UHPC mixtures exhibited adequate resistance to freezing and thawing with durability factors of nearly 100%. The freezing and thawing testing was initiated after 56 days of moist curing given the high volume of SCMs. The excellent frost durability is associated with the very low permeability of the material.

3.4. SUMMARY

A mix design methodology is presented for producing cost-effective UHPC with high-volume SCMs and conventional concrete sand. Based on the reported studies, the following conclusions can be drawn:

The MWC can first be used as an indicator of the packing density of binders in wet condition to narrow down binder systems and reduce the required number of experiments. The binder composition of UHPC can then be optimized with consideration on the HRWR demand, rheological properties, MWC, RWD, and compressive strength properties. A radar chart can be then employed for the analysis. Based on this approach the following binder combinations were selected: G50, G50SF5, FAC60, and FAC40SF5.

The second step is to determine the preliminary w/cm based on the 28-days compressive strength and HRWR demand value for paste mixtures prepared with the optimum binder combinations with w/cm values of 0.18-0.23. The optimum value for the selected binders was 0.20.

The modified Andreasen and Andersen model can be used to optimize sand gradation. In this study, 70 % river sand and 30 % masonry sand were selected to achieve the highest packing density.

The next step involves the determination of the binder-to-sand volume ratio (V_b/V_s). Mortar mixtures made with the selected w/cm and G50SF5 binder were prepared

with V_b/V_s values of 0.6, 0.7, 0.8, 0.9, 1.0 and 1.3. Based on flow properties and 28-days compressive strength, the optimum V_b/V_s was determined to be 1.0.

The optimum fiber content for the UHPC is experimentally determined given the flowability and flexural properties of UHPC made with various fiber contents. For the steel fibers considered in this study, 2% fiber volume was selected.

For the UHPC mixtures prepared with the various binder systems and optimized mixture proportioning, the UHPC mixtures were self-consolidating, stable, and had 28-days compressive strengths of 120-125 MPa under standard curing condition. The strength can reach up to 178 MPa by applying heat curing at a maximum temperature of 90 °C for one day followed by 7-days moist curing. For the selected UHPC mixtures, the 28-days splitting tensile strength, modulus of elasticity, flexural strength, and toughness (T_{150}) were 11.6-14.3 MPa, 48.8-51.6 MPa, 20.2-21.3 MPa and 50 ± 1.5 kN mm, respectively.

The designed UHPC mixtures exhibited relatively low autogenous shrinkage and drying shrinkage. The G50 mixture had the lowest autogenous and drying shrinkage of 255 µm/m at 28 days and 55 µm/m at 98 days, respectively. All tested UHPC mixtures exhibited a very high electrical resistivity and excellent frost durability.

The unit cost per compressive strength of the UHPC mixtures designed with high volume of SCMs and concrete sand can range between 4.1 and 4.7 $\$/m^3/MPa$. The mixture FAC60 was the most cost-effective mixture, which also developed better workability and lower unit cost per compressive strength of 3.7 $\$/m^3/MPa$ than other mixtures.

4. ROBUSTNESS OF UHPC AT DIFFERENT CASTING AND CURING TEMPERATURES

Concrete temperature during mixing and curing can have marked influence on key properties of ultra high performance concrete (UHPC). UHPC was mixed and cured at 10, 23, and 30 ºC to investigate the effect of temperature on rheology, workability, setting time, mechanical properties as well as autogenous and drying shrinkage.

High complexity and some unpredictable performance upon changes of ambient or processing parameters can make special concretes like self-consolidating concrete (SCC) and/or high performance concrete less robust than conventional concrete. For successful applications of such concretes at the job site, they should be robust with respect to variations in processing parameters and the environmental conditions. Robustness is defined as stability against variations in quality and quantity of the constituents, processing parameters, and environmental conditions (Yu et al., 2015). For example, Roy and Asaga (1979) reported that a change from the least severe to the most severe mixing procedure of SCC caused both the yield stress and plastic viscosity to decrease by about 60%. Sakata et al. (1996) reported that SCC made with low water-to-binder ratio (w/b) of 0.33 (powder containing limestone filler), the incorporation of a small concentration of welan gum of 50 g/m^3 can reduce the variability in slump flow of SCC due to changes in cement Blaine (318 to 342 m^2/kg), fineness modulus of sand (2.08 to 3.06), and temperature of fresh concrete (10 to 30°C). Banfill (1982) reported that substitution of up to 60% of the cement by fly ash reduces the yield stress of SCC, but has little effects on the plastic viscosity. The incorporation of cementitious materials of high specific gravity, such as slag, dolomite, or limestone, increases robustness in SCC (Bonen et al., 1982). Higher robustness is also achieved by increasing the viscosity of the mixture via material selection and incorporation of a viscosity-enhancing admixture (VEA) (Gettu et al., 2009; Yurugi et al., 1995) The use of a VEA can increase SCC stability when changes in sand humidity occur (Billberg and Khayat, 2008).

Ultra high performance concrete (UHPC) is a new generation of concrete that exhibits excellent mechanical and durability properties. Unit cost of the material by using locally available materials have been proposed. This includes the replacement of quartz

sand by concrete sand and replacing part of the cement with supplementary cementitious materials (SCMs) through packing density optimization (Meng et al., 2017). As any other high performance concrete, UHPC can be affected by the casting and curing temperature. The mixture design of such high value-added concrete should therefore secure high robustness vis-a-vis temperature variations. Temperature can greatly fluctuate even throughout a single day from 10 and 30 ºC in some parts of the world. Concrete batching in different weather conditions can have significant impact on performance. Ambient temperature can increase concrete temperature, resulting in higher water demand and accelerate hydration process, thus leading to fast slump loss and setting time and can adversely affect mechanical properties of concrete, especially in long term (Neville, 1999). In addition, there is a possibility of reducing effective w/b due to the evaporation of water from fresh concrete in high temperature condition. This can lead to the need for additional water to maintain the concrete in acceptable range of workability for designed application (Mouret et al., 1997). The increase in temperature can increase the risk of plastic and shrinkage cracking and can adversely affect early properties (Soudki et al., 2001; Ortiz e al., 2005).

On the other hand, low temperature can reduce the hydration rate of cementitious materials. This can necessitate special considerations during placement, finishing and curing. A drop in temperature can decelerate setting and delay the time of finishing and strength gain at early age (Nassif and Petrou, 2013).

The mixture design of UHPC necessitates high dosage of high range water reducing admixture (HRWRA) to secure self-consolidating properties. Temperature fluctuation can have significant impact on the rate of hydration and adsorption of HRWRA. HRWRA is adsorbed on the surface of hydration products, such as C_3A, C_4AF, and monosulphate, and in particular ettringite, in particular (Flatt and Houst, 2001). High temperature can accelerate the hydration process causing negative effect on workability. However, the accelerated production of ettringite can increase adsorption sites for the HRWRA which enhances dispersion of the cement and improves flowability (Flatt and Houst, 2001; Goller et al., 2009; Yoshioka et al., 2002). On the other hand, retarding the hydration as a result of low temperature can positively affect workability retention. However, there is not sufficient area to adsorption the high volume of HRWRA

remaining ineffectively in the system due to slow process of hydration (Yoshioka et al., 2002; Plank and Hirsch, 2007; Randl et al., 2014).

Ensuring high robustness of UHPC to temperature variations is key to successful production of UHPC. The objective of this investigation is to evaluate the robustness of UHPC made with silica fume, Class C fly ash, and ground granulated blast-furnace slag that at different casting and curing temperatures of 10, 23, and 30 ºC. The investigated properties included rheology, workability, setting time, mechanical properties as well as autogenous and drying shrinkage.

4.1. MATERIAL AND MIXTURE PROPORTIONS

Table 4-1 summarizes the physical and chemical characteristics of cementitious materials. A Type III portland cement, densified silica fume (SF), a Class C fly ash (FA), and ground granulated blast-furnace slag (GGBS) were employed for the binder. Two natural siliceous sands of 0-4.75 mm (sand A) and 0-2 mm (sand B) with specific gravity of 2.6 were used. The sands were proportioned at 70:30 mass ratio, which was found to yield the highest packing density for the proposed UHPC mixtures (Meng et al., 2017). A quartz sand (0-0.6 mm) was used for the reference UHPC. A polycarboxylate-based HRWRA with a solid content of 23% and specific gravity of 1.05 was used to enhance fluidity retention and fiber distribution of the UHPC. Brass coated straight steel fibers measuring 13 mm in length and 0.2 mm in diameter were incorporated at 2% volumetric ratio, to improve ductility. The aspect ratio and tensile strength of the fibers are 40 and 2.16 GPa, respectively.

Table 4-2 summarizes mixture proportioning of the investigated UHPC mixtures. The w/b was fixed at 0.20, and the sand-to-cementitious materials ratio was held at 1.0, by volume. HRWRA dosage was adjusted to secure initial mini-slump value of 270 ± 10 mm, which is necessary to secure self-consolidating characteristic.

4.2. MIXING PROCEDURE AND SAMPLE PREPARATIONS

In order to provide low temperature condition of 10 ± 1 °C, all solid materials and mixing water were stored in a controlled chamber at 2 °C for 24 hr before mixing. Half of the mixing water was replaced with crushed ice, and the ice was introduced into mixer 15 min prior to mixing to cool down the mixer pan. For the UHPC at 23 ± 1 °C, only the

mixing water was cooled down. Finally, for the 30 ± 1 °C mixtures, no special preparation was required.

A 150-l high-shear concrete mixer with an inclined drum and adjustable vane speed was used. The mixing procedure consisted of mixing the sand and cementitious materials for 2 min at 1 rps. This was followed by adding of 90% of the mixing water with 90 % of the HRWRA and mixing the material 2 min at 6 rps; (3) the remainder of the liquid was added, and the material was mixed for 4 min at 6 rps; (4) the fibers were introduced gradually over a period of 1 min and total materials were mixed for 2 min at 10 rps. Specimens were cast in one lift without any mechanical consolidation and covered with wet burlap and plastic sheet for 24 hours. They were demolded and cured in lime-saturated water at 10, 23, and 30 °C.

Table 4-1 Physical and chemical characteristics of cementitious materials

Compositions	Cement (Type III)	Fly ash (Class C)	GGBS	Silica fume
SiO_2 (%)	19.72	36.5	36.8	95.5
Al_2O_3 (%)	5.10	24.8	9.2	0.7
Fe_2O_3 (%)	2.76	5.2	0.76	0.3
CaO (%)	64.50	28.1	37.1	0.4
MgO (%)	2.30	5	9.5	0.5
SO_3 (%)	3.25	2.5	0.06	0
Na_2O (%)	0.33	0	0.34	0.4
C_3S (%)	65.23	-	-	-
C_2S (%)	7.33	-	-	-
C_3A (%)	8.85	-	-	-
C_4AF (%)	8.40	-	-	-
Blaine surface area (m^2/kg)	562	465	589	-
Specific gravity	3.15	2.70	2.90	2.2
Loss of ignition (%)	2.6	0.3	5.1	2.6

4.3. EXPERIMENTAL PROGRAM

4.3.1. Fresh Properties. Mini-slump flow was conducted in accordance with ASTM C230 using a truncated cone measuring 60 mm in height with upper and lower diameters of 70 and 100 mm, respectively. The flow time test was measured using a mini V-funnel with an opening of 32 × 32 mm. A UHPC sample of 1.15 l was cast in the funnel, and after 30 sec of rest the bottom outlet was opened allowing the mortar to flow.

The flow time was determined at the end of continuous flow. Air content of UHPC mixtures was determined by the pressure method in accordance with ASTM C 231.

Table 4-2 UHPC mixtures compositions

Code	reference	G50	G50SF5	FA60	FA60SF5
Cement (kg/m^3)	712	593	548	486	663
Silica fume (kg/m^3)	231	-	42	-	42
Fly ash (kg/m^3)	-	-	-	556	367
GGBS (kg/m^3)	-	546	535	-	-
Sand A (kg/m^3)	-	698	694	715	703
Sand B (kg/m^3)	-	295	304	304	308
Fine sand (kg/m^3)	211	-	-	-	-
Quartz sand (kg/m^3)	1020	-	-	-	-
HRWRA (%*)	0.9	1.09	1.42	0.53	0.98
Mixing water (L/m^3)	164	167	182	171	188
Fiber (%)	2	2	2	2	2

*By active mass of HRWRA compared to binder mass

4.3.2. Rheological Properties. A co-axial viscometer ConTech 5 was employed to evaluate the rheological properties of the UHPC. The outer and the inner radius are 145 and 100 mm, respectively, and the height of the vane that is submerged in mixture is 160 mm. The torque was measured at the fixed inner cylinder, while the outer cylinder was rotating. The measurement started at 20 min of age and was repeated at 40 and 60 min of elapsed time. The UHPC samples were subjected to pre-shear at a rotational velocity of 0.50 rps during 25 s, followed by a stepwise reduction in rotational velocity till zero. The yield stress and plastic viscosity of the UHPC mixtures were calculated using the Bingham model (Tattersall and Banfill, 1983).

4.3.3. Mechanical Properties. Compressive strength was determined on cubes measuring 50 mm, in accordance with ASTM C109. The splitting tensile strength and the modulus of elasticity were evaluated using 100 × 200 mm cylinders, in accordance with ASTM C 496 and C 469, respectively. Three replicates were used for each test.

4.3.4. Shrinkage. Autogenous shrinkage was monitored in accordance with ASTM C 1698. For each mixture, the final setting time was determined in accordance with ASTM C 403, which was used as the starting time for autogenous shrinkage.

Drying shrinkage was evaluated using 25 × 25 × 285 mm prismatic bars, in accordance with ASTM C 596. After demolding, the specimens were immersed in water for 7 d before exposing them to air-drying in controlled environment with the desired temperature. Three specimens were used for shrinkage test.

4.4. RESULTS AND DISCUSSION

4.4.1. Fresh Properties. Figure 4-1 presents the HRWRA demand to obtain a mini-slump flow of 270 ± 10 mm of UHPC at different temperatures. The HRWRA demand varied between 0.46% and 1.58% (expressed as percent of active solid content of HRWRA compared to binder mass). The HRWRA demand increased in all investigated UHPC mixtures with the increase in temperature from 10 to 30 °C. The FA60 mixture with 0.46% at 10 °C and the G50SF5 mixture with 1.58% at 30 °C exhibited the lowest and highest HRWRA dosages, respectively. UHPC made with FA required less HRWRA compared to that made with GGBS and the reference mixture where the FA60 mixture had the lowest HRWRA demand with 0.46%, 0.53% and 0.77% HRWRA at 10, 23, and 30 °C, respectively. On the other hand, UHPC made with GGBS necessitated higher dosages compared to other UHPC mixtures. For example, the G50SF5 mixture required the highest HRWRA dosages of 1.33%, 1.42%, and 1.58% at 10, 23, and 30 °C, respectively. The reference mixture showed the highest variation rates of HRWRA demand when temperature increased from 10 to 23 °C and from 23 to 30 °C requiring 0.16% and 0.37% more HRWRA, respectively.

The fresh properties including mini slump flow and mini V-funnel flow time of the five investigated UHPC mixtures are summarized in Table 4-3 and are discussed below.

Mini slump flow: the initial mini-slump flow values of all UHPC mixtures were targeted at 270 ± 10 mm by adjusting the HRWRA dosage. This was necessary to secure self-consolidating characteristic of the UHPC mixtures (Meng et al., 2017).

Mini V-funnel flow time: as shown in Table 4-3, the mini V-funnel flow time decreased with the increase in temperature varying from 12 to 63 sec. The flow time accelerated as the temperature increased from 10 to 23 °C and 23 to 30 °C by up to 26

and 23 sec, respectively. The FA60 mixture with 12 sec at 30 °C and the G50SF5 mixture with 63 sec at 30 °C exhibited the lowest and highest mini V-funnel flow time.

Air content: results indicated that air content decreased with the increase in temperature varying from 6.2% to 3.2%. The G50SF5 and FA60 mixtures exhibited the highest and lowest values of air volume with 6.2% and 3.2% at 10 and 30 ºC, respectively. The FA60 mixture had the lowest air content values of 5%, 3.5%, and 3.2% at corresponding temperatures of 10, 23, and 30 ºC, respectively.

Setting time:

Figure 4-2 illustrates the initial and final setting times of UHPC mixtures at different temperatures ranging from 1.8 to 11 hr and 5 to 17 hr, respectively. Increasing the temperature from 10 to 30 ºC accelerated the initial and final setting times by up to 4.5 and 5 hr, respectively. The shortest and longest values of final setting time corresponded to the G50SF5 and FA40SF5 mixtures with 5 hr at 30 ºC and 17 hr at 10 ºC, respectively.

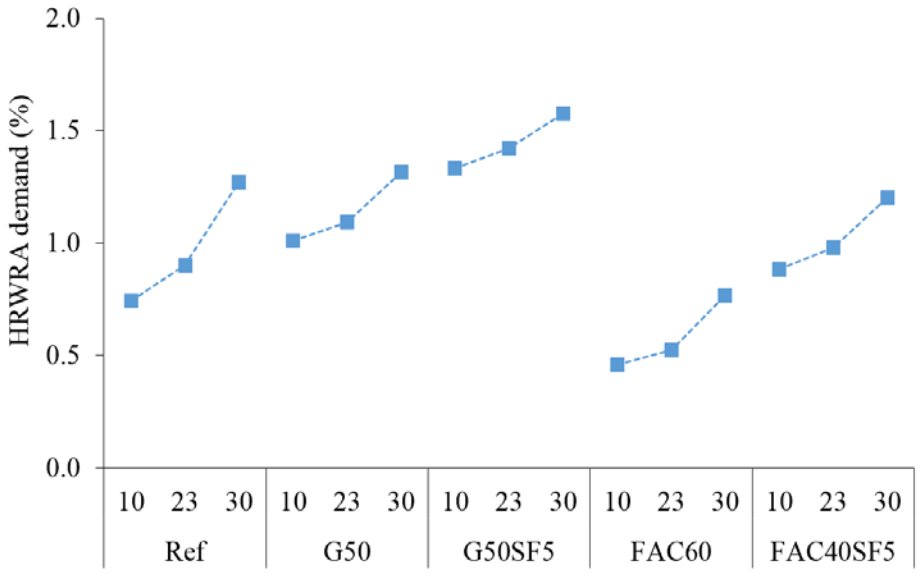

Figure 4-1 HRWR demand for UHPC mixtures at different temperatures

Figure 4-3 and Figure 4-4 illustrate the variations in yield stress and plastic viscosity with three measurement times of 20, 40, and 60 min for the UHPC mixtures at 10, 23, and 30 ºC, respectively, and are discussed below.

Table 4-3 Fresh properties of four optimized UHPC mixtures at different temperatures

Code	Target temperature (°C)	Measured temperature (°C)	Air content (%)	Mini-slump value (mm)	Mini V-funnel (sec)
reference	10	11	6	260	23
	23	24	4.2	260	16
	30	29	3.8	270	13
G50	10	9	5.5	280	41
	23	24	5.6	270	35
	30	29	3.8	280	20
G50SF5	10	11	6.2	260	63
	23	23	5.0	270	37
	30	29	4.2	275	14
FA60	10	9	5.0	260	46
	23	21	3.5	270	30
	30	29	3.2	280	12
FA40SF5	10	9	5.5	260	52
	23	22	4.5	280	39
	30	30	4.3	260	16

Yield Stress: yield stress increased by up to 55% with increasing the temperature from 10 to 30 ºC ranging from 19 to 53 Pa. UHPC made with GGBS exhibited lower yield stress for all three measurement times compared to other mixtures. The G50 mixture had the lowest yield stress values of 19, 21, and 23 Pa for the first (20 min) measurement time at 10, 23, and 30 ºC, respectively. On the other hand, the reference mixture exhibited the highest values of 35, 37, and 41 Pa for the same condition, respectively. As shown, yield stress increased over the elapsed time at all temperatures. For example, the FA40SF5 mixture had yield stress values of 36, 41, 45 Pa for 20, 40, and 60 min elapsed times, respectively, at 30 ºC. UHPC made with GGBS exhibited the lowest variations in the increase rate of yield stress with elapsed time. For example, the G50SF5 mixture had 2 and 3 Pa further increase in yield stress when elapsed time increased from 20 to 40 min and 40 to 60 min, respectively, at 10 ºC. However, these values were 9 and 6 Pa in the case of the FA60 mixture for the same condition.

Plastic Viscosity: plastic viscosity values decreased by up to 45% with the increase in temperature from 10 to 30 ºC for all investigated UHPC mixtures varying

from 15 to 60 Pa.s. UHPC made with GGBS exhibited the higher values of viscosity compared to the reference mixture and UHPC made with FA. For example, the G50SF5 mixture with viscosity values of 60, 48, and 32 Pa.s had the highest values for the first measurement time (20 min) at 10, 23, and 30 ºC, respectively. On the other hand, the FA60 mixture with 24 Pa.s and the reference mixture with 19 and 15 Pa.s showed the lowest viscosity values at 20 min of 10, 23, and 30 ºC, respectively. As shown, plastic viscosity increased over the elapsed time regardless of temperature. For example, the FA60 mixture showed viscosity values of 24, 34, and 42 Pa.s for the first (20 min), second (40 min), and third (60 min) of elapsed time.

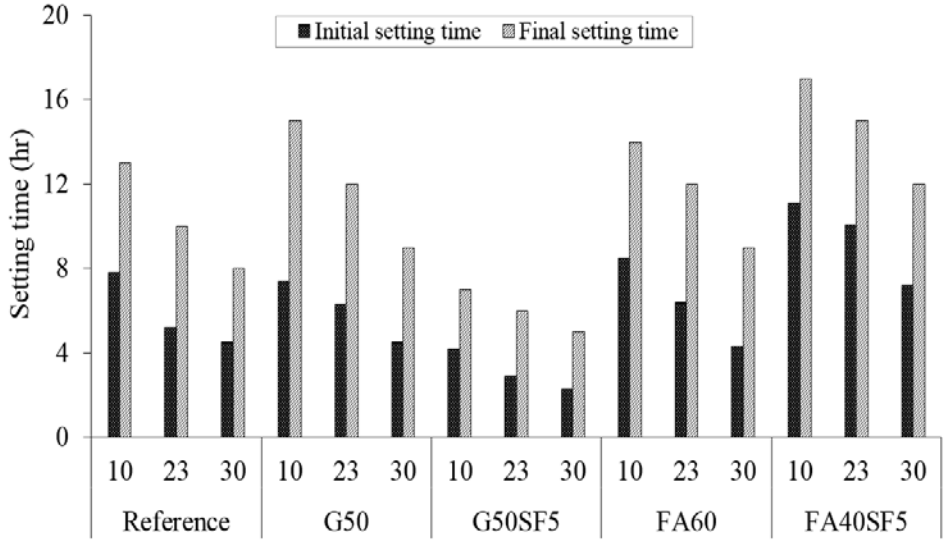

Figure 4-2 Results of setting time

4.4.2. Hardened Properties. Figure 4-5 illustrates the 28-d compressive strength results of the investigated UHPC mixtures at different temperatures. Compressive strength enhanced with the increase in age and temperature varying from 68 to 142 MPa. The lowest and highest values of 28-d compressive strengths belonged to the reference mixture at 10 and 30 ºC with 68 and 142 MPa, respectively. Increasing temperature from 10 to 30 ºC improved the 28-d compressive strength by 65%, 70%, 43%, and 42% for the G50, G50SF5, FA60, and FA40SF5 mixtures, respectively. This is in agreement with the findings of (Soliman and Nehdi, 2011) that concluded higher curing temperature resulted

in higher compressive strength. Lower compressive strength of the reference mixture at 10 ºC can be attributed to higher air content with was 1.8% and 2.2% higher than that of at 23 ºC and 30 ºC. The agglomeration of SF particles can be other possible reason that can reduce its effectiveness (Soliman and Nehdi, 2011). It is reported that the pozzolanic activity of agglomerated SF can be low and the size of such agglomerates can be larger than cement particles leading to higher porosity and limiting its fine particle filler effect (Soliman and Nehdi, 2011).

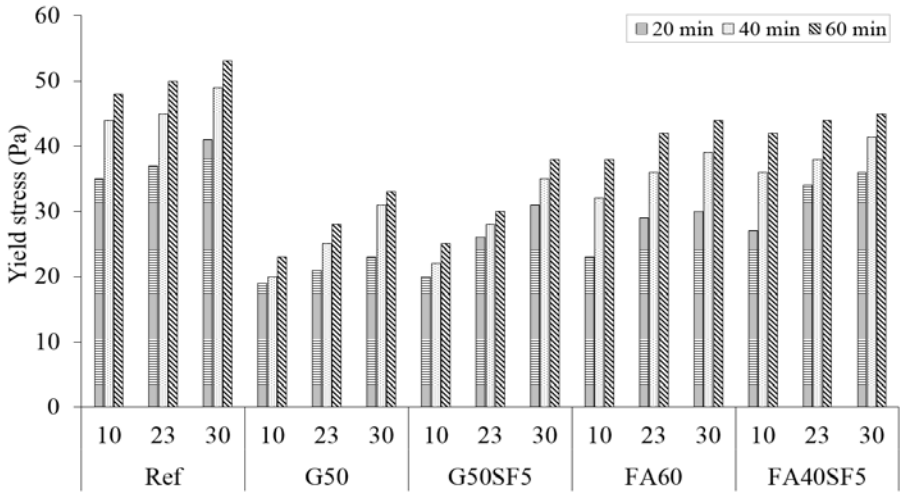

Figure 4-3 Yield Stress results at various temperature

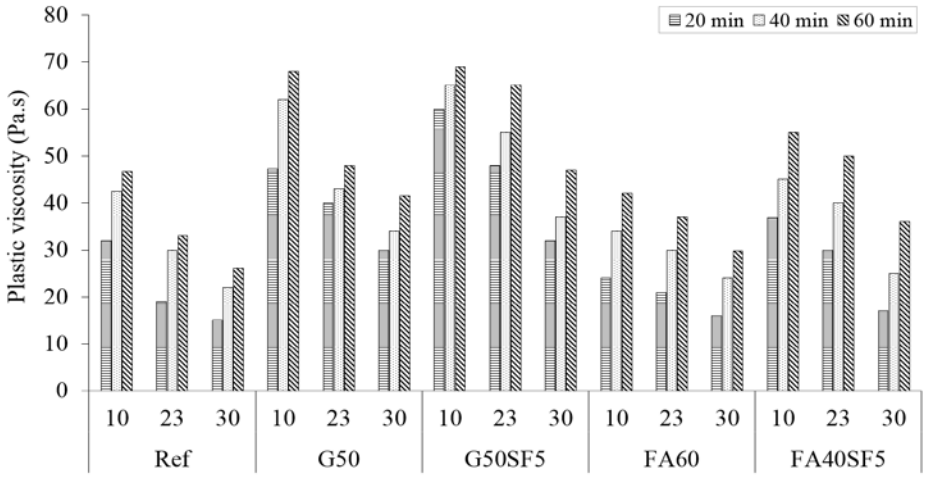

Figure 4-4 Plastic Viscosity results at various temperature

Splitting tensile strength: The 28-d splitting tensile strength results of the investigated UHPC mixtures at different temperatures are presented in Figure 4-6. Results indicated that the tensile strength enhanced with the increase in temperature varying between 8 and 16.5 MPa. These lowest and highest values were belonged to the reference mixture at 10 ºC and the G50SF5 mixture at 30 ºC, respectively.

Elastic modulus: Figure 4-7 compares the 28-d MOE results of UHPC mixtures at different temperatures. The MOE values enhanced with the increase in temperature for all investigated UHPC mixtures ranging from 41 to 56 GPa. The G50 and reference mixtures exhibited the lowest and highest values of 41 GPa at 10 ºC and 56 GPa at 30 ºC, respectively. The MOE values of UHPC made with GGBS or FA showed by up to 3 and 7 GPa lower values than that of the reference mixture at ambient temperature (23 ºC).

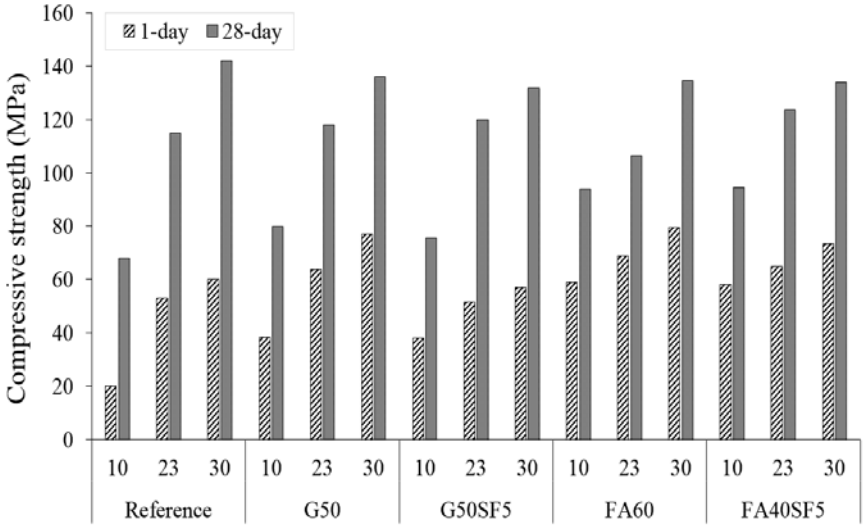

Figure 4-5 Compressive strength results for 28 days tests

Flexural Strength: Table 4-4 presents the test results of the 28-d flexural properties of the investigated UHPC mixtures at different temperatures. The flexural properties enhanced with the increase in temperature. The G50 mixture exhibited the lowest flexural strength with 13 MPa at 10 ºC. However, the flexural strengths at 23 and 30 ºC were close and varied between 21 and 22 MPa. Results indicates that increasing temperature from 10 to 23 ºC had greater impact on flexural properties than that from 23 to 30 ºC. For example, the flexural strength improvements were 3, 8, 6, 5, and 3 MPa for

the reference, G50, G50SF5, FA60, and FA40SF5 mixtures, respectively, with increasing the temperature from 10 to 23 ºC. However, these enhancements were 1 to 2 MPa for the increase in temperature from 23 to 30 ºC. The same trend was observed for first cracking load and toughness values. The G50 mixture exhibited the highest first cracking load, peak load, and toughness (T150) with 25, 35, and 54 kN-mm, respectively, at 30 ºC.

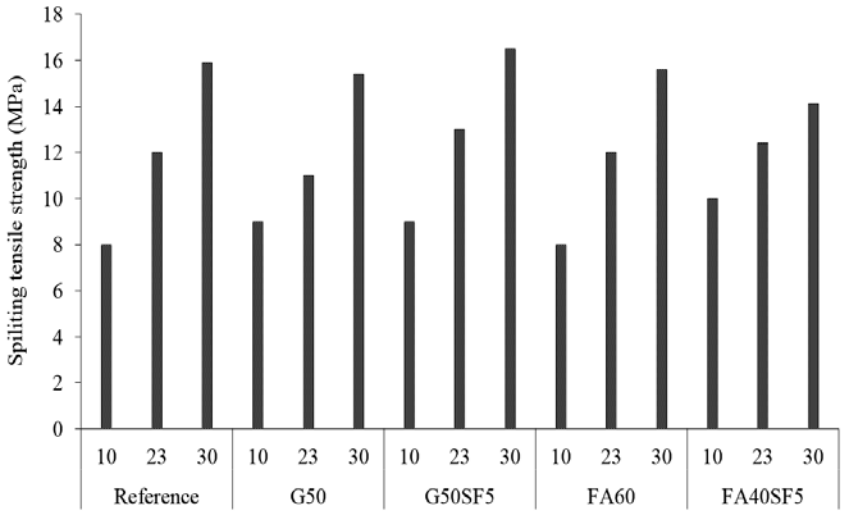

Figure 4-6 Splitting tensile strength results for 28 days tests

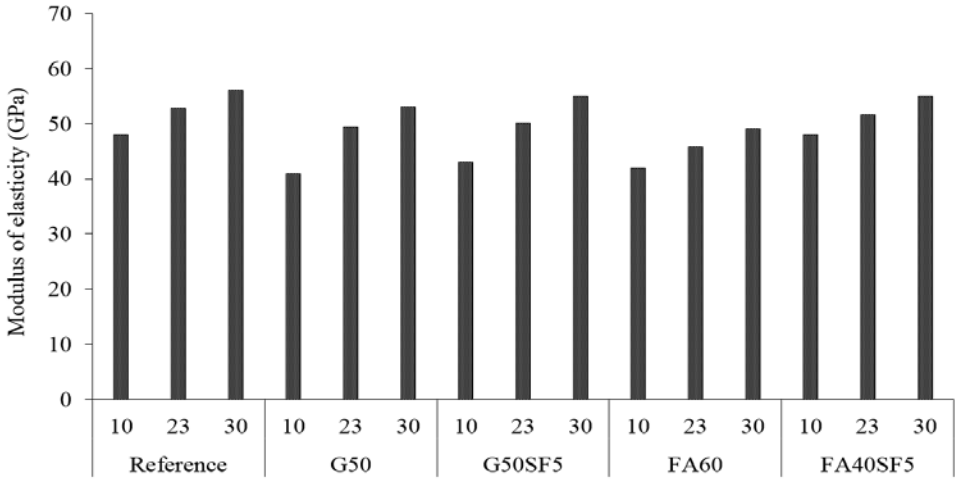

Figure 4-7 Modulus of elasticity results for 28 days tests

Table 4-4 Results of flexural behavior at different temperatures

Code	Target temperature (°C)	First cracking load (kN)	Peak load (kN)	Flexural strength (MPa)	T150 (kN-mm)
reference	10	19	19	17	38
	23	22	21	20	40
	30	24	28	21	52
G50	10	15	20	13	35
	23	24	33	21	51
	30	25	35	22	54
G50SF5	10	17	20	14	35
	23	21	29	20	49
	30	25	31	21	52
FA60	10	16	22	15	36
	23	20	29	20	49
	30	22	32	22	54
FA40SF5	10	19	28	19	32
	23	21	31	21	50
	30	22	33	22	53

4.4.3. Shrinkage. Figure 4-8 presents the autogenous shrinkage results for UHPC mixtures at different temperatures. Results indicated that the higher curing temperature resulted in greater shrinkage with faster growth rate, particularly at early ages which were in agreement with the reported results (Soliman and Nehdi, 2011). For example, increasing temperature from 10 ºC to 30 ºC led to increase in autogenous shrinkage by up to 60% and 45% for GGBSs and FACs, respectively. This increase was 35% for the REF mixture. This can be attributed to higher chemical shrinkage due to the acceleration of hydration. As seen, the mixtures at 30 ºC were the first mixtures to set and started to shrink, followed by 23 ºC and 10 ºC which can be due to the development of a strong solid skeleton at high temperatures (Soliman and Nehdi, 2011). Increasing the temperature from 10 ºC to 30 ºC accelerated the shrinkage developments with high rate during the first 24 h, which can be due to the expedition of cement hydration, leading to higher chemical shrinkage (Soliman and Nehdi, 2011).

The REF mixture with 25 % SF achieved the highest shrinkage development, having ultimate values of 650 µm/m, 730 µm/m and 870 µm/m at 10 ºC, 23 ºC and 30 ºC, respectively. Incorporation of SF significantly reduces the coarse pore while there is no

effect on total pore space resulted in increasing fine pores (Russell and Graybeal, 2013; Yu et al., 2015). This causes an increase in negative pressure of capillary tube which generally leads to autogenous shrinkage increase. Moreover, silica fume consumes $Ca(OH)_2$ in order to produce C-S-H gel which creates denser structure (Yu et al., 2015; Neville, 1999). This accelerates the hydration of cement which improves the self-drying degree within the concrete, resulting in increasing the autogenous shrinkage of concrete (Schober and Flatt, 2006; Göller et al., 2009).

Considerable reduction was observed with the replacement of SF with high volume GGBS or FAC. The FAC60 mixture decreased autogenous shrinkage significantly compared to the REF mixture in corresponding temperatures. This reductions were up to 25% and 20% at 10 ºC and 30 ºC. Results showed that increase in fly ash replacement level from 40% to 60% with addition of 5% SF decreased the shrinkage development up to 10%. It has been reported that the autogenous shrinkage of concrete decreases with increase in fly ash amount (Jensen and Hansen, 1999). This can be attributed to the fact that fly ash is not participating in the hydration process with pozzolanic reactions at very early ages and acts as a filler. On the other hand, since it replaces some portion of cement, early-age efficient water cement ratio increases due to lower content of cement which also decreases the heat of hydration. Therefore, it leads to a decrease in early-age self-drying results in reduction of autogenous shrinkage (Loukili et al., 1999).

The addition of silica fume in GGBS mixture increased the autogenous shrinkage up to 25% at 30 ºC. The G50 mixture had the lowest shrinkage development among all mixtures at corresponding temperatures with ultimate shrinkage values of 350 µm/m, 420 µm/m and -560 µm/m at 10 ºC, 23 ºC and 30 ºC. The literature shows that the influence of GGBS on the autogenous shrinkage is controversial. However, it has been frequently reported that the fineness and replacement level are the main factors of GGBS impressed its influence on autogenous shrinkage (Ortiz et al., 2005). The autogenous shrinkage of concrete reduces with an increase of GGBS amount given the same fineness as cement. However, an increase in autogenous shrinkage is observed with increasing the level of replacement when the fineness of GGBS exceeds 4000 cm^2/g (Ortiz et al., 2005).

The results of drying shrinkage of UHPC mixtures subjected to different mixing and curing temperatures are displayed in Figure 4- 9. Results showed that drying shrinkage increased with an increase in temperature by up to 30%, 60%, and 50% for the REF, GGBSs, and FACs mixtures, respectively, as temperature went up from 10 ºC to 30 ºC. High temperature changes the development trend of the concrete shrinkage deformation which demonstrates that shrinkage develops so fast at early age. In the case of 30 ºC, during first 8-10 days the development rate reached to a smooth trend and in later ages, the shrinkage values were higher than those of in 10 ºC and 23 ºC. Comparing the results at low and high temperature showed that strain variations were stabilized at 30 ºC sooner than 10 ºC. It could be concluded that mixing and curing temperatures impressed the hydration reaction of cement, which affected the structure of concrete. Therefore, temperature variations impacted the drying shrinkage of concrete. This can be due to the fact that at high temperature, cement hydration reactions are faster than low temperature, resulting in reduction of the internal relative humidity due to increase in evaporation rate (Jianyong and Yan, 2001). The REF mixture had the highest shrinkage development with -756 µm/m, -856 µm/m and -978 µm/m corresponding to 10 ºC, 23 ºC and 30 ºC. SF particles have high specific surface area and very high activity which can expedite the hydration process, resulting in reduction in internal relative humidity at early and later ages. This can increase the autogenous shrinkage of concrete continuously. In particular, at high temperature, high drying shrinkage of concrete incorporating silica fume is predictable (Lura et al., 2001).

Results showed that the replacement of SF with GGBS or FAC considerably reduced drying shrinkage. For example, the G50 and G50SF5 mixtures with ultimate shrinkage of 642 µm/m and -530 µm/m, reduced the shrinkages up to 25% and 40% compared to the REF mixture, respectively, at 28 days under environmental temperature of 23 ºC. At the same condition, the FAC60 and FAC40SF5 mixtures ended up with 35% and 30% reduction in shrinkage. From the results, it can be concluded that increasing FAC replacement level from 40% to 60% decreased the shrinkage up to 10%. Fly ash can delay the cement hydration at early age resulted in reduction in the early internal drying speed of concrete. This can lead to reduced early autogenous shrinkage. On the other hand, pastes incorporating fly ash have a lower stiffness at earlier ages leading to increase

possibility of shrinkage. Additionally, later continues hydration of fly ash induce increment in internal self-desiccation leading to refinement of pore structure, which results in a higher drying shrinkage. In case of GGBS, low activity at early age delayed the hydration reaction of cement meaning limited water were consumed and in the later ages the hard slag particles constrained the shrinkage of cement (Jianyong and Yan, 2001; Lura et al., 2001).

4.5. EVALUATION OF ROBUSTNESS OF UHPC AT DIFFERENT TEMPERATURES

Total 16 properties of UHPC were considered for robustness evaluation including eight fresh characteristics, five mechanical properties, and three shrinkage deformations. The COVs of the responses resulted for the three temperatures were determined to calculate the relative spread of each response for each property, as shown in Table 4-5. The UHPC mixtures were ranked in descending order based on the calculated COV values. For each property the lowest COV indicated the best robustness yielding 14 different rankings for the investigated UHPC mixtures. Table 4-6 summarizes the properties with their calculated COVs associated with determined rankings for each mixture. The sum of the final rankings is normalized using Eq. 4.1.

$$\text{Normalized sum of ranking (\%)} = \frac{(SR_{max} - SR_i)}{(SR_{max} - SR_{min})} \tag{4.1}$$

where *SRi* represents the sum of the ranking of the element *i* and *SR* denotes the average of *SRi*. As indicted in Table 4-7, the robustness of the investigated UHPC mixtures is classified into three categories. The FA60 and FA40SF5 mixtures belong to category I with a normalized sum of ranking >85% as the highest level of robustness. UHPC made with GGBS exhibited medium level of robustness classified under Category II with a normalized sum of ranking between 35% and 85%. Category III, with a normalized sum of ranking ≤35% which can be considered as the lowest level of robustness, includes the reference mixture (Naji et al., 2011).

4.6. SUMMARY

The HRWRA demand increased regardless of the investigated UHPC mixture with the increase in temperature. UHPC made with FA required less HRWRA compared

to that with GGBS and the reference mixture (25% SF). The FA60 mixture with 0.46% HRWRA at 10°C and G50SF5 mixture with 1.58% HRWRA at 30°C exhibited the lowest and highest HRWRA demands, respectively.

Mini V-funnel flow time decreased by up to 45%, with the increase in temperature (10 to 30 ºC).

Increasing the temperature accelerated the initial and final setting times by up to 4.5 and 5 hr, respectively.

Yield stress increased by up to 55% and plastic viscosity decreased by up to 45% with increasing the temperature from 10 to 30 ºC. UHPC made with GGBS exhibited the highest values of viscosity and the lowest yield stresses compared to the reference mixture and UHPC made with FA.

Temperature variation can significantly affect the development of mechanical properties of UHPC. Results indicated that mechanical properties of different UHPC improved with the increase in temperature. Increasing temperature from 10 to 30 ºC improved the 28-d compressive strength of the G50, G50SF5, FA60, and FA40SF5 mixtures by 65%, 70%, 45%, and 40%, respectively.

The flexural toughness (T150) enhanced by up to 65% with the increase in temperature where all mixtures had their minimum and maximum toughness at 10 and 30 ºC, respectively.

Increasing the temperature from 10 to 30 ºC led to increase in autogenous and drying shrinkage by up to 60% and 70%. UHPC made with GGBS or FA exhibited a reduction in autogenous and drying shrinkage by up to 300 and 350 μm/m, respectively, compared to the reference mixture at 56 d.

UHPC made with FAC and GGBS were more robust than the reference mixture made with 25% SF. In general, the FA60 and FA40SF5 mixtures resulted in greater robustness than other UHPC mixtures.

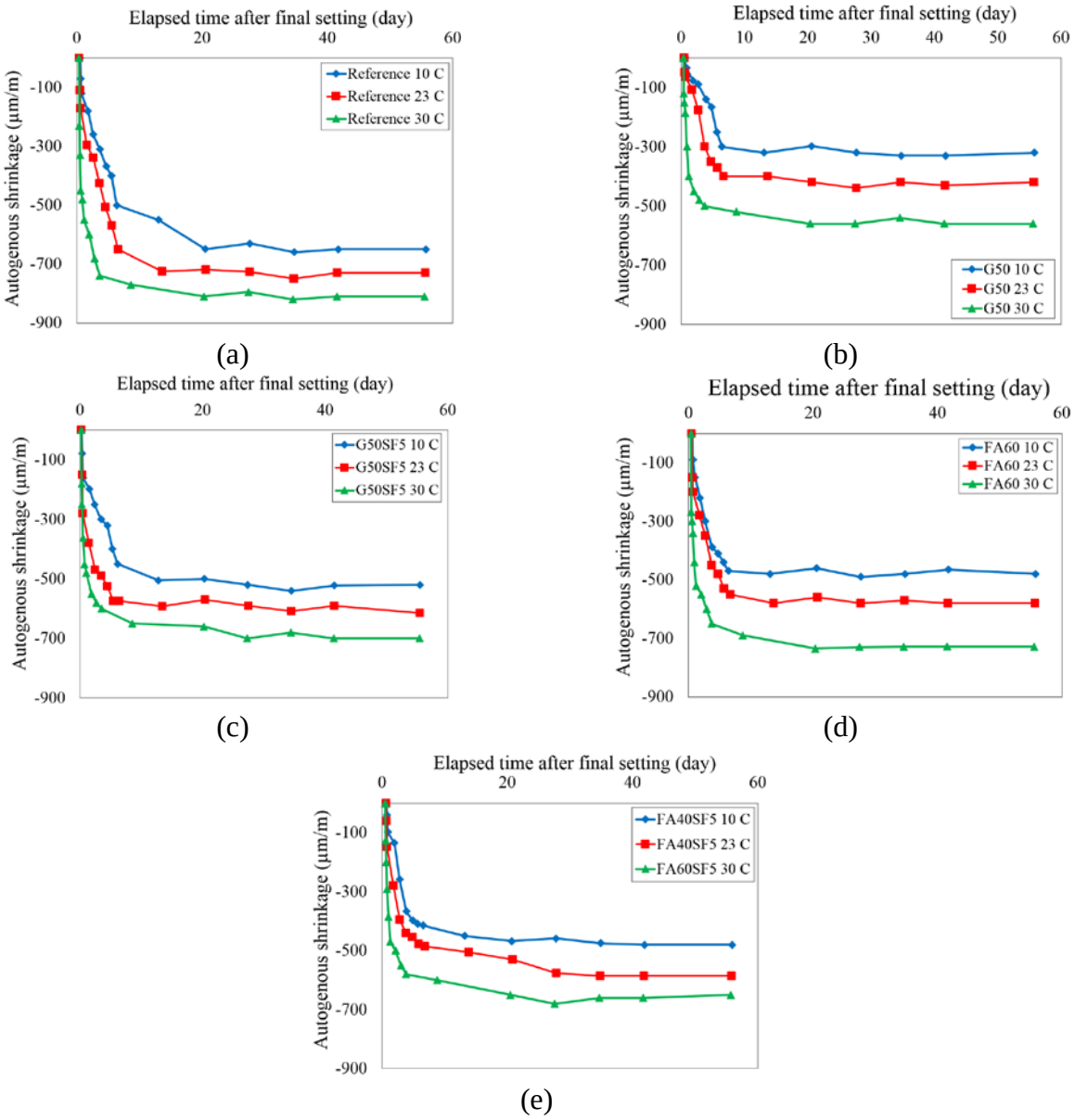

Figure 4-8 Autogenous shrinkage results at different temperatures

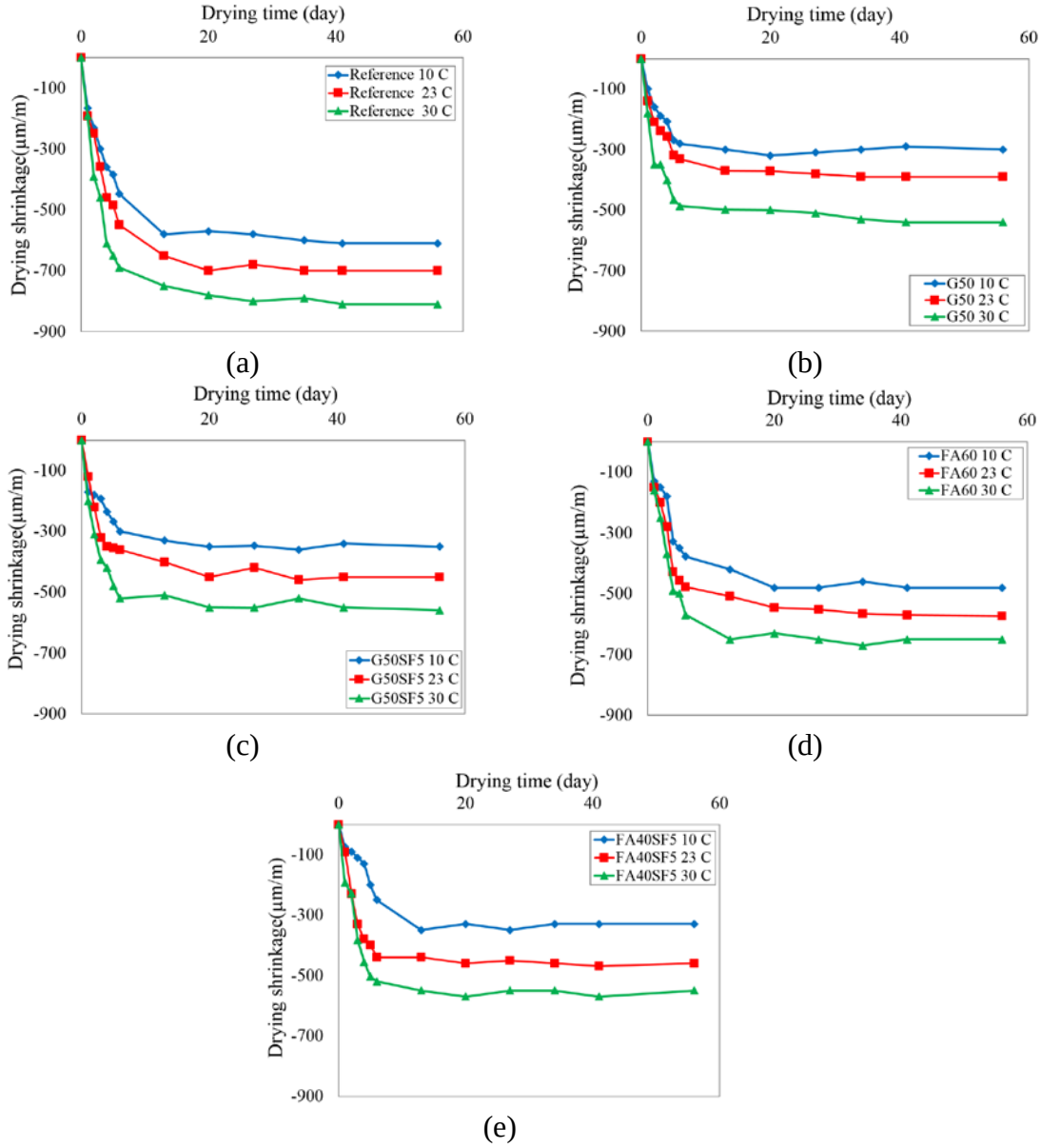

Figure 4- 9 Drying shrinkage results at different temperatures

Table 4-5 Key properties and robustness ranking of UHPC mixtures prepared at different temperatures

		Reference	G50	G50SF5	FA60	FA40SF5
HRWRA demand (%)	T: 10; 23; 30	0.74; 0.90; 1.3	1.01; 1.09; 1.32	1.33; 1.42; 1.58	0.46; 0.53; 0.77	0.89; 0.98; 1.20
	COV, %	28	13.9	8.5	27.8	15.9
	Rank	5	2	1	4	3
V-funnel flow time (sec)	T: 10; 23; 30	23; 16; 13	41; 35; 20	63; 37; 14	46; 30; 12	52; 39; 16
	COV, %	29.6	33.8	64.5	58	51.1
	Rank	1	2	5	4	3
Air content (%)	T: 10; 23; 30	6; 4.2; 3.8	5.9; 5.6; 3.8	6.2; 5; 4.2	5; 3.5; 3.2	5.5; 4.5; 4.1
	COV, %	25.1	22.3	19.6	24.7	15.3
	Rank	5	3	2	4	1
Yield stress (Pa) at 20 min	T: 10; 23; 30	35; 37; 41	19; 21; 23	20; 26; 31	23; 29; 30	27; 34; 36
	COV, %	8.1	9.5	21.5	13.9	14.6
	Rank	1	2	5	3	4
Yield stress (Pa) at 60 min	T: 10; 23; 30	48; 50; 53	23; 28; 33	25; 30; 38	38; 42; 44	42; 44; 45
	COV, %	5	17.9	21.2	7.4	3.5
	Rank	2	4	5	3	1
Plastic viscosity (Pa.s) at 20 min	T: 10; 23; 30	32; 19; 15	47; 40; 30	60; 48; 32	24; 21; 16	37; 30; 17
	COV, %	40.2	22.3	30.1	19.9	36
	Rank	5	2	3	1	4
Plastic viscosity (Pa.s) at 60 min	T: 10; 23; 30	47; 33; 26	68; 48; 41	69; 65; 47	42; 37; 30	55; 50; 36
	COV, %	30	26.3	19.4	16.8	21
	Rank	5	4	2	1	3
Initial setting time (hr)	T: 10; 23; 30	7.5; 5; 4.5	7; 6; 4	3; 2; 1.8	8.5; 6; 4	11; 10; 7
	COV, %	28.5	27	28	36.6	22.3
	Rank	4	2	3	5	1
1-d compressive strength (MPa)	T: 10; 23; 30	20; 53; 60	39; 64; 78	39; 51; 57	59; 69; 80	58; 65; 74
	COV, %	56.6	33	20	14.9	11.7
	Rank	5	4	3	2	1
28-d compressive strength (MPa)	T: 10; 23; 30	68; 115; 142	80; 118; 136	76; 120; 132	94; 107; 135	95; 124; 134
	COV, %	47	26.2	27.7	18.7	17.5
	Rank	5	3	4	2	1
28-d tensile strength (MPa)	T: 10; 23; 30	8; 12; 16	9; 10; 15	7; 14; 16	8; 12; 16	10; 12; 14
	COV, %	44.6	38.5	36.8	35.9	10.8
	Rank	5	4	3	2	1
28-d MOE (GPa)	T: 10; 23; 30	48; 52.7; 56	41; 49.5; 53	43; 50.1; 55	42; 45.8; 49	48; 51.6; 55
	COV, %	7.8	12.9	12.2	7.6	6.8
	Rank	3	5	4	2	1
28-d flexural Strength (MPa)	T: 10; 23; 30	17; 20; 21	13; 21; 22	14; 20; 21	15; 20; 22	19; 21; 22
	COV, %	19.3	18.7	18.3	19	20.7
	Rank	4	2	1	3	5
3-d autogenous shrinkage (μm/m)	T: 10; 23; 30	230; 340; 500	89; 175; 200	250; 470; 450	300; 450; 450	260; 395; 385
	COV, %	38.1	37.6	31.2	21.7	22
	Rank	5	4	3	1	2
56-d autogenous shrinkage (μm/m)	T: 10; 23; 30	580; 700; 850	350; 450; 560	520; 614; 700	510; 570; 730	480; 585; 690
	COV, %	19.1	23.2	14.7	18.8	17.9
	Rank	4	5	1	3	2
56-d drying shrinkage (μm/m)	T: 10; 23; 30	700; 920; 990	580; 640; 800	450; 530; 720	480; 575; 650	479; 610; 725
	COV, %	17.4	16.9	24.5	125	20.3
	Rank	3	2	5	1	4

Table 4-6 Sum of ranking of UHPC mixtures according to COV of all properties

	HRWRA demand (%)	V-funnel flow time (sec)	Air content (%)	Initial setting time (hr)	Final setting time (hr)	Yield stress (Pa) at 20 min	Yield stress (Pa) at 60 min	Plastic viscosity (Pa.s) at 20 min	Plastic viscosity (Pa.s) at 60 min	1-d compressive strength (MPa)	28-d compressive strength (MPa)	28-d tensile strength (MPa)	28-d MOE (GPa)	28-d flexural Strength (MPa)	3-d autogenous shrinkage (μm/m)	56-d autogenous shrinkage (μm/m)	56-d drying shrinkage (μm/m)	Sum of ranking (SR)	Ranking based on SR (16 properties)
Refer	5	1	5	4	4	1	2	5	5	5	5	5	3	4	5	4	3	68	5
G50	2	2	3	2	5	2	4	2	4	4	3	4	5	2	4	5	2	56	4
G50SF5	1	5	2	3	1	5	5	3	2	3	4	3	4	1	3	1	5	54	3
FA60	4	4	4	5	3	3	3	1	1	2	2	2	2	3	1	3	1	48	2
FA40SF5	3	3	1	1	2	4	1	4	3	1	1	1	1	5	2	2	4	44	1

Table 4-7 Robustness evaluation of UHPC

	Sum of ranking given by 16 selected properties	Normalized sum of ranking, %	Category	Robustness
Reference	68	0	III (≤35%)	Low
G50	56	50	II (35% to 85%)	Medium
G50SF5	54	58	II (35% to 85%)	
FA60	48	83	I (>85%)	High
FA40SF5	44	100	I (>85%)	

5. COUPLED EFFECT OF SATURATED LIGHTWEIGHT SAND AND SHRINKAGE-MITIGATING ADMIXTURES IN REDUCING SHRINKAGE OF UHPC

This chapter evaluates the efficiency of various shrinkage mitigation approaches in reducing autogenous and drying shrinkage of ultra high performance concrete (UHPC). This included the use of various contents of CaO-based and MgO-based expansive agents, shrinkage-reducing admixture, and pre-saturated lightweight sand. Workability, compressive strength development, autogenous and drying shrinkage were evaluated for UHPC mixtures subjected to moist curing periods of 1, 3, and 7 d.

The superior strength and unique strain-hardening characteristics of UHPC make it an attractive option for some civil engineering construction and repair applications (Ahlborn et al., 2008; Russel and Graybeal, 2013). Given its very low w/b and high volume of cementitious materials, UHPC can exhibit high degree of self-desiccation that can cause significant autogenous shrinkage, that may lead to cracking, particularly in the presence of restraint (Aïtcin, 2011; Cusson and Hoogeveen, 2007; Tazawa, 1998). This can limit some of the potential use of UHPC where shrinkage can play a major role in the performance of the mixture. This includes the use of UHPC for thin bonded overlays for concrete pavements. Bernardi et al. (2016) reported successful use of UHPC in thin overlay of 45 mm in thickness reinforced with UHPC made with 3.25% steel fibers for bridge deck rehabilitation in Switzerland in 2014. The overlay repair included reinforcing rebar and UHPC to strengthen the existing deck that was damaged from alkali silica reactivity. Similarly, a successful use of UHPC measuring 38 mm in thickness applied on a 30-m long bridge was also reported in Iowa, USA. The control of shrinkage characteristics of such novel application is critical for the service life of the repair. I addition to water loss due to drying, chemical shrinkage, and self-desiccation, the UHPC overlay is highly effected by restrained shrinkage at the interface. This can cause tensile stresses in the overlay that can lead to cracking, compressive and bending stresses in the substrate that can lead to debonding, and shear stresses across the interface at the free ends (joints) that can cause curling and cracking (Orta and Bartlett, 2014). Lowering these stresses is critical especially in thin overlay elements in order to enhance the efficiency and durability of the repair.

Various methods have been investigated to mitigate the shrinkage of high performance concrete and UHPC, including the use of saturated lightweight sand (LWS), the incorporation of an expansive agent (EX) and/or a shrinkage reducing admixture (SRA) (Hwang et al., 2013; Barrett et al., 2012; Bentz and Peltz, 2008). SRA can reduce the potential for shrinkage-induced stresses that can lead to cracking. SRA is composed of non-ionic organic surfactant that can decrease the surface tension of the pore solution, thus resulting in lower capillary stress upon moisture loss (Rajabipour et al., 2008). The drop in capillary stress can reduce drying shrinkage as well as plastic and autogenous shrinkage at early age (Rajabipour et al., 2008; Liu et al., 2017). The incorporation of SRA can also decrease the amount of water evaporation, hence reducing residual stresses (Liu et al., 2017). The reduction of water evaporation as a result of use of SRA can preserve the higher internal relative humidity (Lura et al., 2007; Weiss et al., 2008; Wyrzykowski et al., 2015). In spite of the aforementioned advantages of SRA, there have been some reported side effects associated with SRA, including reduction in the rate of cement hydration, loss of entrained air, and delay in setting time and development of mechanical properties at early age (Weiss et al., 2008; Wyrzykowski et al., 2015).

Expansive agents (EX) are widely used alternatives that compensate for shrinkage of cementitious materials due to expansion produced upon hydration (Nagataki and Gomi, 1998). They are categorized as CaO-based (EXC), ettringite-based, or MgO-based (EXM), depending on the type of the main ingredients in use (Mo et al., 2014). The expansion of ettringite-based and CaO-based EXs occurs at an early age and is characterized by its rapid development and ability to stabilize before 28 d. The use of CaO-based EX can lead to fast hydration of CaO and the relatively high solubility of portlandite (Higuchi et al., 2014). The incorporation of CaO-based EX can enhance the interfacial zone especially at early hydration period for high performance concrete with w/b of 0.32 using an EX accounted for 12% of the total binder amount by mass (Higuchi et al., 2014). Additionally, an improvement in the pore structure of concrete was noted, which can reduce drying shrinkage (Sun et al., 2001). Unlike traditional EXs, the expansion property of MgO-based agent is affected by the calcination temperature and residence time (Qi et al., 2002). In addition to the chemical stability of Mg $(OH)_2$

hydration product, relatively little water is required for the hydration of MgO (Qi et al., 2002; Mo et al., 2010).

The use of steel fibers in cement-based materials made with an expansive agent can act as internal restraint. This can lead to a self-stressing, which can improve mechanical properties (Shuguang and Yue, 1999; He et al., 2011). He et al. (He et al., 2011) reported under expansion, steel fibers are tensioned, thus resulting in a compressive pre-stressing of the composite material in the range of 3 to 6 MPa.

The degree of expansion of CaO-based and MgO-based EXs is dependent on the availability of water in the pore solution. Given the very low w/b of UHPC, expansion can be limited. In the case of UHPC, Meng and Khayat (2017) showed that the use of LWS in UHPC made with 0.20 w/b and 4% of silica fume and 34% of Class C fly ash can significantly reduce the relative humidity and autogenous shrinkage. Mixtures made without any LWS and with 75% LWS had relative humidity values of approximately 83% and 87%, respectively, at the 7 d. The relative humidity values of the 48 hr were 87% and 100%. The autogenous shrinkage of UHPC mixtures made with 0, 60%, and 75% LWS were approximately 500, 275, and 175 μm/m, relatively, after 28 d. Due to their porous microstructures, lightweight aggregate can be saturated to accumulate water prior to mixing and used for internal curing. The stored water can then be gradually released into the system during cement hydration to compensate for moisture loss and reduce shrinkage caused by evaporation and reduce chemical shrinkage and self-desiccation (RILEM, 2007; ACI SP-256, 2008; ACI, 2010).

Given the critical effect of autogenous and drying shrinkage on the performance of thin overlays made with UHPC, a study is carried out to evaluate the benefits of using combined addition of SRA and EX in the presence of LWS in UHPC. The effect of initial moist curing of the UHPC on shrinkage and compressive strength is also of special interest.

5.1. EXPERIMENTAL PROGRAM

5.1.1. Materials. The cementitious materials used in this investigation included a Type III portland cement with a Blaine fineness of 385 m^2/kg. GGBS with a Blaine fineness of 590 m^2/kg was used. A CaO-based expansive agent (EXC) and an MgO-based

expansive agent (EXM) were used in powder form. The specific gravity and recommended content of former material are 3.14 and 3%-10%, by the mass of cementitious materials, respectively. These values for the EXM are 2.26 and 2%-7%, respectively. A propylene glycol ether-based SRA with specific gravity of 0.98 was used.

Two natural sands with nominal maximum sizes of 4.75 mm (sand A) and 2 mm (sand B) and a specific gravity of 2.6 were used. The sands were proportioned at 70:30 mass ratio, which was found to yield the highest packing density for the UHPC mixture (Meng et al., 2017). Pre-saturated LWS with nominal maximum size of 4.75 mm and specific gravity of 1.81 was used. The LWS has a 24-hr absorption rate of 17.5% by dry mass, and a desorption rate of 96.4% determined according to ASTM C1761. Based on this standard, the minimum required amount of LWS should be 237 kg/m^3 to compensate for chemical shrinkage, which corresponds to 35% of the total volume of sand for the proposed UHPC mixture.

A polycarboxylate-based HRWR with a solid content of 23% and specific gravity of 1.05 was employed. The HRWR was used to secure self-consolidating characteristic of the UHPC. It is important to note that water present in all liquid-based chemical admixtures was accounted for to maintain a fixed w/b for all mixtures. High strength straight steel fibers measuring 13 mm in length and 0.2 in diameter were incorporated. The aspect ratio and tensile strength of the selected fiber are 40 and 2160 MPa, respectively.

5.1.2. Mixture Proportioning. As indicated in Table 5-1, 12 UHPC mixtures were investigated. The mixtures had a fixed w/b of 0.20 and 2% fiber content, by volume. UHPC mixtures were proportioned with different dosage rates of EXC corresponding to 5%, 7.5%, and 10%, by mass of binder. The EXM dosage for UHPC was 5% and 7%, by mass of total cementitious materials. UHPC mixtures were also prepared with SRA dosage of 1.5% and 3%, by volume of water content.

Sand A was substituted by LWS at different volumetric replacement ratios of 25%, 40% and 60%. The HRWR demand was adjusted to secure an initial mini-slump value of 270 ± 10 mm, which is necessary to secure self-consolidating characteristic of the UHPC (Meng et al., 2017).

A 12-L Hobart mixer was used to prepare the UHPC that was mixed at room temperature (23 ± 2 °C). The mixing procedure was consisted of four steps: (1) dry cementitious materials and sand were added and mixed for 2 min at 1 rps; (2) 90 % of the mixing water with 90 % of the HRWR were introduced and the material was mixed for 3 min more at 2 rps; (3) the remainder of water and HRWR were added, and the material was mixed for 7 min at 2 rps; and finally (4) steel fibers were added gradually over 1 min, and then the material was mixed for 2 min at 10 rps.

Table 5-1 Composition of investigated mixtures

Mixtures	Cement	GGBS	Sand A	Sand B	LWS	EXC	EXM	SRA	Mixing water	HRWR	Fibers
	(kg/m^3)	(kg/m^3)	(kg/m^3)	(kg/m^3)	(kg/m^3)	(kg/m^3)	(kg/m^3)	(L/m^3)	(L/m^3)	(%)	(%)
G50	593	546	704	298	-	-	-	-	235	2.02	2
LWS60	593	546	103	298	405	-	-	-	237	1.14	2
EXC7.5	571	526	704	298	-	44	-	-	250	2.37	2
EXC7.5LWS25	571	526	454	298	169	44	-	-	230	1.23	2
EXC7.5LWS40	571	526	303	298	270	44	-	-	235	1.14	2
EXC7.5LWS60	571	526	103	298	405	44	-	-	238	1.05	2
EXC5LWS60	578	532	103	298	405	30	-	-	236	0.97	2
EXC10LWS60	563	519	103	298	405	59	-	-	240	1.05	2
EXM5LWS60	572	529	103	298	405	-	29	-	242	1.14	2
EXM7LWS60	563	522	103	298	405	-	40	-	252	1.40	2
SRA1.5LWS60	593	546	103	298	405	-	-	17	213	1.14	2
SRA3LWS60	593	546	103	298	405	-	-	34	206	1.14	2

5.1.3. Testing Program. The mini-slump flow and mini-V-funnel flow time tests were used to evaluate the flowability of the UHPC at 10 and 70 min of age. The latter test can also be considered as an indication of plastic viscosity (Erdem et al., 2009). Between 10 and 70 min, the UHPC mixture was left in the mixer covered to avoid any water evaporation. The UHPC was then remixed for 2 min before testing at 70 min.

For the mini-slump test, a truncated cone measuring 60 mm in height with upper and lower diameter of 70 and 100 mm, respectively, was used. The UHPC was cast in the mini-cone in a single lift without any mechanical consolidation, and the cone was lift after 30 sec to determine the mean spread diameter at the end of the flow. The opening of the V-funnel measures 32 × 32 mm^2, and the sample volume is 1.15 L. The bottom outlet was opened 30 sec after casting the UHPC. The flow time was determined at the end of continuous flow. All tested mixtures exhibited continuous flow.

50-mm cubes were used to determine compressive strength at 7, 28, 56 and 91 d. Three specimens were employed for each test. The specimens were initially covered with

wet burlap and plastic sheet. They were demolded at 24 ± 1 hr then subjected to different initial curing times of 0, 2, 6, or continuous in lime-saturated water at 23 ± 2 °C. These curing conditions are referred to as: air-drying (AD), 3 d of initial moist curing (3MC), 7 d of moist curing (7MC), and continuous moist curing (MC), respectively.

Autogenous shrinkage was measured using three replicated samples. The UHPC was cast in rigid corrugated polyethylene tubes that were capped at both ends to prevent any loss of moisture. Linear deformations were recorded right at the final setting time using a digital comparator with a linear variable differential transformer (LVDT). The samples were kept in a controlled environmental chamber at 23 ± 2 °C and 50% ± 4% relative humidity throughout the test period. The initial and final settings were assessed by the penetration test according to ASTM C 403.

Drying shrinkage was determined according to ASTM C 596 at 23 ± 2 ºC and 50% ± 4% relative humidity. Three prismatic specimens with dimensions of 285×25×25 mm^3 were prepared for each mixture. The samples were demolded after one day and subjected to the AD, 3MC, and 7MC moist curing conditions. The drying shrinkage was measured over a period of 91 d.

5.2. RESULTS AND DISCUSSION

5.2.1. Fresh Properties. Table 5-2 summarizes the fresh properties of the 12 investigated UHPC mixtures. The dosage rates of the HRWR required to secure mini-slump flow of 270 ± 10 mm ranged between 0.97% and 2.37% (expressed as percent of active solid content of the HRWR compared to binder mass). The lowest and highest values correspond to the EXC5LW60 and EXC7.5 mixtures, respectively. The majority of the mixtures had HRWR demand of 0.96% to 1.40%, in exception of the EXC7.5 and G50 mixtures which had high HRWR demand of 2.37% and 2.02%, respectively. Compared to the EXC7.5 mixture, the incorporation of 25% to 60 % of LWS resulted in considerable decrease in HRWR demand (1.23% to 1.05%).

The mini-slump values at 70 min ranged between 230 and 265 mm. The loss in mini-slump over 60 min was therefore limited to 15 to 40 mm. The G50 and SRA1.5LWS60 mixtures exhibited the lowest and highest 70-min mini-slump flow

values of 230 and 265 mm, respectively. The use of 60% LWS with EXC, EXM, and SRA had a positive effect on reducing mini-slump loss.

Table 5-2 Fresh properties and compressive strength results

Test		G50	LWS60	EXC7.5	LWS+EXC7.5			EXC+LWS60		EXM+LWS60		SRA+LWS60	
					25	40	60	5	10	5	7	1.5	3
Mini-slump flow (mm)	10 min	270	260	280	260	280	275	275	265	270	265	280	260
	70 min	230	240	240	230	255	260	260	235	245	235	265	245
Mini-V-funnel (sec)	10 min	19	16	21	20	18	17	18	23	17	20	18	20
	70 min	32	23	34	29	25	21	24	32	23	27	25	29
Air content (%)		4.8	3.1	4.5	3.3	3.7	4	3.8	4.3	3.5	4	3.4	3.8
Initial setting (hr)		11	5	9	3.5	4	4.5	5	4	5.5	5	6	7
Final setting (hr)		17.5	9.2	16	6	7	8	9.5	7	11	9	10.5	11.8

The mini-V-funnel flow times varied from 16 to 23 sec at 10 min and 21 to 34 sec at 70 min. The LW60 and EXC10LW60 mixtures exhibited the lowest and highest initial V-funnel values of 16 and 23 sec, respectively. On the other hand, the fastest and slowest flow times after 70 min belonged to the EXC7.5LWS60 and EXC7.5 mixtures with 21 and 34 sec. The use of LWS decreased the loss in V-funnel time; 7.5% EXC with 25%, 40%, or 60% of LWS had V-funnel flow time losses of 9, 7 and 4 sec, respectively. Increasing the replacement level of EXC (5%, 7.5%, and 10%), EXM (5% and 7%), and SRA (1.5% and 3%) increased slightly (10% to 25%) the mini-V-funnel at 10 and 70 min but had no significant effect on the loss of V-funnel time.

The air content of the UHPC mixtures varied between 3.1% and 4.8% which corresponded to the LWS60 and G50 mixtures, respectively. As presented in Table 5-6, the initial setting times varied between 3.5 and 11 hr and the final setting times between 6 and 17.5 hr. The G50 and EXC7.5LWS25 mixtures had the longest and shortest setting times, respectively. The combined use of EXC, EXM, or SRA with LWS significantly shortened the setting time. For example, the initial and final setting times of the EXC7.5LW25 were 3.5 and 6 hr compared to 9 and 16 hr, respectively, for the EXC7.5 mixture. This significant acceleration of setting can be due to the sharp drop in HRWR demand when 25% LWS was incorporated. The increase of the EXC content from 5% to 10%, the EXM dosage from 5% to 7% delayed the setting time by 2.5 and 2 hr whereas

the increase of the SRA from 1.5% to 3% resulted in slight acceleration in setting time by 1 hr.

5.2.2. Shrinkage

5.2.2.1 Autogenous shrinkage. As shown in Figure 5-, the incorporation of LWS at replacement levels of 25%, 40%, and 60%, by volume of sand, combined with 7.5% EXC resulted in considerable decrease in autogenous shrinkage compared to the reference G50 mixture. As illustrated in Figure 5-a, the expansion increased with the LWS content where UHPC with 25%, 40%, and 60% LWS replacements exhibited early-age maximum expansions at 7 d of 80, 300, and 375 μm/m, respectively. Given the higher relative humidity associated with greater use of LWS (Meng and khayat, 2017), greater expansion observed from the use of 7.5% CaO-based EX. Following peak values, the deformation decreased gradually until started to exhibit net shrinkage. For example, the EXC7.5LWS60 mixture had a net expansion of 5 μm/m after 91 d compared to the shrinkage of 296 μm/m for the EXC7.5LWS25 mixture.

The combined use of different EXC replacements coupled with 60% LWS exhibited a significant effect on autogenous shrinkage. As shown in Figure 5-b, the use of the EXC developed substantial expansion of 865 μm/m at 15 d in the case of the EXC10LWS60 mixture, which was the highest expansion value among the investigated mixtures. The expansion increased with the EXC replacement level with the EXC5, EXC7.5, and EXC10 mixtures exhibiting shrinkage values of 275, 375, and 865 μm/m, respectively. Following peak values, the shrinkage gradually increased and leveled off after 80 d; the EXC5LWS60 and EXC7.5LWS60 mixtures had 0 to 5 μm/m and the EXC10LWS60 mixture had an expansion of 580 μm/m.

As shown in Figure 5-c, the incorporation of 5% EXM coupled with 60% LWS did not have considerable effect on autogenous shrinkage where its shrinkage ended up at 140 μm/m compared to 35 μm/m shrinkage of the LWS60 mixture after 91 d. On the other hand, a greater dosage of 7% EXM with 60% LWS led to an expansion of 250 μm/m at 28 d. As indicated in Figure 5-c, compared to the LWS60 mixture, the incorporation of SRA did not further reduce autogenous shrinkage, which may be due to the low capillary water in the UHPC system.

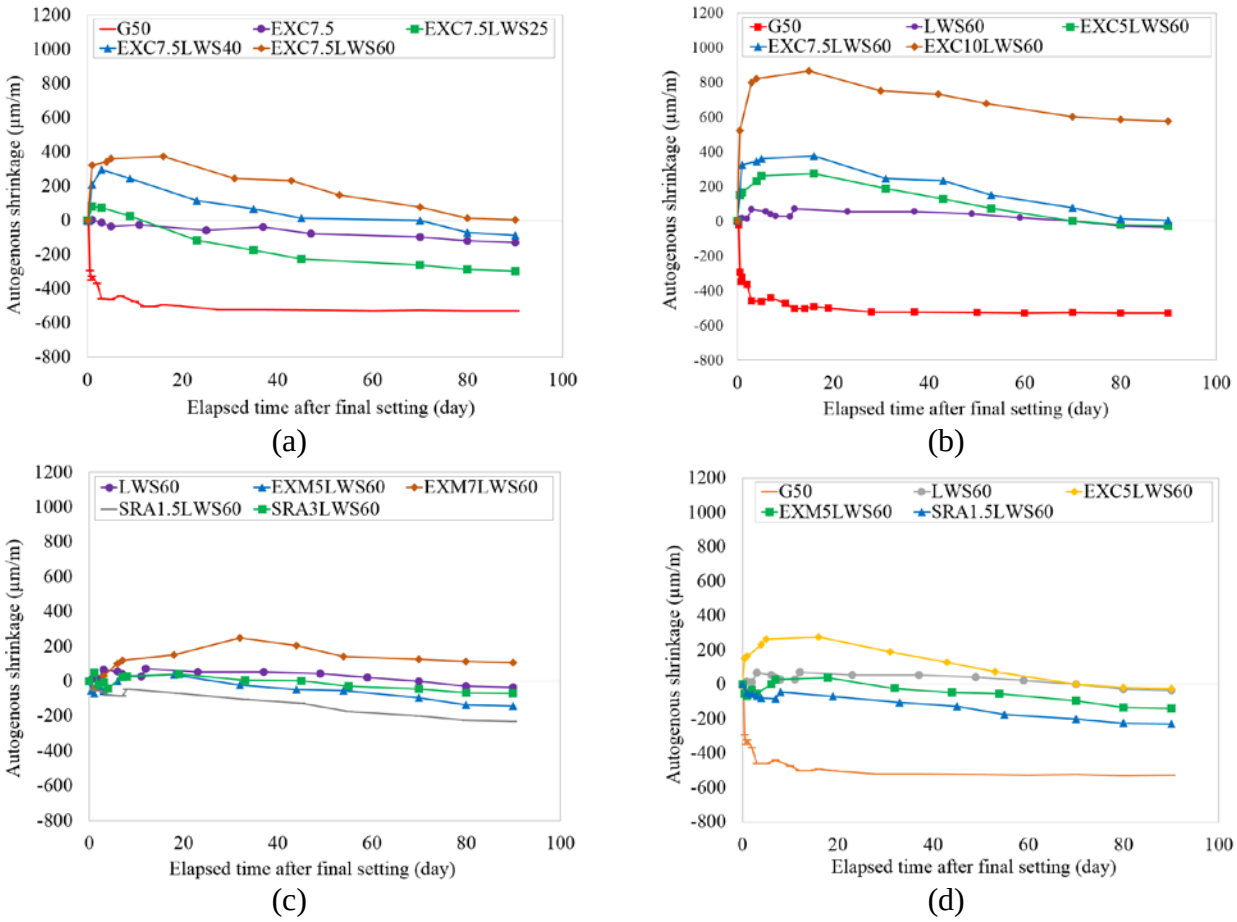

Figure 5-1 Variations in autogenous shrinkage for mixtures with different: (a) LWS contents; (b) EXC dosages; (c) EXM and SRA dosages; (d) shrinkage mitigating strategies at the low dosages

Figure 5-d compares the autogenous shrinkage of UHPC mixtures made with the lower contents of the EXC, EXM, and SRA to those of the G50 and LWS60 mixtures. Compare to the reference G50 mixture that had shrinkage of 528 µm/m at 91 d, the other mixtures had 5 to 230 µm/m at 91 d with the EXC5LWS60 mixture exhibiting the highest expansion at early age (270 µm/m).

A regression analysis of variance was performed to determine the effect of saturated LWS content coupled with shrinkage mitigating admixture type and content on autogenous shrinkage of UHPC. The autogenous shrinkage relationship is given in Eq. 5.1 and is valid for the range of variables that considered in this study.

Autogenous shrinkage = - 486 × t $^{0.00288}$ + 8.15 LWS + 57.7 EXC + 11.4 EXM + 1.0 SRA (5.1) (R^2 = 87 %)

where t (d) denotes UHPC age after final setting, LWS (% of sand volume), EXC, and EXM indicate the, CaO-based and MgO-based, respectively, expressed as percentage of binder mass, and finally SRA expressed as percentage of total water volume. The predicted autogenous shrinkage results are compared in Figure 5-2 with the experimental values. The comparison yields adequate results with R^2 of 0.93.

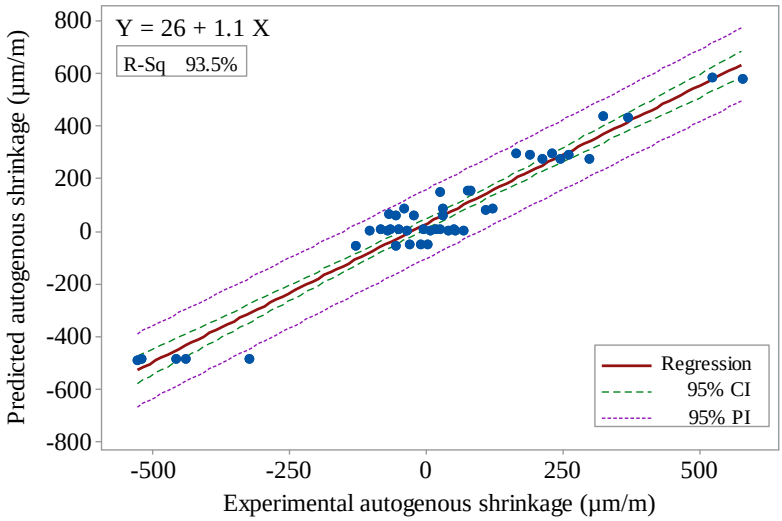

Figure 5-2 Correlation of experimental autogenous shrinkage and predicted values from Eq. 5.1.

5.2.2.2 Total shrinkage. Drying shrinkage was initiated following either 1, 3, or 7 d moist curing corresponding to curing conditions AD, 3MC, and 7MC, respectively. Drying shrinkage was monitored for 91 d, and the majority of the shrinkage occurred by 28 d. The total shrinkage is considered here as the sum of drying shrinkage at any given age and the autogenous shrinkage at the time of demolding. The total shrinkage results at different ages and curing conditions are reported in Table 5-1. The initial expansion observed during moist curing increased with LWS replacement level, regardless of the curing condition. The EXC7.5LWS60, EXC7.5LWS40, and EXC7.5LWS25 mixtures exhibited initial expansions of 240, 210, and 80 µm/m, respectively, in the case of the AD condition, compared to the reference EXC7.5 mixture that had no residual shrinkage of

early age. The maximum total shrinkage values of 25% and 60% LWS replacements were 580 and 465 μm/m, respectively.

The increase in moist-curing from 3 d to 7 d had slight enhancement of initial expansion at early age. For example, the EXC7.5LWS60 mixture had initial expansion value of 520 μm/m at the end of 3 d (3MC condition) and exhibited 530 μm/m expansion at the end of 7 d for the 7MC condition.

The increase of EXC dosage led to a significant reduction in shrinkage compared to the LWS60 mixture, especially for 10% EXC where the total shrinkage dropped from 535 to 110 μm/m for the AD condition. This reduction of the total shrinkage was even enhanced with moist curing. For example, the EXC10LWS60 mixture achieved the highest initial expansion of 900 μm/m in the 7MC condition ending up with a net expansion of 105 μm/m after 91 d, compared to initial expansion of 520 μm/m and total shrinkage of 110 μm/m at 91 d when no moist curing was applied.

The shrinkage mitigating performance of the UHPC mixtures containing EXM 60% LWS improved with moist curing duration where a reduction of shrinkage by up to 30% at the end of 91 d of the 7MC condition was observed. The use of SRA in combination with 60% LWS was found to be effective in reducing the total shrinkage. For UHPC that had curing condition of AD, the incorporation of 1.5% and 3% SRA with 60% LWS led to the total shrinkage values of 680 and 450 μm/m, respectively, compared to the LWS60 mixture with 830 μm/m at 91 d. The initial expansion during moist curing period and shrinkage reduction after air drying slightly increased with moist curing. For example, the SRA3LWS60 mixture ended up with total shrinkage of 310 μm/m with the 7MC condition compared to 455 μm/m for the mixture without any moist curing (AD).

The variation of total shrinkage with time for the UHPC mixtures containing EXC in combination with 60% LWS is illustrated in Figure 5-3 for mixtures subjected to AD, 3MC, and 7MC curing conditions. Applying 3 d of moist curing is shown to significantly increase the initial expansion. However, no significant improvement of initial expansion was observed after extending the moist curing period from 3 to 7 d. For example, the EXC10LWS60 mixture exhibited a maximum initial expansion of 520, 870, and 910 μm/m for curing conditions of AD, 3MC, and 7MC, respectively. The total shrinkage variations became stabilized after 28 d, regardless of curing condition. The same trend

was observed in Figure 5-d for the EXC5LWS60 mixture under AD, 3MC, and 7MC moist curing conditions where an increase in initial expansion from 165 to 365 μm/m was observed for the mixture subjected to 3 d of initial moist curing compared to AD, and no significant additional expansion was exhibited for 7 d of moist curing.

Table 5-3 Results for total shrinkage* of UHPC under different curing conditions

Mixture	1 d			3 d			7 d			28 d			91 d		
	AD	3MC	7MC	AD	3MC	7MC	AD	3MC	7MC	AD	3MC	7MC	AD	3MC	7MC
G50	-324	-324	-324	-536	-200	-208	-700	-632	-132	-782	-780	-728	-810	-820	-730
LWS60	18	18	18	-322	178	113	-598	-438	142	-780	-698	-580	-830	-750	-630
EXC7.5	3	3	3	-193	217	251	-420	-305	343	-517	-413	-350	-580	-465	-410
EXC7.5LWS25	81	81	81	-251	220	193	-368	-256	301	-623	-519	-460	-680	-575	-470
EXC7.5LWS40	211	239	239	-121	383	351	-225	-86	421	-430	-333	-289	-465	-370	-350
EXC7.5LWS60	239	245	245	-141	519	487	-377	-189	529	-513	-400	-273	-535	-453	-321
EXC5LWS60	165	165	165	-231	365	309	-455	-295	370	-570	-500	-371	-600	-551	-415
EXC10LWS60	522	522	522	122	862	800	2	162	910	-94	-26	254	-110	-30	105
EXM5LWS60	-68	-68	-68	-410	84	45	-600	-438	92	-730	-690	-560	-815	-750	-600
EXM7LWS60	-40	-40	-40	-310	152	110	-530	-330	175	-690	-528	-480	-756	-610	-520
SRA1.5LWS60	-50	-50	-50	-234	-10	6	-390	-310	46	-565	-550	-468	-680	-750	-550
SRA3LWS60	50	50	50	122	102	98	-222	-110	126	-318	-280	-250	-455	-366	-310

*Negative and positive values denote shrinkage and expansion, respectively.

Figure 5-4 compares the total shrinkage of the tested UHPC mixtures at 91 d for samples subjected to 1, 3 and 7 d of initial moist curing. The total shrinkage includes the autogenous shrinkage at 1 d in addition to the drying shrinkage after the remaining drying period of the moist curing. All mixtures exhibited lower shrinkage with the increase of moist curing duration. Unlike UHPC mixtures of 60% LWS and other EXs, the G50 reference mixture had shrinkage values regardless of the moist curing regime. The LWS60 mixture with no EX had an initial expansion of 180 μm/m at the end of 3 d. As expected, the increase of replacement level of LWS from 25% to 60%, EXC dosage from 5% to 10%, EXM content from 5% to 7%, and SRA concentration from 1.5% to 3% resulted in greater initial expansion during the moist curing period and lower total shrinkage upon drying. The EXC10LWS60 mixture had the best performance in terms of total shrinkage reduction where it obtained the highest expansion of 850 and 910 μm/m at

3 d and 7 d of the 3MC and 7MC conditions, respectively. It was also the only UHPC mixture ended up with the expansion of 110 μm/m at 91 d of the 7MC condition.

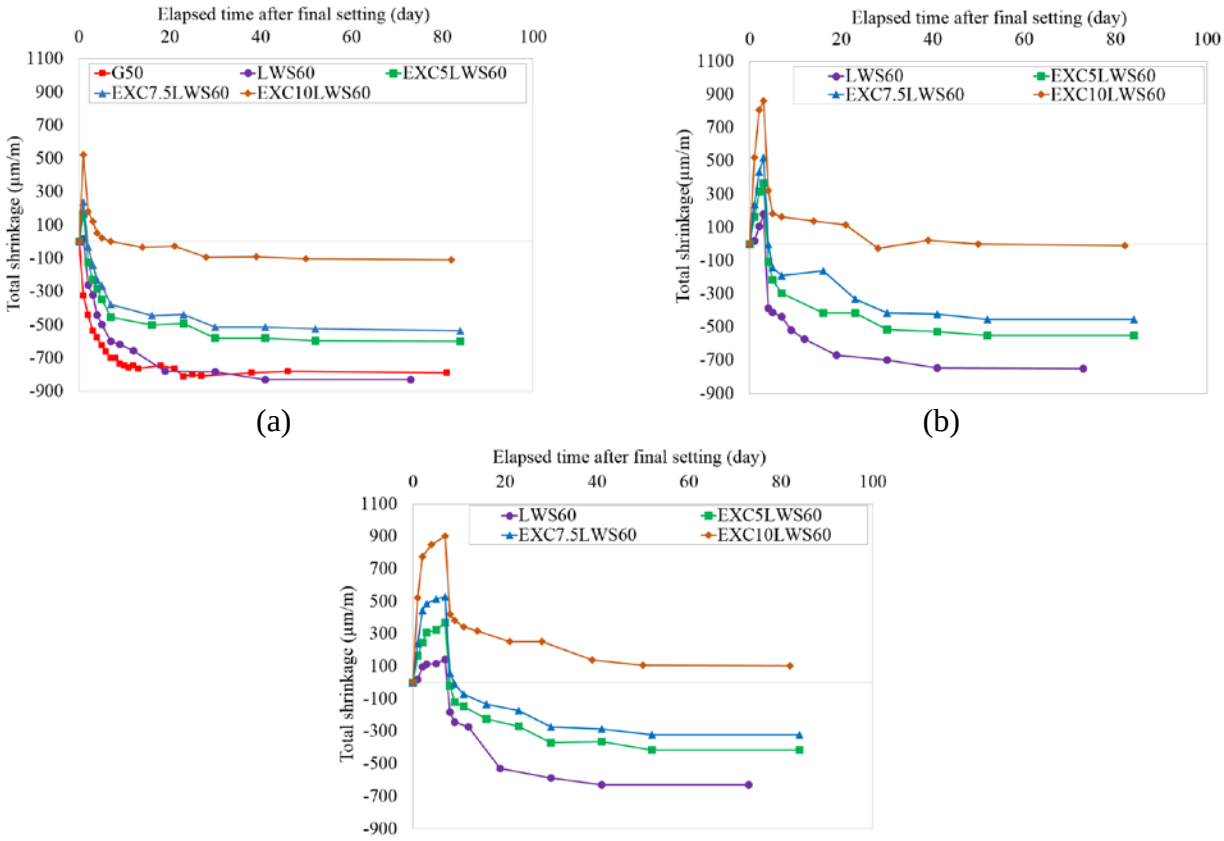

Figure 5-3 Variations in total shrinkage of UHPC mixtures with 60% LWS and different EXC contents and initial moist curing periods: (a) 1 d; (b) 3 d; and (c) 7 d of curing condition.

A regression analysis of variance was conducted to determine the effect of the LWS content coupled with a shrinkage mitigating admixture type and content and moist curing duration on total shrinkage. The total shrinkage relationship is given in Eq. 2 and is valid for the range of variables considered in this study.

$$\text{Total shrinkage} = -472 \times t^{0.1987} + 46.8\,MC + 3.5\,LWS + 53.1\,EXC + 9.3\,EXM + 82.4\,SRA \quad (2)$$

($R^2 = 90\ \%$)

where t (d) denotes specimen age after final setting, LWS (% of sand volume), EXC, and EXM indicate the, CaO-based and MgO-based, respectively, expressed as percentage of

binder mass, and finally SRA expressed as percentage of total water volume. Predicted total shrinkage results are compared in Figure 5-5 to the experimental values. The comparison yields adequate results with R^2 of 0.92.

Figure 5-6 illustrates contour diagrams based on Eq. 5.1 and 5.2 indicate the coupled effect of different EXC used in combination with LWS on autogenous shrinkage and total shrinkage at 91 d for the mixture subjected to the 7MC curing condition. The increase of LWS and EXC dosages are shown to reduce shrinkage. The highest values of expansion occurred where 60% of LWS coupled with 10% EXC and the G50 reference mixture without any LWS and EXC had the highest shrinkage.

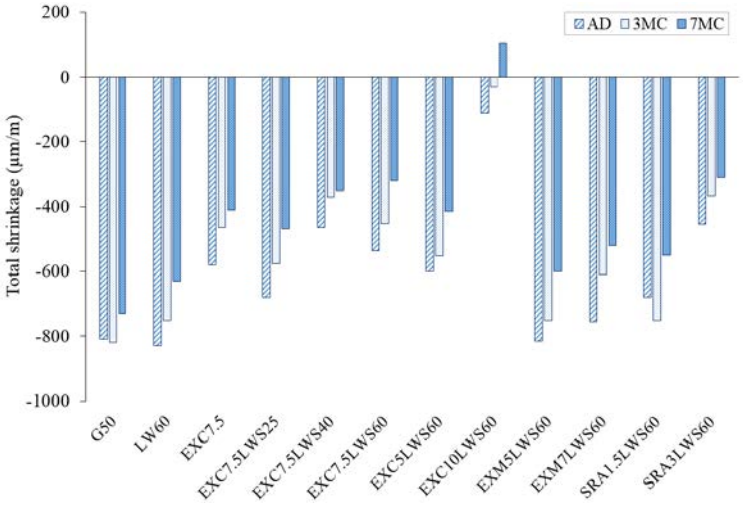

Figure 5-4 Total shrinkage results of UHPC mixtures at 1 d of AD, 3 d of 3MC, 7 d of 7MC, and 91 d of each curing regime, respectively

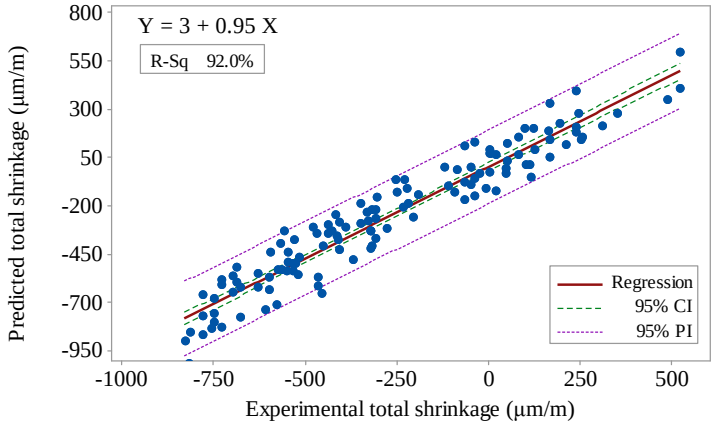

Figure 5-5 Correlation of experimental total shrinkage and predicted values from Eq.5.2.

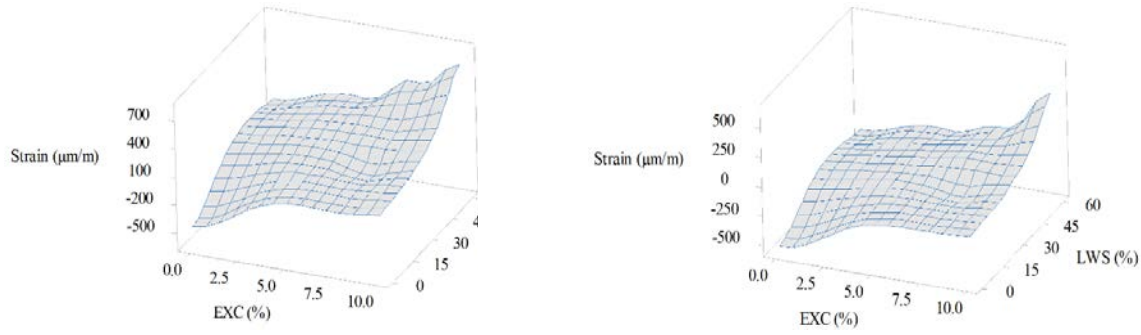

(a) (b)

Figure 5-6 Coupled effect of LWS and EXC on the 91-d variations of: (a) autogenous shrinkage; and (b) total shrinkage of 7MC curing condition.

5.2.3. Compressive Strength. Table 5-4 presents the mean compressive strength results of the 12 investigated mixtures subjected to different curing conditions. The coefficient of variation (COV) of the strength results are also reported and ranged between 0.2% and 5.5%, which indicates good reproducibility of test results. The lowest 91-d compressive strength was 87 MPa and was obtained for the G50 mixture that was air cured (AD). The LW60 mixture subjected to 7 d of moist curing (7MC) had the highest compressive strength of 148 MPa.

As shown in Figure 5-7a, regardless of the moist curing regime, the use of LWS showed clear benefit in enhancing compressive strength. The mixtures with LWS had greater compressive strength than the G50 and EXC7.5 mixtures without LWS. The latter mixture exhibited lower compressive strength than the G50 mixture. The use of LWS with 7.5% EXC enhanced compressive strength by up to 45% compared to the EXC7.5 mixture without any LWS. Higher LWS replacements led to slightly greater compressive strength. The use of 25% LWS increased compressive strength by 10% to 30% compared to the reference EXC7.5 mixture. Further increase in LWS had limited effect on compressive strength (less than 10%). The enhancement of compressive strength with the inclusion of the LWS is attributed to its internal curing function, given the very low w/b of the tested material. Similar observations were reported by Meng and Khayat (2017) where the use of LWS up to 75% in UHPC with 0.20 w/b was shown to increase the degree of hydration and increase mechanical properties.

Compared to the LWS60 mixture, the combined use of either EXC, EXM, or SRA with 60% LWS decreased compressive strength by up to 30%, 40%, and 40%, respectively. Strength loss increased with the dosage of the shrinkage mitigating admixture. As shown in Figure 5-7b, for the UHPC mixtures made with different EXC contents with 60% LWS, increasing the replacement level of the EXC (5% to 10%), resulted in compressive strength decrease from 140 to 130 MPa. The same trend was observed for the EXM (5% to 7%), and the SRA (1.5% to 3%) where shrinkage drop was 128 to 122 MPa, and 138 to 133 MPa, respectively, at 91 d for the 7MC condition.

It can be stated that the impact factor of the EX on mechanical properties of the concrete relies on the effect of the expansion volume generated in the microstructure (Higuchi et al., 2014). The expansion can refine the microstructure, thus resulting in a decreased size and volume of the total porosity, which enhances mechanical properties. However, excessive expansion can cause damage to the microstructure resulting in cracks, and particularly, deteriorating of the interface with aggregate (Higuchi et al., 2014).

Table 5-4 Compressive strength results for investigated UHPC mixtures

Test		G50	LWS60	EXC7.5	LWS?+EXC7.5			EXC?+LWS60		EXM?+LWS60		SRA?+LWS60	
					25	40	60	5	10	5	7	1.5	3
Comp. str.-AD (MPa)	7	66 (1.5*)	99 (2.3)	66 (2.6)	84 (2.6)	87 (2.3)	96 (2.4)	98 (3.2)	88 (4.4)	85 (2.7)	77 (2.8)	80 (1.8)	71 (3.4)
	28	80 (1.8)	120 (1.7)	83 (5.0)	104 (1.0)	108 (3.3)	110 (3.3)	115 (2.6)	108 (4.4)	102 (4.8)	98 (4.2)	123 (3.0)	118 (1.6)
	56	85 (3.6)	127 (4.4)	88 (3.8)	111 (1.2)	114 (4.6)	119 (3.7)	124 (2.1)	118 (4.1)	110 (4.7)	104 (1.6)	128 (2.4)	123 (2.6)
	91	87 (2.2)	130 (1.8)	90 (0.2)	115 (0.9)	118 (1.5)	122 (4.1)	129 (0.8)	120 (5.2)	114 (3.2)	107 (1.7)	131 (1.1)	127 (0.6)
Comp. str.-3MC (MPa)	7	77 (0.8)	112 (1.6)	68 (3.5)	89 (3.8)	93 (0.9)	102 (0.5)	102 (3.6)	92 (2.3)	90 (3.2)	79 (2.8)	83 (1.9)	74 (3.1)
	28	96 (1.5)	132 (2.7)	93 (3.5)	112 (2.2)	115 (4.4)	118 (2.9)	120 (2.4)	107 (2.4)	112 (5.2)	107 (2.2)	125 (2.7)	122 (0.6)
	56	103 (0.4)	139 (2.5)	101 (0.9)	118 (4.6)	120 (0.4)	128 (0.7)	128 (1.5)	122 (3.1)	117 (1.5)	112 (4.5)	131 (3.4)	126 (4.7)
	91	105 (3.2)	142 (0.8)	104 (4.2)	122 (2.2)	124 (1.5)	131 (3.4)	134 (1.1)	126 (3.1)	125 (1.0)	119 (1.8)	135 (3.3)	129 (1.1)
Comp. str.-7MC (MPa)	7	83 (3.5)	119 (1.4)	72 (3.0)	92 (3.7)	97 (1.0)	104 (1.8)	107 (3.0)	93 (3.2)	94 (4.6)	80 (4.2)	86 (2.3)	79 (1.9)
	28	106 (2.2)	142 (4.6)	97 (1.9)	117 (3.9)	120 (5.5)	123 (2.3)	126 (0.8)	111 (2.0)	119 (1.3)	111 (2.7)	127 (1.9)	124 (2.4)
	56	112 (3.0)	146 (1.3)	105 (4.6)	126 (2.9)	129 (0.6)	131 (1.0)	135 (3.4)	126 (3.9)	124 (0.6)	118 (4.6)	134 (1.7)	131 (1.3)
	91	115 (1.7)	148 (2.0)	110 (2.3)	129 (1.1)	132 (1.1)	136 (0.6)	140 (0.9)	130 (3.3)	128 (3.0)	122 (1.1)	138 (3.6)	133 (1.4)
Comp. str.-MC (MPa)	28	108 (2.0)	129 (2.0)	98 (3.4)	109 (3.6)	108 (4.2)	111 (3.7)	117 (4.4)	109 (4.6)	107 (2.4)	98 (3.6)	118 (1.9)	115 (3.7)
	56	115 (1.3)	139 (4.6)	109 (2)	114 (1.2)	117 (3.6)	126 (2.3)	131 (3.6)	126 (1.2)	125 (2.0)	103 (4.0)	128 (2.4)	130 (4.7)
	91	120 (0.6)	143 (3.1)	112 (2.2)	120 (2.4)	124 (1.2)	130 (0.5)	133 (2.1)	127 (1.8)	129 (3.3)	115 (2.9)	130 (5.1)	132 (3.9)

* C.O.V. (%)

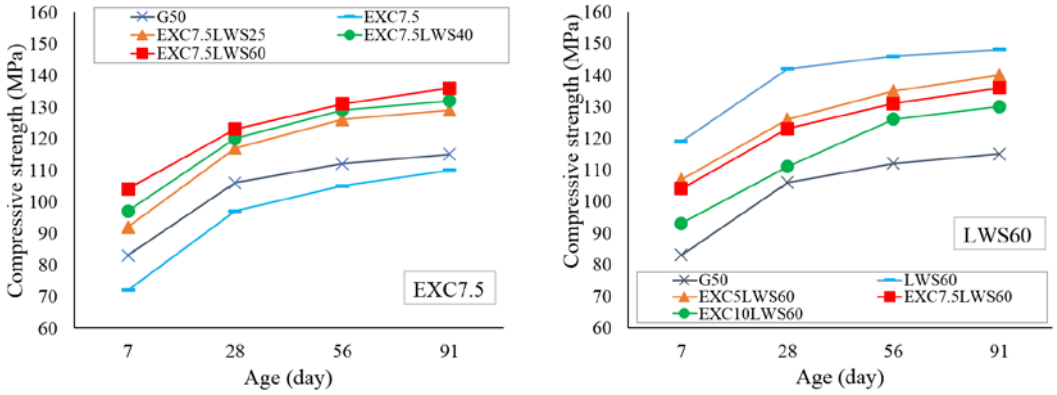

(a) (b)

Figure 5-7 Variations of compressive strength of investigated UHPC over age at 7MC curing condition: (a) LWS contents; (b) EXC dosages

As indicated in Figure 5-8, the increase in the period of moist curing from 1 to 3 and 7 d had significant effect on the 91-d compressive strength of UHPC, especially when no LWS was used. The two reference mixtures, G50 and EXC7.5, showed consistent increase in compressive strength with the duration of moist curing. For example, the compressive strengths of the G50 and EXC7.5 mixtures increased from 87 and 90 MPa under air-dried (AD) condition to 115 and 110 MPa, respectively, under 7MC curing condition. These mixtures exhibited slight increase in compressive strength at 91 d under continuously moist cured (120 and 112 MPa, respectively).

On the other hand, the benefit of moist curing condition was limited in UHPC with LWS. For example, Figure 5- illustrated that the compressive strength of the EXC10LWS60 mixture of 91 d for curing conditions of the AD and 7MC were 122 and 136 MPa, respectively. Further increase in moist curing (MC) led to lower 91-d compressive strength. For example, mixtures containing the 7.5% EXC and 60% LWS had approximately 10% lower at 91 d than concrete that subjected to 7 d of moist curing followed by air drying. This can be due to the relatively lower relative humidity of the 7 MC concrete at the time of testing (91 d) than the MC specimens, which can increase strength.

As indicated in Table 5-8, regardless of the shrinkage-mitigating admixture, the highest compressive strength was obtained for the EXC7.5LW60 mixture (136 MPa)

subjected to 7 d of moist-curing (7MC). The compressive strengths of UHPC mixtures made with combinations of EXC, EXM, or SRA with 60% LWS were greater than the G50 mixture but lower than the LWS60 mixture, regardless of the curing condition. The same trend occurred for mixtures containing EXC, EXM, or SRA combined with 60% LWS where extending moist curing period up to 7 d enhanced compressive strength. However, it is important to note that the 91-d compressive strengths of all UHPC mixtures, except the reference G50 mixture, were lower than those subjected to 7 d of moist curing followed by air-drying, as shown in Figure 5-a and b. For example, the 91-d compressive strength of the EXC10LWS60 mixture increased from 120 MPa in the AD condition to 126 and 130 MPa at the 3MC and 7MC conditions, respectively, but dropped to 126 MPa with the MC curing condition.

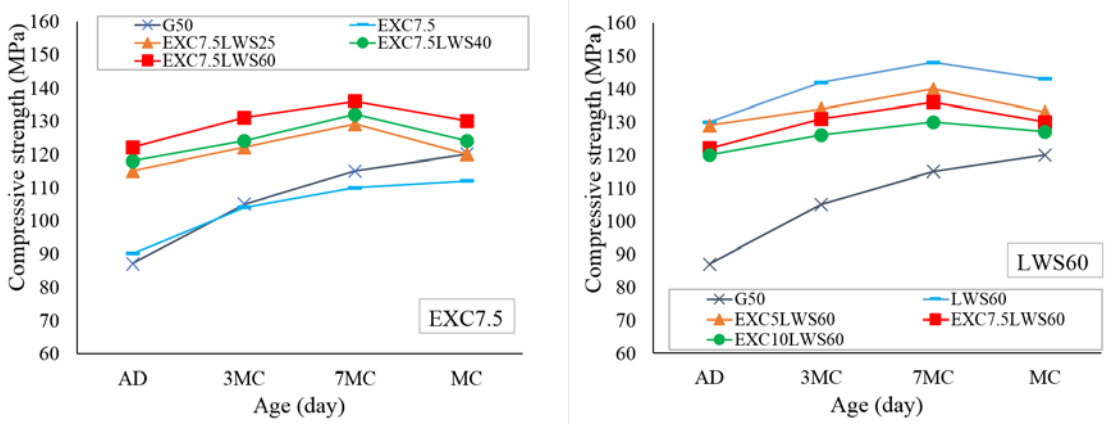

(a) (b)

Figure 5-8 Variations of compressive strength of the investigated UHPC mixtures over different curing conditions at 91 d: (a) LWS contents; (b) EXC dosages

Coupled effect of shrinkage mitigation measures on compressive strength: A regression analysis of variance was performed to determine the effect of saturated LWS content coupled with shrinkage mitigating admixture type and content on compressive strength of UHPC. The predicted coefficient of multiple determinations (pre-R^2) 90.2% was in a good agreement with the adjusted coefficient of multiple determinations (adj-R^2) with 91.2% for the responses. The compressive strength relationship is given in Eq. 5.3 and is valid for the range of variables that were considered in this study, including strengths between 7 d and 91 d.

$$f_c = 58 \times t^{0.151} + 0.46\ LWS - 0.97\ EXC - 3.45\ EXM - 4.85\ SRA \quad (5.3)$$

(R^2 = 89%)

where, f_c (MPa) represents compressive strength, t (d) denotes testing age, LWS (% of sand volume), EXC, and EXM indicate the, CaO-based and MgO-based, respectively, expressed as percentage of binder mass, and finally SRA expressed as percentage of total water volume. The predicted compressive strength results are compared in Figure 5-9 to the experimental values. The comparison yields adequate results with R^2 of 0.92.

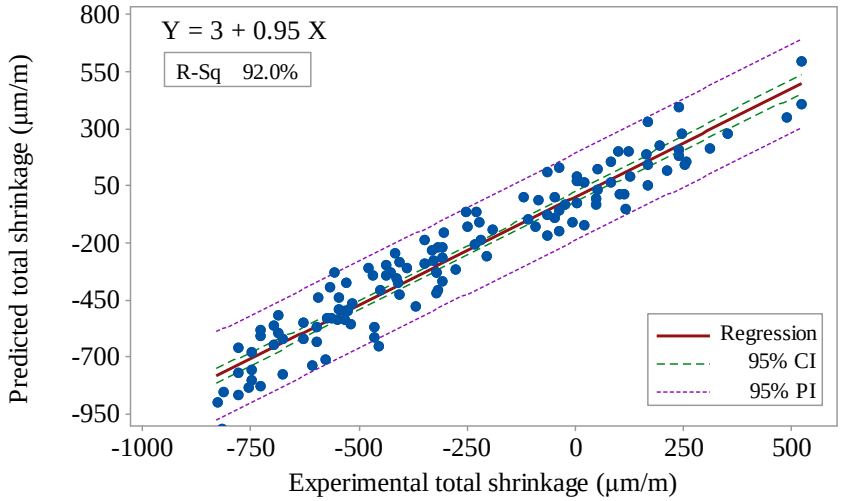

Figure 5-9 Correlation of experimental compressive strengths and predicted values from Eq.5.3

5.3. SUMMARY

The incorporation of 25% to 60% pre-saturated LWS resulted in considerable decrease in HRWRA demand (1.23% to 1.05%) compared to the EXC7.5 mixture (2.3%) required to secure self-consolidating characteristics. The lowest and highest values of HRWRA demand corresponded to the EXC5LW60 and EXC7.5 mixtures, respectively. The content of LWS necessary to compensate for chemical shrinkage for the investigated UHPC corresponds to 35% by volume of sand.

The use of 60% LWS with EXC, EXM, or SRA had a positive effect on reducing mini-slump flow and mini V-funnel losses with time. The fastest and slowest flow times after 70 min belonged to the EXC7.5LWS60 and EXC7.5 mixtures.

The combined use of EXC, EXM, or SRA with LWS significantly shortened the final setting times from 17.5 hr for the G50 mixture to 6-8 hr for those with LWS combined with 7.5% EXC.

The coupled effect of incorporating an EXC with 60% LWS resulted in a significant effect on controlling autogenous shrinkage of UHPC. The EXC10LWS60 mixture had the highest expansion of 865 μm/m and exhibited expansion value of 580 μm/m at 91 d compared to the reference G50 mixture that had a shrinkage of 530 at 91 d.

The coupled effect of LWS and EXC for different curing conditions indicate that increasing LWS and EXC replacement levels along with extending moist curing significantly improved expansion during moist curing period and reduced total shrinkage thereafter. The EXC10LWS60 mixture had the best performance in terms of total shrinkage (expansion of 110 μm/m at 91 d) following 7 d of moist curing.

The use of SRA or EXM in combination with 60% LWS was effective in reducing total shrinkage by up to 30%.

The increase in the period of moist curing from 1 to 3 and 7 d had significant effect on the 91-d compressive strength of UHPC. Such increase was by up to 35% for UHPC with no LWS and 15% for that with 60% LWS.

The combined use of either EXC, EXM, or SRA with 60% LWS decreased 91-d compressive strength under 7MC ranging from 8 to 20 MPa compared to 60% LWS. Further increase in EXC from 5% to 10%, EXM from 5% to 7%, and SRA from 1.5% to 3% in mixtures subjected to 7d of moist curing resulted in 91-d compressive losses of 10, 6, and 5 MPa, respectively.

6. PERFORMANCE OF UHPC AS BONDED OVERLAYS

The function of a bonded overlay is significantly dependent on a well implemented bonding at the interface layer as well as to the choice of concrete material. These factors have been investigated individually in previous chapters. The main purpose of this chapter is to verify the feasibility of UHPC as bonded concrete overlay as described in detail below.

6.1. PREPARATION OF SUBSTRATE

Total 11 slabs, each measuring 2 × 1.5 m^2 and a depth of 150 mm, were cast outdoor in June 2016 using a local concrete ready mix company, as shown in Figure 6-1. The conventional concrete mixture for the slabs was designed according to typical MoDOT mix design for bridge decks. All slabs were reinforced with two reinforcement mats of longitudinal #4 bars spaced at 250 mm which were placed at the top and bottom parts of slabs. The top and bottom rebar mats were located 25 mm and 50 mm from the top and bottom of the concrete, respectively. The slabs were demolded after 24 hr and then moisture cured for 14 days using wet burlap and plastic sheet. They were then allowed to air dry outdoor for about 12 months prior to applying UHPC overlays in order to ensure that the slabs would dry sufficiently under real seasonal variations.

Figure 6-1 Concrete pavement sections as substrate

6.2. SURFACE PREPARATION

Concrete surface retarder was used to provide aggregate exposed surface. The retarder was uniformly applied with a low pressure pump-up type garden sprayer onto the surface of the concrete immediately after final finishing operations. The retarded mortar were flushed off with a stream of water and removed by scrubbing with a stiff brush in 24 hr after application to expose the aggregate. The final prepared surface is shown in Figure 6-2.

Figure 6-2 Substrate surface preparation

6.3. INSTRUMENTATION PLAN

The substrate slabs were fully instrumented by strain gauges, relative humidity sensors, and thermocouples after adequate air drying. The instrumentation plan aimed to monitor the concrete shrinkage deformation, humidity and temperature variations at the interface layer over time after overlay application.

The embedment type of strain gauges manufactured by KYOWA (120-120-H2-11) were used to measure the shrinkage deformations. Figure 6-3 displays the embedment strain gage. The sensors are designed with the outer body of 120 mm sensing grid with an effective gauge length of 75 mm. The sensor consists of a 75 mm 120 ohm (Ω) foil strain gage (nickelchromium alloy on polymide backing). The gages feature a specially treated

surface with a honeycomb pattern providing adequate bond to concrete. They provide suitable waterproofness and elastic modulus to be able to embed in fresh mortar or concrete to measuring the internal stress.

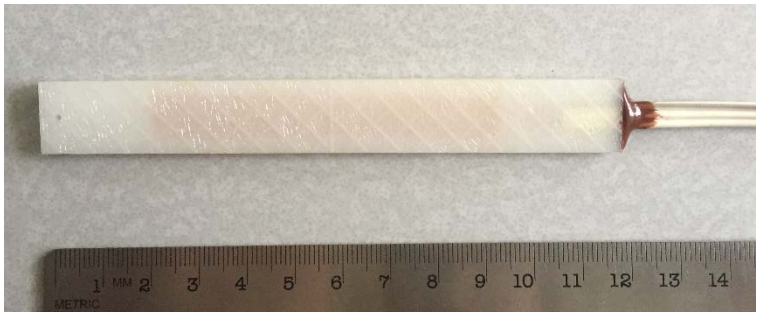

Figure 6-3 Embedded strain gauge for monitoring shrinkage deformation

Type T 20 gage wire produced by Coleparmer (UX-08542-24) were used as thermocouple. These thermocouple are functional between -250 °C and +250 °C as they consist of copper and constantan wires. In order to make sure an adequate electrical connection, the ends of the solid thermocouple wires were twisted and then soldered.

The capacitive relative humidity sensor manufactured by Sparkfun (HIH-4030), measuring 6 × 20 mm, was used to measure the relative humidity at the interface layer. The accuracy of the sensors is ±2% RH between 10% and 90% RH, and range up to ±4% at 100% RH, as reported by the manufacturer. Each RH sensor was encased in a 1/2” PVC tube with covered ends to be able to embedded inside concrete as the sensors were not waterproof. The end intended to position inside concrete at the interface layer was covered with stretch gauze to allow humidity transmission while preventing the penetration of UHPC inside the pipe that could lead to erroneous measurements. The encapsulated RH sensor, prepared for embedding in concrete, is shown in Figure 6-4.

Figure 6-5 demonstrates the instrumentation layout, including embedded concrete strain gauge, relative humidity sensor, and thermocouple for monitoring the shrinkage deformation of UHPC at the interface layer. Each slab was instrumented at three different locations to monitor the concrete shrinkage behavior at the corner, edge, and center of the slab, corresponding to points A, B, and C, respectively.

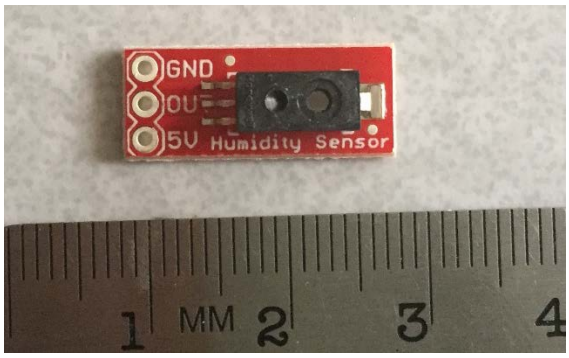

Figure 6-4 Relative humidity sensor

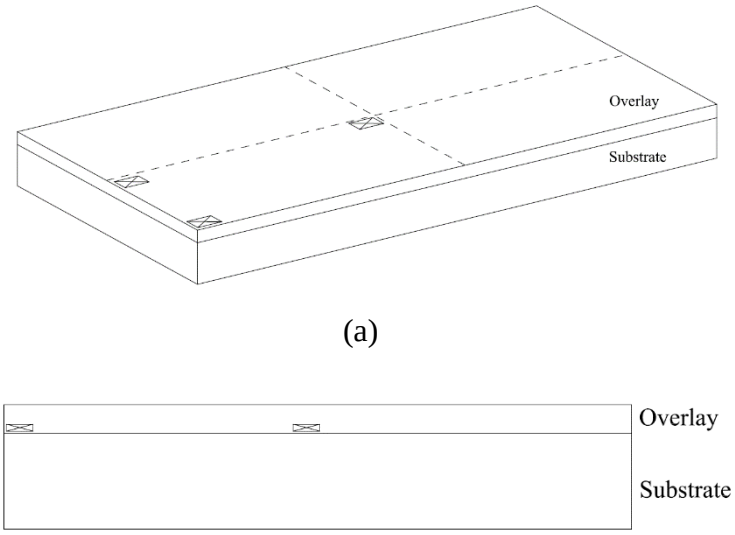

Figure 6-5 Sensor locations (a) overall view (b) lateral view of experimental pavement sections

All variations were recorded using Campbell Scientific data acquisition hardware and software. Lead wires from the strain gages were routed through AM16-32 multiplexer, using a separate completion module for each gage on the multiplexer. The data logger used was a Campbell Scientific CR1000. The thermocouple wires were routed through an AM25T multiplexer, which has an internal RTD (resistance temperature detector) to measure the cold junction temperature required to compute the temperature at the soldered end of the thermocouple. The multiplexer was controlled by

the CR1000 data logger. In addition to the strain and temperature instrumentation, relative humidity sensors were collected. Table 6-1 presents the mixture characteristics of the substrate concrete.

Table 6-1 Cast slabs characteristics

Slab no.	Overlay type	Mixture characteristics	Thickness (mm)	Steel fiber volume (%)
1	UHPC 1	EXC 10% - LWS 60%	25	2
2	UHPC 1	EXC 10% - LWS 60%	38	2
3	UHPC 1	EXC 10% - LWS 60%	50	2
4	UHPC 1	EXC 10% - LWS 60%	38 (Repeat)	2
5	UHPC 2	EXC 10% - LWS 60%	25	3.25
6	UHPC 2	EXC 10% - LWS 60%	38	3.25
7	UHPC 2	EXC 10% - LWS 60%	50	3.25
8	UHPC 3	EXC 5% - LWS 60%	38	2
9	UHPC 3	EXC 5% - LWS 60%	25	2
10	UHPC 4	EXC 0% - LWS 60%	38	2
11	UHPC 5	EXC 0% - LWS 0%	38	2

After casting, the top surface of the beams was covered with wet burlap and plastic sheeting, and a wet surface was maintained for seven days to retain moisture for a proper initial moist curing.

After seven days, the burlaps and plastic sheets were removed, and the slabs were demolded and exposed to air drying in the lab environment. Shrinkage of the investigated concrete mixtures is not affected by humidity and temperature variations caused by seasonal changes. Therefore, the shrinkage results of the investigated concrete mixtures can be isolated from warping and curling deformations caused by seasonal variations. The slab construction procedures, including concrete mixing, placement, and finishing are presented in Figure 6-6.

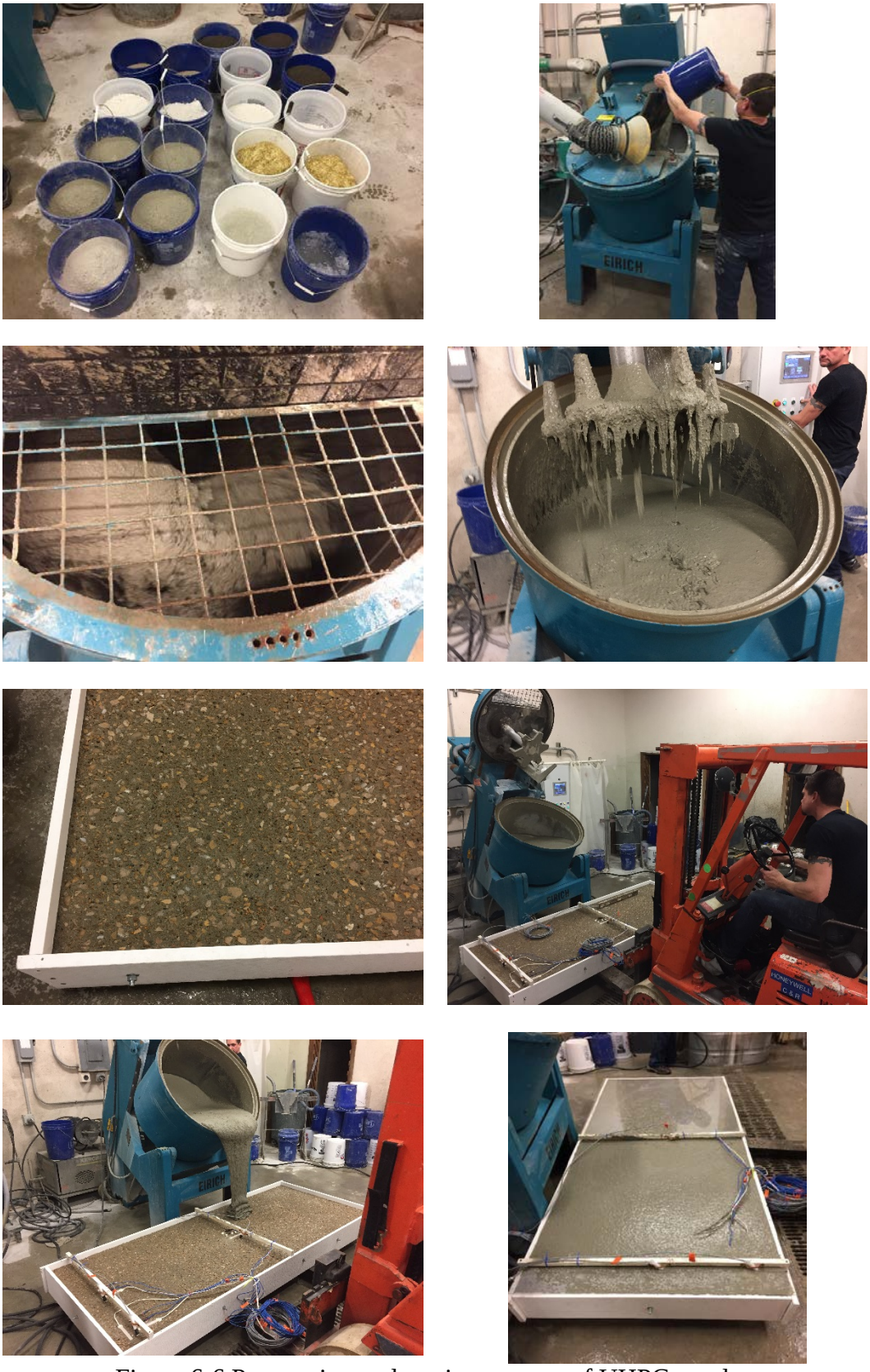

Figure 6-6 Preparation and casting process of UHPC overlay

6.4. SHRINKAGE, RH, AND TEMPERATURE MEASUREMENTS

Figure 6-7 presents the results of total shrinkage deformation at the interface layer of different measurement stations in the investigated slabs. Negative and positive values of this figure correspond to shrinkage and expansion, respectively. As mentioned earlier, all slabs were subjected to wet curing using wet burlap and plastic sheet for seven days before exposure to air drying. The results of shrinkage deformation were shown to be a function of UHPC mix design, location, and overlay thickness. As expected, the overlay made with 10% EXC combined with 60% LWS with 25 mm in thickness exhibited the highest expansion of 820 μm/m. On the other hand, the UHPC overlay made with 50% GGBS without any LWS and EX ended up with total shrinkage of 100 μm/m after 130 days of casting. As shown, all UHPC overlays exhibited slight increase of expansion during seven days of wet curing under burlap and plastic sheet. However, shrinkage gradually began to dominate as UHPC overlays were exposed to air drying after seven days. The expansion rate decreased with increase in UHPC overlay thickness from 25 mm to 50 mm. For example, the EXC10LWS60 mixture with 25, 38, and 50 mm thicknesses exhibited maximum expansion of 820, 630, and 500 μm/m, respectively. After the EXC10LWS60 mixture, the EXC5LWS60 mixture showed the highest expansion values of 300 and 220 μm/m, respectively. The LWS60 and G50 mixtures had the lowest deformation with maximum expansions of 100 and 20 μm/m, respectively. It should be noted that the deformations of the investigated UHPC mixtures were not affected by humidity and temperature variations caused by seasonal fluctuations as all slabs were stored and investigated indoor. Visual and microscopic inspections of UHPC overlays at the surface and interface layer showed no signs of cracking nor debonding after 150 days of casting. It should be noted that the variations of deformation are being monitored over time and the results will be updated.

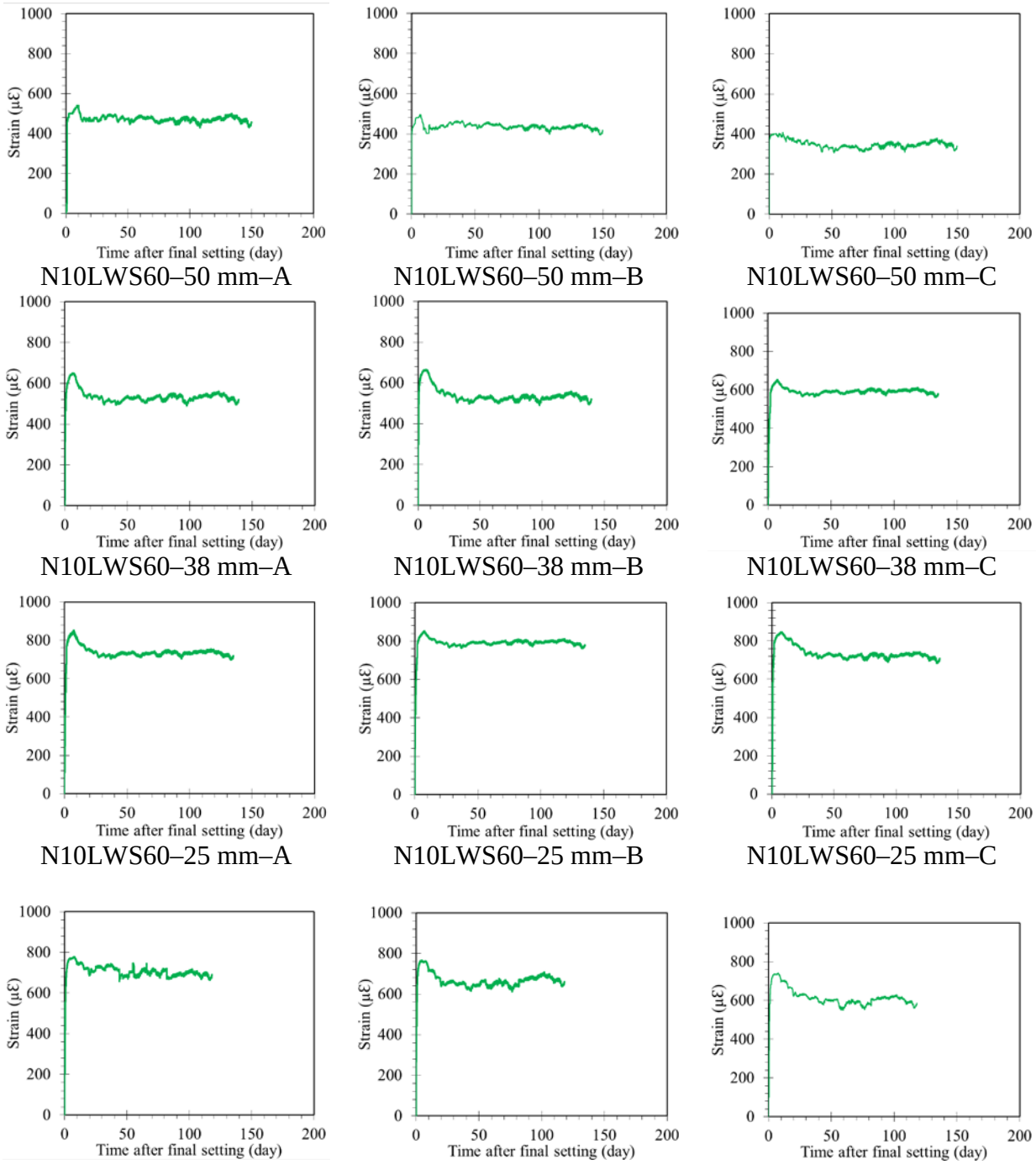

Figure 6-7 Total shrinkage deformation at the interface layer of different stations

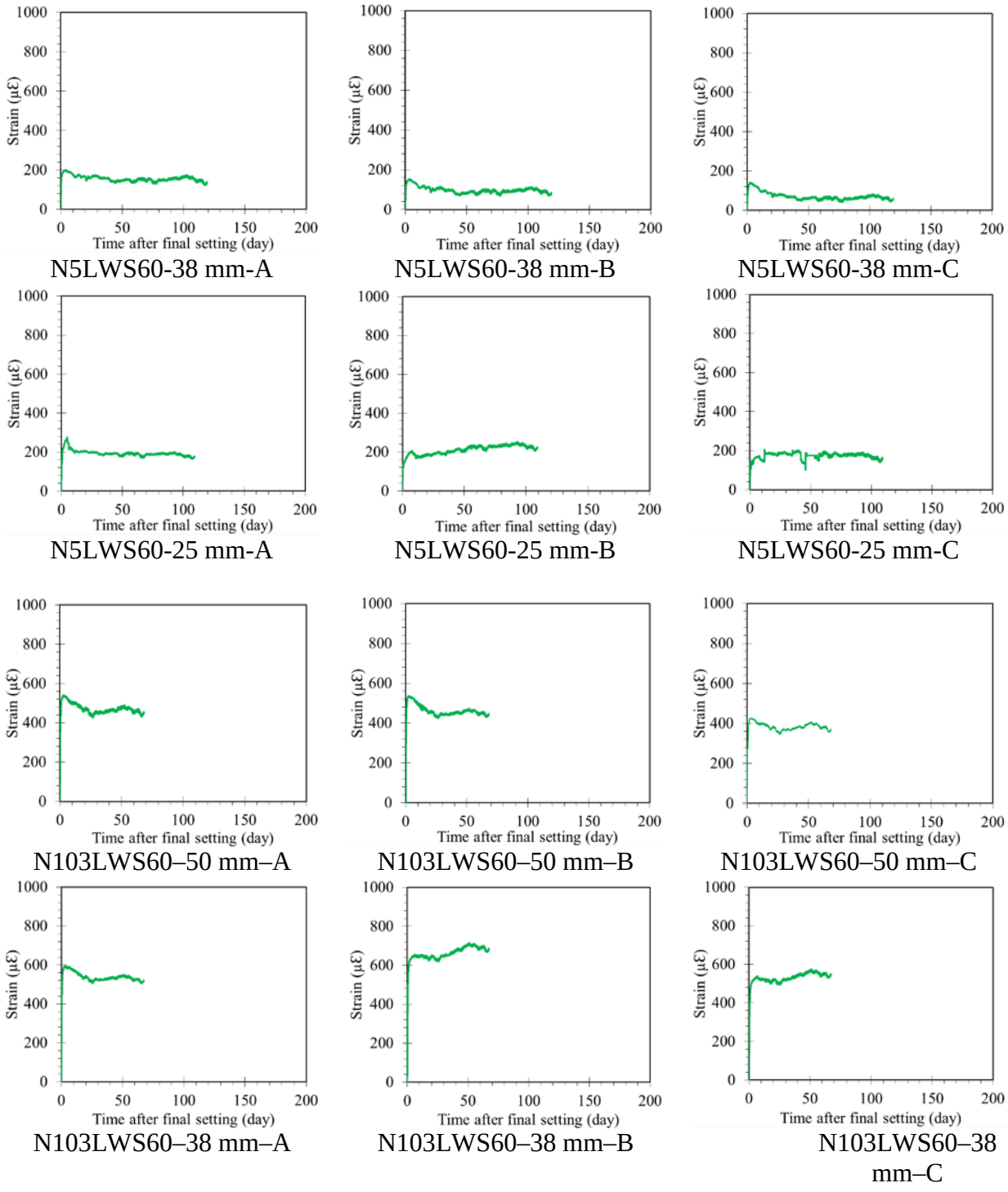

Figure 6-7 Total shrinkage deformation at the interface layer of different stations (Cont')

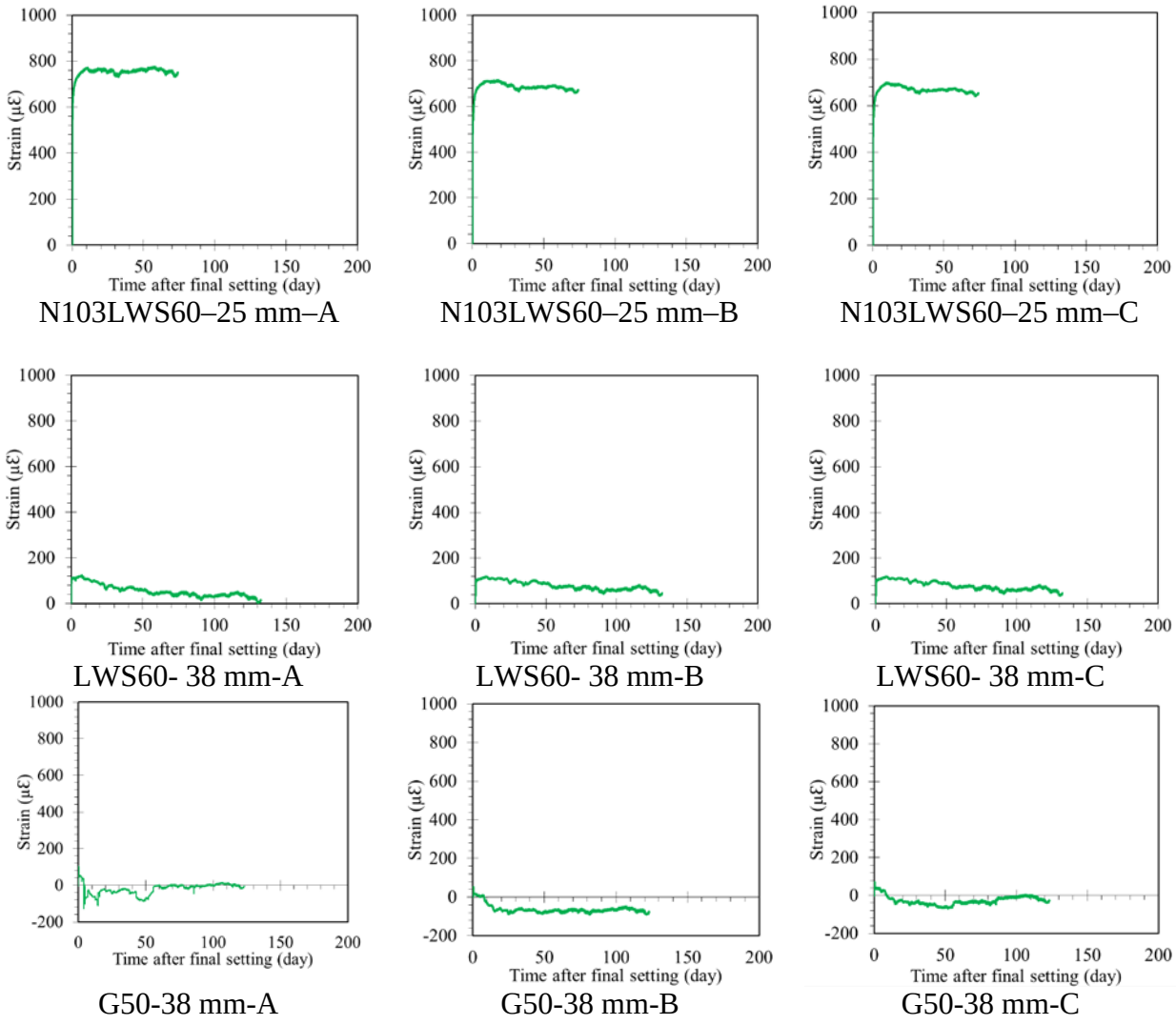

Figure 6-7 Total shrinkage deformation at the interface layer of different stations (Cont')

Figure 6-8 and Figure 6-9 presents the variations of relative humidity and temperature over time at different locations of investigated UHPC mixtures with different thicknesses, respectively. Results indicated that UHPC overlay had a relative humidity of 100% (saturated) at the early ages. However, as time passed, the relative humidity dropped to around 70% – 80% depending on the UHPC mixture and overlay thickness.

As illustrated in Figure 6-9, temperature variations showed a high temperature at the first 24 hr by up to 35 °C for most of UHPC mixtures. However, after 24 hr, the temperature gradually reached the ambient temperature around 20-25 °C.

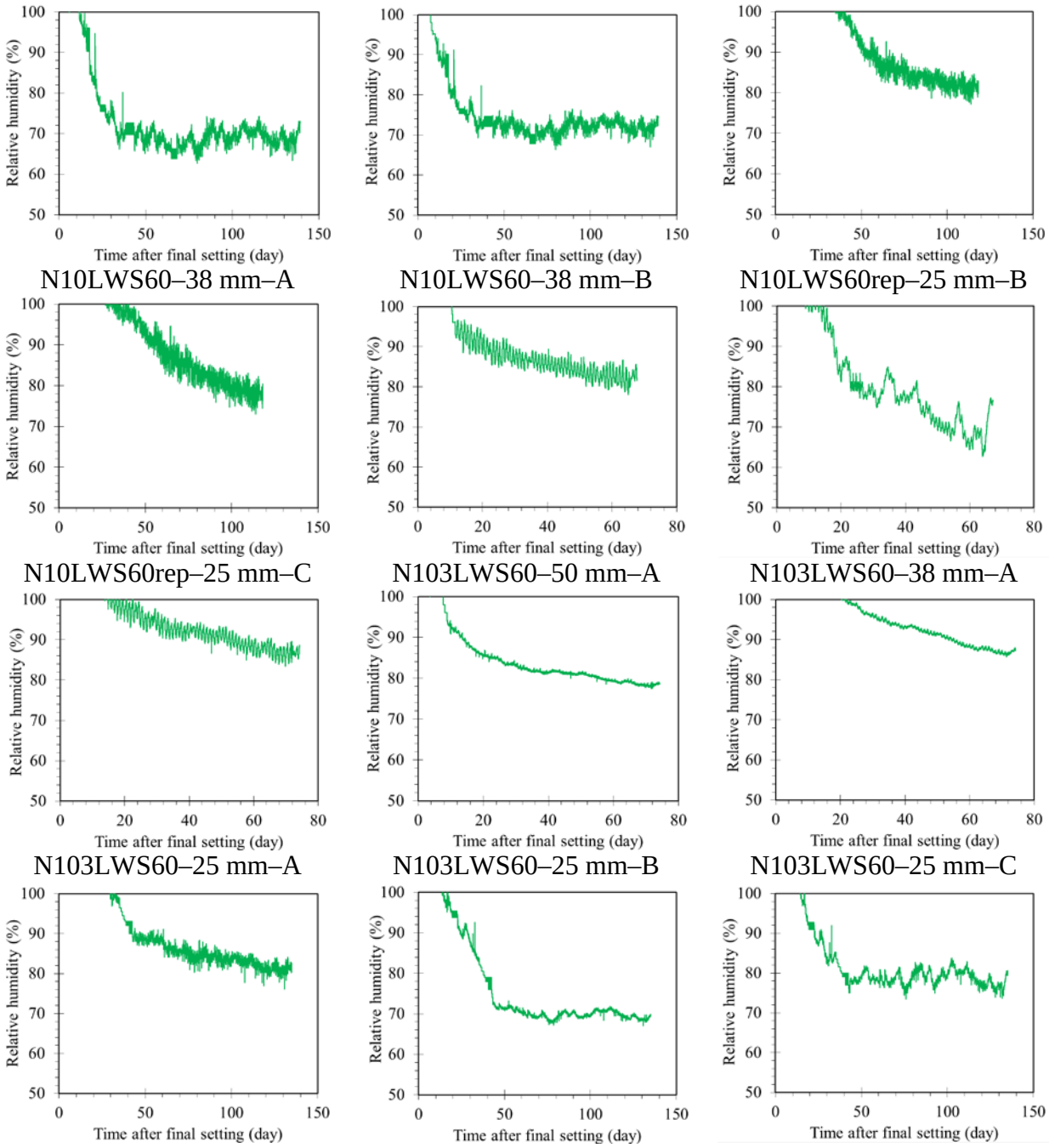

Figure 6-8 Relative humidity variations at the interface layer of different locations

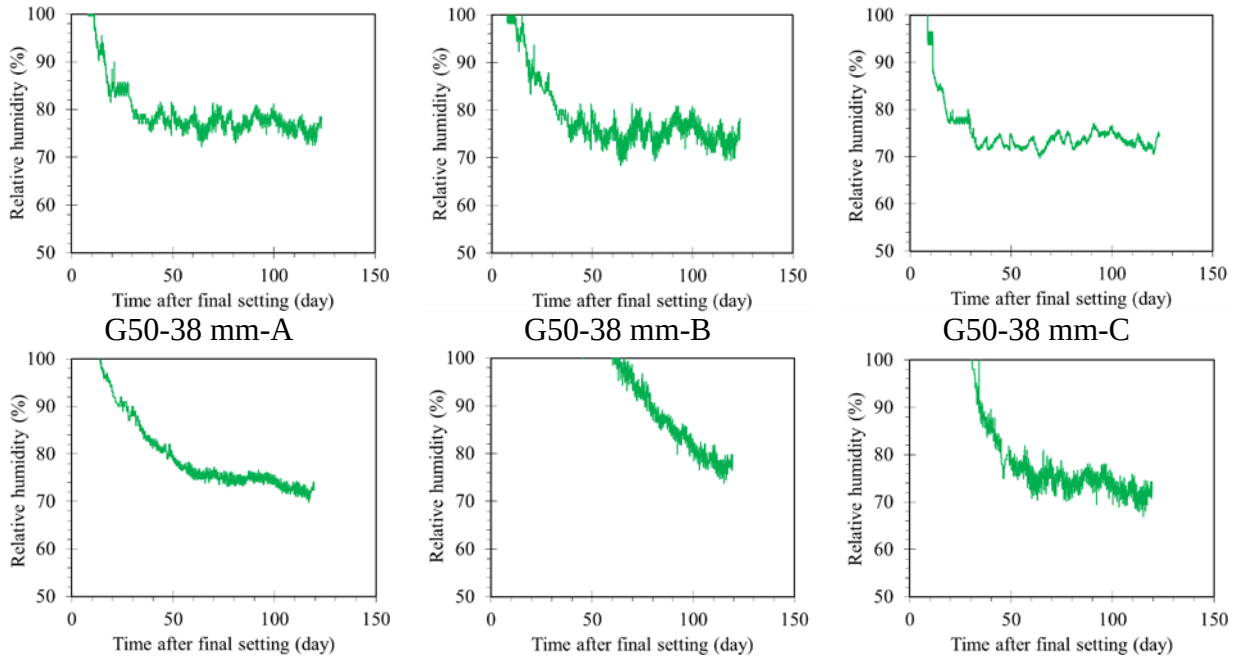

Figure 6-8 Relative humidity variations at the interface layer of different locations (Cont')

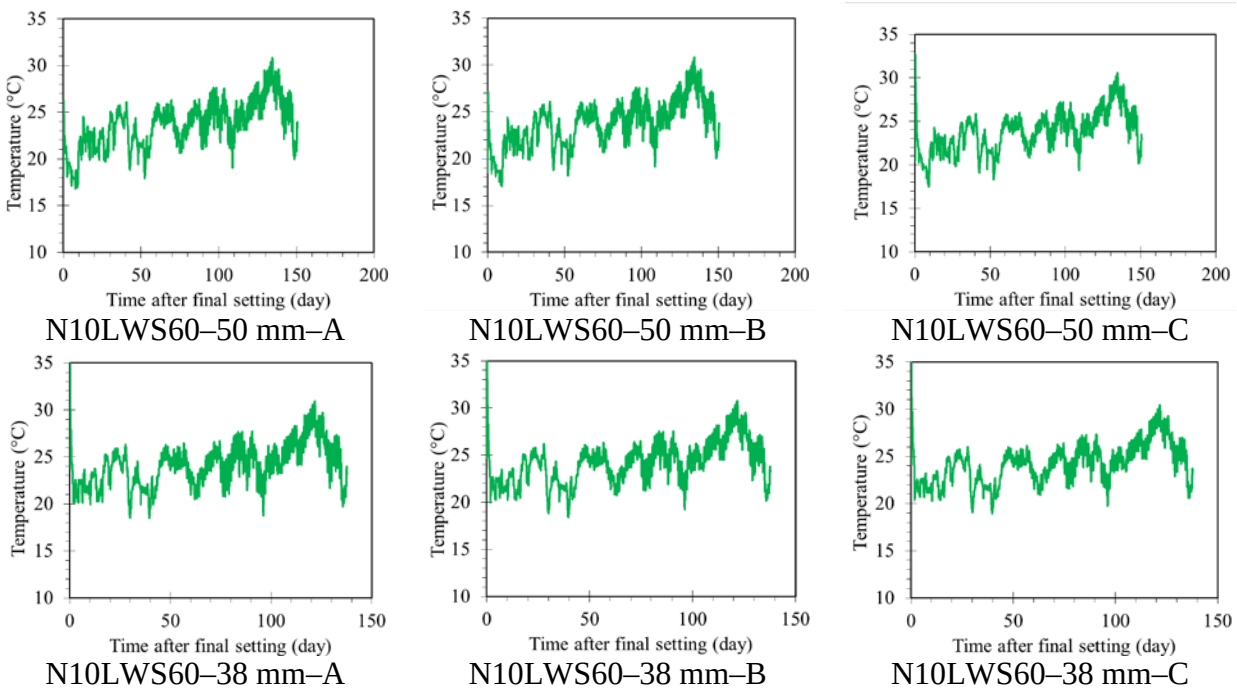

Figure 6-9 Temperature variations at the interface layer of different locations

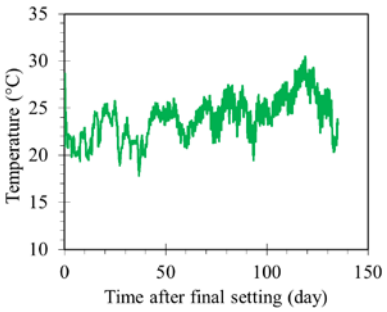

N10LWS60–25 mm–A

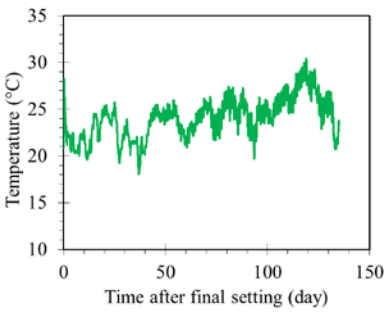

N10LWS60–25 mm–B

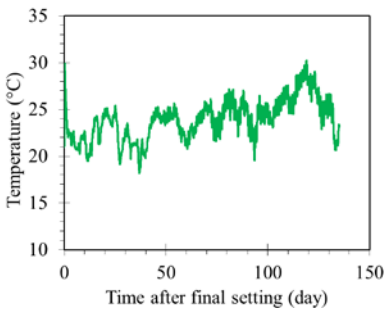

N10LWS60–25 mm–C

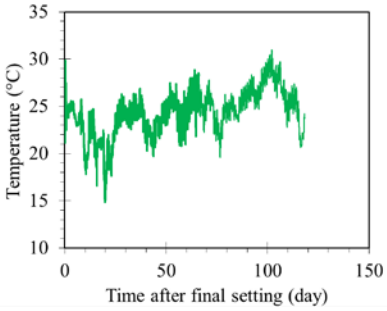

N10LWS60rep–25 mm–A

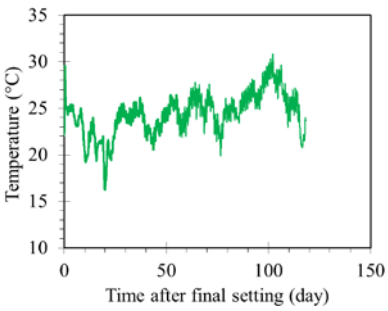

N10LWS60rep–25 mm–B

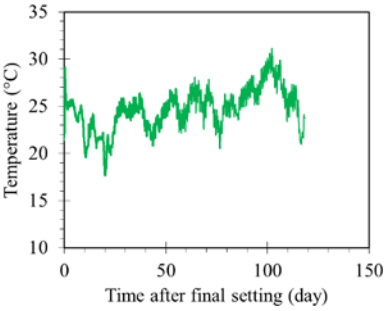

N10LWS60rep–25 mm–C

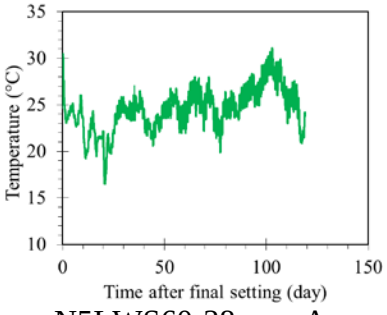

N5LWS60-38 mm-A

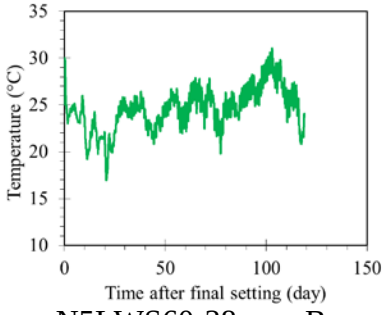

N5LWS60-38 mm-B

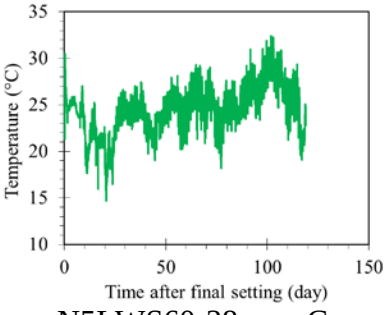

N5LWS60-38 mm-C

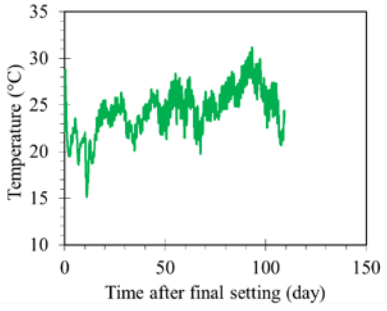

N5LWS60-25 mm-A

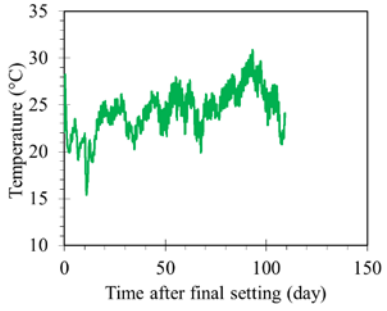

N5LWS60-25 mm-B

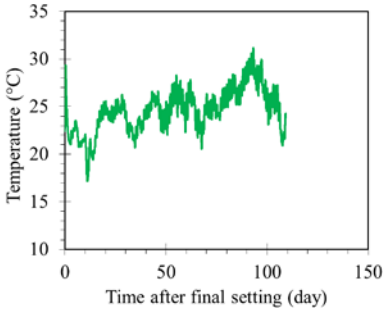

N5LWS60-25 mm-C

Figure 6-9 Temperature variations at the interface layer of different locations (Cont')

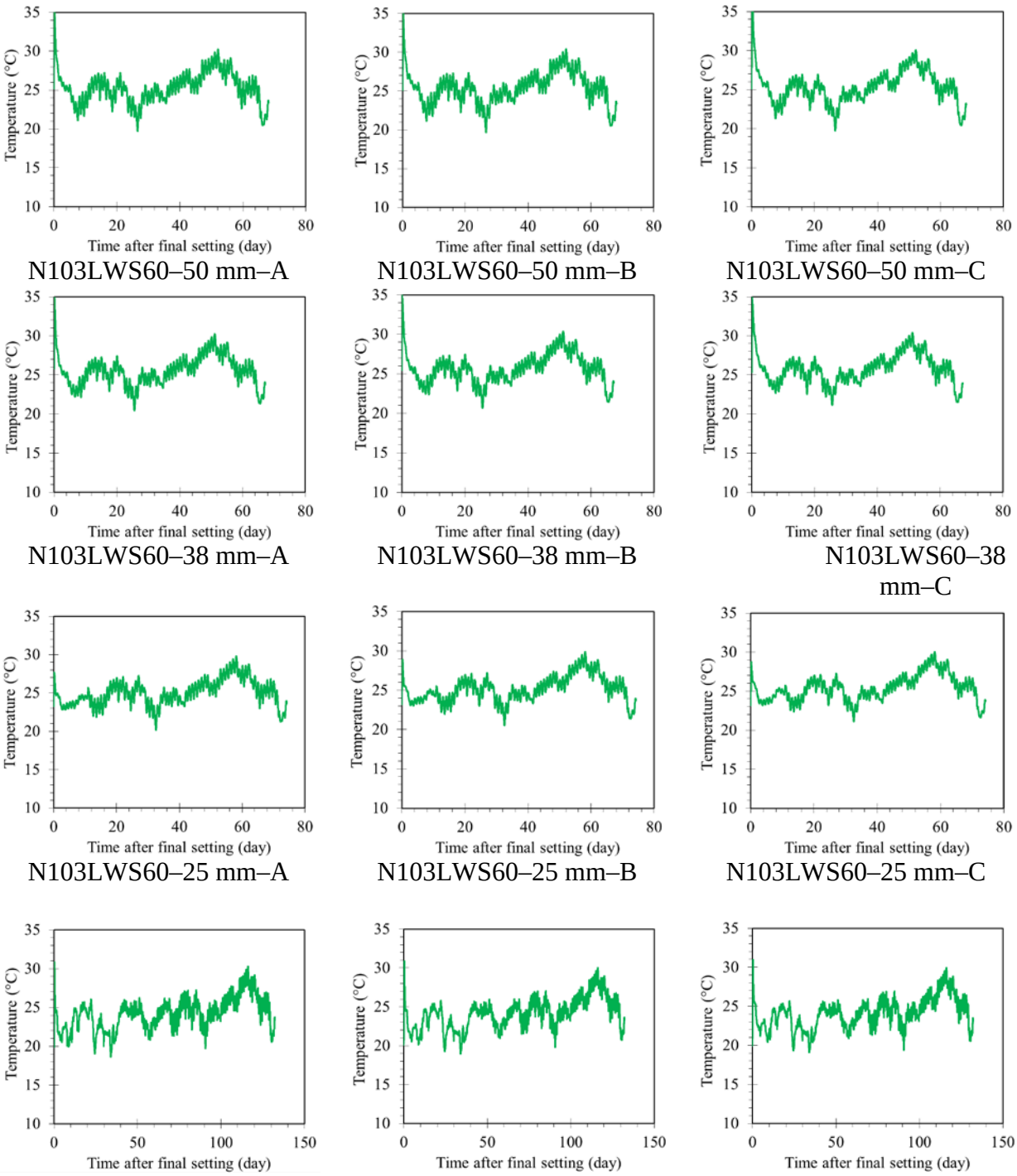

Figure 6-9 Temperature variations at the interface layer of different locations (Cont')

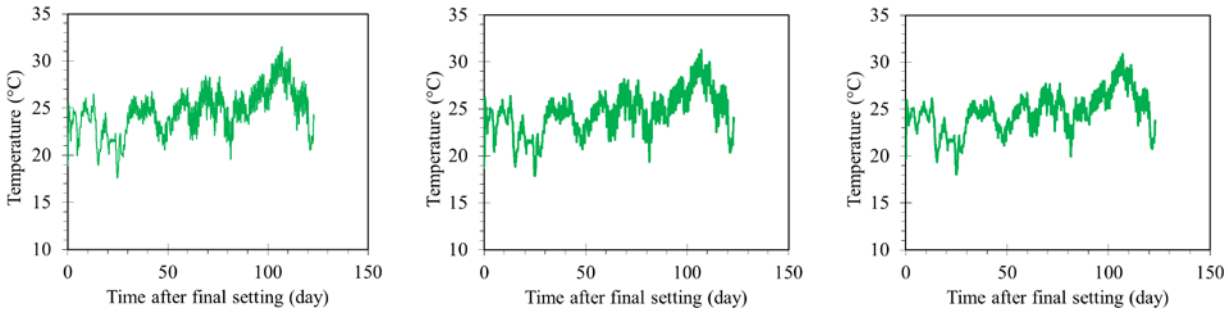

Figure 6-9 Temperature variations at the interface layer of different locations (Cont')

6.5. EVALUATION OF BOND IN THIS OVERLAYS

UHPC can be a promising material for accelerated rehabilitation of existing concrete infrastructures. However, there are some fundamental challenges of bond behavior and interplay with substrate material in overlay/repair systems. This study was carried out to assess the bond strength between UHPC and underlying concrete. The complications related to the use of conventional test methods were addressed. As a solution, a modified test method was proposed in order to evaluate the interface bond behavior properly.

6.5.1. Material Properties. The mixture design for substrate concrete was representative of a conventional bridge deck mix design used in the U.S. Type I/II Portland cement was used with a w/b of 0.4, and the maximum size for the coarse aggregate was 21 mm. For the UHPC mix design, the cementitious materials used in this investigation were Type III portland cement and GGBS with w/b of 0.20. Two local natural sands with 4.75 mm and 2 mm nominal maximum size of aggregate with the same specific gravity of 2.6 were employed. In addition, 2% of high strength steel fibers were incorporated by volume. The physical and chemical characteristics of cementitious materials used in this research are presented in Table 6-2. The mix proportions for both concretes are shown in Table 6-3

6.5.2. Casting and Preparation. Casting and preparation of concretes are explained as followings.

6.5.2.1 Normal-strength concrete (NSC) preparation. After the substrate concrete mixing process was completed, the concrete was placed into the relevant molds and was then covered with wet burlap and plastic sheet for 24 hr. The NSC was then

demolded and cured in lime-saturated water at 23 ± 2 ºC for additional 27 days. At the end of the desired moist-curing period, the surface preparation was applied using a sandblasting system, which has already proven to be the one of the best surface preparation methods for achieving a high bond strength (Tayeh et al., 2013).

Table 6-2 Physical and chemical characteristics of cementitious materials

Compositions	Portland cement (Type I/II)	Portland cement (Type III)	Fly ash (Class C)	GGBS
SiO_2 (%)	19.8	22	36.5	36.8
Al_2O_3 (%)	4.5	6	24.8	9.2
Fe_2O_3 (%)	3.2	3	5.2	0.76
CaO (%)	64.2	65	28.1	37.1
MgO (%)	2.7	3	5	9.5
SO_3	3.4	3.1	2.5	0.06
Na_2O (%)	-	-	-	0.34
Blaine surface area (m^2/kg)	385	400	465	590
Specific gravity	3.14	3.15	2.71	2.86
LOI (%)	1.5	1.5	0.5	-

Table 6-3 Mixture proportioning for UHPC and substrate concretes

Code	Cement (kg/m^3)	FAC (kg/m^3)	GGBS (kg/m^3)	Fine sand I (0-5 mm) ($/m^3$)	Fine sand II (0-2 mm) (kg/m^3)	Coarse sand (0-21 mm) (kg/m^3)	HRWR (l/m^3)	Water (l/m^3)	Steel fibers (kg/m^3)
UHPC	593	-	546	704	298	-	54.2	173.7	156
Substrate	323.3	81	-	791.5	-	1045.6	0.8	129.4	-

6.5.2.2 UHPC preparation. Before the UHPC overlay was placed, the NSC was submerged in water for a period of at least 24 hr to provide a saturated surface dry condition. The UHPC mixture was then prepared to be cast on top of the NSC. The casting was launched in one corner, allowing the mixture to flow to the other end due to its flowing, self-consolidating property. The specimens were then fully covered with wet

burlap and plastic sheets for 24 hr. They were then demolded and stored in lime-saturated water for curing purpose until the desired testing age.

6.5.3. Testing Procedures. Testing procedures of this study are explained as followings.

6.5.3.1 Pull-off test. The pull-off test was performed in compliance with ASTM C 1583. In order to achieve an adequate bond strength between the disk and the UHPC surface, the test area was abraded with a metallic wire brush to eliminate any contamination. A partial core with a diameter of 50 mm was then drilled through the composite system. The core bit was carefully positioned perpendicularly to the UHPC surface in order to eliminate any eccentricities during loading. After the cored area was cleaned by pressurized air, an aluminum disk with a diameter of 50 mm was adhered to the surface of the partial core using a rapid-setting epoxy. A high-precision spirit bubble level, as shown in Figure 6-10, was used to equalize the disk precisely to prevent any eccentricities during loading. After ensuring that the epoxy was properly set, the pull-off tester was attached to the disk. The device was adjusted so that the load was applied as perpendicularly as possible to the horizontal axis of the core. Eventually, the vertical tensile load was applied to the core by manually rotating a crank handle on the tester until the specimen reached a failure mode. Considering that it is difficult to manually apply the load at a constant rate, great care was taken to apply the load for each specimen at identical intervals of a specific duration using a timer. After the test was completed, all of the details such as the failure load, the mode and the fracture location were recorded.

6.5.3.2 Modified pull-off test. As mentioned earlier, a conventional pull-off test requires drilling a partial core into the composite specimen. The results of conventional test showed that the fracture locations in all tested samples were inside the substrate concrete. This can be attributed to some potential issues in the sample preparation process, such as during core drilling. Due to the significant difference in the stiffness of the UHPC, compared to underlying concrete, drilling operation can induce some stresses to the substrate concrete through the UHPC, and/or the drill core bit itself. These stresses are able to damage the interface-layer zone and/or the substrate concrete by creating micro cracks. Therefore, it was attempted to modify the sample preparation procedure in order to eliminate the possible problem causes through omitting the need for the coring

process. Thus, a thin piece of PVC tube was located on top of the substrate after surface preparation of substrate was carried out. Another modification that was implemented involved reducing the bonded area of the UHPC with NSC. The reason behind this adjustment was to lead stress concentration induced by tensile loading at the interface layer. To do this, an ultra-thin and hollow washer-like metal plate was used underneath the PVC tube as shown in Figure 6-11.

Figure 6-10 High-precision spirit bubble level

The main objective of these two aforementioned design modifications was to preserve the substrate concrete from any operation that could potentially induce damages. The underside of the metal plate was sealed with silicon to prevent any leakage of UHPC during casting. The tube was placed on top of the plate, and the outer circumference of the PVC tube was sealed using silicon as a glue to prevent any leakage. In order to eliminate the friction between the UHPC and the set-up, the whole inside surface of the set-up was lubricated with grease, prior to the UHPC casting, except for the surface of the substrate concrete where it was supposed to become in contact with the UHPC.

6.5.3.3 Modified splitting tensile test for UHPC overlay. A modification of splitting tensile test has been reported in the spirit of ASTM C 496 in order to investigate the bond performance of the composite system. However, there have been some challenges with this method. The main concern is the casting direction of concrete in testing specimen, which is different than the reality in field situations. The overlay/repair concrete in real conditions is cast and cured perpendicular to the substrate. This can have a negative influence on the bond strength, in particular, the way the fibers are positioned

with the substrate surface in fiber-reinforced concretes. Additionally, it is difficult to apply the uniformly-distributed load along the length of the bonded line in the cylinder during testing, as is the standard test method. Therefore, the test explained in ASTM C 1245 was modified in order to eliminate, or reduce, the aforementioned issues with the current modified splitting tensile tests. The standard test is intended to determine the relative bond between the different layers of roller-compacted concrete, or other hardened concrete, that is cast in multiple-lift forms. The relative bond strength is investigated in cylindrically-shape specimens where the bond surface is essentially normal to the longitudinal axis at mid-length. The test consists of using a point load test at the joint between the two materials, as presented in Figure 6-12. The sample is confined by small barrier walls that have been fabricated on the lateral sides of the specimens in order to preserve the specimen from any loading eccentricities caused by slipping from its original position. A splitting tensile stress normal to the bond surface is produced by applying a point load at the joint. Several 100 × 200 mm cylinders were used to determine the bond strength. First, conventional concrete was cast up to the halfway mark of each cylinder. The specimens were then demolded after 24 hr and water-cured for 14 days. At the end of the curing, the top surface of the specimens were sandblasted to ensure of having adequate bond between the concretes. Afterward, the specimens were washed with a high pressure water jet to remove all of the dirt and contamination. It was assured to have a saturated surface dry condition before casting the UHPC, which is required for a better bond between the two layers. Then, the empty half of the cylinders were filled with UHPC. After 24 hr maintaining the specimens under we burlap and plastic sheet, demolded composite specimens were then water-cured for an additional 27 days. At the desired testing age, the cylinders with two layers were subjected to a point loading, using the test assembly setup that was fabricated for the point loading. During testing, the cylinders were completely fixed without any movement in both horizontal and vertical directions. The load was applied in the vertical direction directly onto the interface layer, and the cylinder was placed firmly on one point on the bottom support to ensure pure tension without any bending movement.

6.5.4. Results and Discussion. After the aforementioned pre-test preparation procedures were completed for each test, all of the specimens were tested. The failure stress and mode of fracture were determined after each test, as the fracture mode can reveal crucial details about the bond performance.

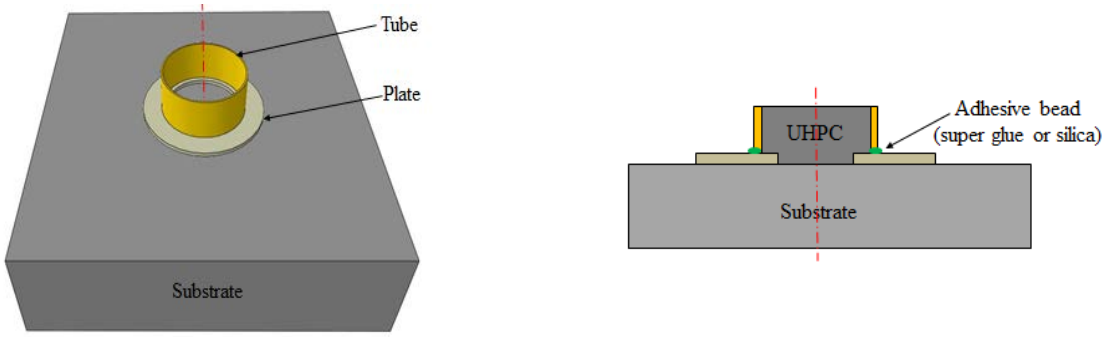

Figure 6-11 Schematic illustration of modified pull-off test

6.5.4.1 Mechanical properties of UHPC and NSC. In order to gain a better understanding of the differences in the properties of the two concretes involved in this investigation, related tests were conducted such as compressive strength, splitting tensile strength, flexural performance, and modulus of elasticity. The test results are presented in Table 6-4 for UHPC as overlay and NSC as substrate. The results indicated that the properties of the two concretes significantly differed from each other, as expected. The compressive strength at 1 and 28 days for UHPC were 64 and 124 MPa, which were 197% and 175% higher than those of NSC, respectively. For the 28-day tests, the differences were 233% for the splitting tensile strength and 43% for the modulus of elasticity. Furthermore, the flexural performance for the UHPC with 51.5 kN-mm was higher than NSC.

6.5.4.2 Pull-off test. The pull-off tests were carried out on a composite slab system with 280 × 280 mm^2, UHPC on NSC. The investigated thicknesses of UHPC were 6, 12, 19 and 25 mm. The tests were performed on the top side of the NSC slab itself in order to obtain an understanding about the differences in the results in case the fracture mode occurred in the substrate section. The bottom side of the substrate was also tested in order to discern the effect of the concrete casting direction on the pull-off test results and to learn more about possible segregation. The results are presented in Table 6-

5, as the displayed tensile stresses are the average of the number of tested samples indicated in the Table. Different statuses of fracture modes for different thicknesses are shown in Figure 6-13.

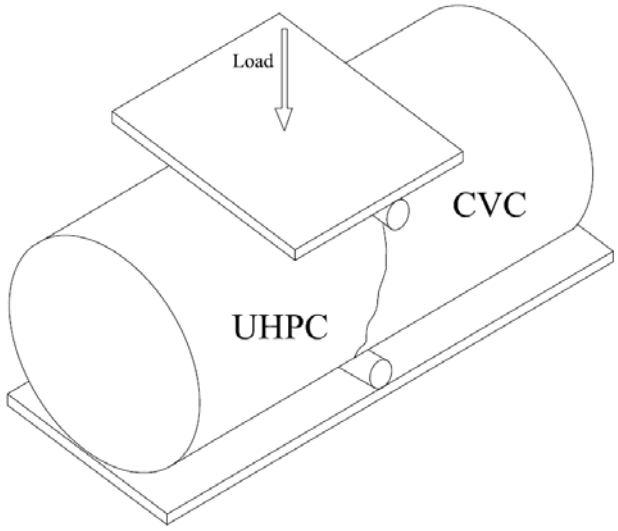

Figure 6-12 Schematic of set-up for Modified splitting tensile test

Table 6-4 Mechanical properties of UHPC and substrate concrete

Tests	NSC				UHPC			
	1-day	COV (%)	28-day	COV (%)	1-day	COV (%)	28-day	COV (%)
Compressive strength (MPa)	21.5	3.9	45	2.1	64	8	124	3.5
Splitting Tensile Strength(MPa)	-	-	3.3	7.5	-	-	11	1.5
Modulus of elasticity(GPa)	-	-	35	3.4	-	-	50	3.2
Flexural (kN-mm)	-	-	3.2	3.9	-	-	51.5	2.6

Table 6-5 Summary of pull-off tests on composite system

Samples	Number of Samples	pull-off tensile stress	COV (%)	Fracture mode
UHPC	3	5	6.2	N.A.
Composite (6 mm)	5	0.45	27.5	A
Composite (12 mm)	5	0.5	41.6	A
Composite (19 mm)	5	0.45	44.8	A
Composite (25 mm)	5	0.52	67.4	A

In cases of sole systems (NSC slab), as shown in Figure 6-13f, there was no significant difference between the results of two tests on top and bottom sides. This can mean that the casting direction had no meaningful influence on test results. It also implies that the inside texture of substrate concrete was uniform having no segregation. The same tests were attempted on the UHPC itself, but fracture mode D as shown in Figure 6-13e, failure plane in the epoxy material, always took place due to the greater stiffness of UHPC. Results indicated that all of the composite system failures occurred inside the substrate, as shown in Figure 6-13a, b, c, d. This signified that the UHPC overlay and the bond at the interface layer were always stronger than the underlying concrete. As a result, the repair can be considered successful in terms of the interface bond quality. However, an accurate bond strength value between the two concretes cannot be achieved in this failure mode, particularly not if it is needed for simulation or design purposes. The observed fracture modes showed that the common issue with pull-off testing in UHPC cases occurred in this study as well, which was that the failure locations were inside the substrate. As shown, regardless of the overlay thickness, all tests in the composite systems showed failure mode A. More importantly, comparisons of the results between sole and composite systems exhibited a significant difference. The test results of the composite systems were significantly lower than those of the sole system. It is interesting that although the fracture of all specimens in the composite systems took place inside of the substrate, the results were lower than those of the substrate concrete in the sole system which had the same concrete and fracture mode. Since the core drilling and surface preparation process were the same for both the solo and composite systems, this could possibly be attributed to micro-cracks that occurred during the drilling process. In terms of the influence of the UHPC thickness, there was no meaningful trend between the different thicknesses. The maximum difference was 15.5% for UHPC with 25 mm, compared to 12 mm and 19 mm.

The COVs exhibited significantly high fluctuations in this test, ranging from 5% to 67%, which shows one of the major challenges with this test. These high range variations have also been reported by other researchers using similar methodologies. A COV of 39% was yielded in the pull-off testing performed by Bonaldo et al. (2005). In other research carried out by Robins and Austin (1995), COVs ranging from 8% to 40%

were reported. As a result, the outcomes of this research were in agreement with those in the literature, which indicates that the issue is common for this test. The COVs obtained from the testing of sole system (unit material), either UHPC or NSC, showed very low COVs compared to those of the composite systems. Consequently, it was proven that this cannot be due to the methodology or the equipment.

(a) Composite – 25 mm

(b) Composite – 19 mm

(c) Composite – 12 mm

(d) Composite – 6 mm

(e)UHPC – sole system

(f) Substrate – Sole system

Figure 6-13 Fracture modes for different pull-off tests on solo and composite systems

6.5.4.3 Modified pull-off test. The results from the modified pull-off tests are presented in Table 6-6. Two types of surface conditions were used to prepare the surfaces

of the specimens: virgin and sandblasted. These were used to investigate the general effect that surface preparation had on the fracture mode. Before the UHPC was cast, the virgin surfaces were prepared by carefully cleaning the surface of the specimens with pressurized air, and then it was cast in the saturated surface dry condition. The virgin specimen tests were carried out at 1, 3, 7, 14 and 28 days, but only the 28-day test was applied for the sandblasted samples.

As shown, the fracture mode for all virgin specimens was type B as they failed at the interface layer between the two concretes; whereas, in terms of the sandblasted cases, the mode was altered to type A which shows that the fracture occurred inside NSC. These results highlighted the effect of surface preparation on bond characterization in the interface layer of a composite system. The bond strength increased as the testing age increased, and the maximum strength was gained at 28 days, but that strength was still lower than the required minimum, according to ACI 546-06. In contrast to the virgin specimens, sandblasting the surface increased the bond quality and led to the fracture location being inside of the NSC. This implied that the bond performance was successful from a quality point of view, even though the bond strength value was still much lower than that of the virgin specimens and the limit recommended by ACI 546-06. This indicated the importance of obtaining the correct value of the bond strength in a laboratory testing, for design purposes, when needed for comparing with the standard values.

The results illustrated that the fracture mode should be taken into account when analyzing the data for the bond strength of composite systems. As shown, according to the bond strength values, the virgin specimens should have had better quality bond performance, but the fracture mode suggests that the conclusion was the opposite. It was interesting to observe fracture mode A in this test where the substrate was unaffected when the drilling process was eliminated. This showed the excellence and power of the bond strength that is attainable when UHPC is used. This is one of the unique characteristics of UHPC that assures it is a promising material for rehabilitation purposes.

In general, the results showed that the modified method significantly reduced the COV values. The minimum COV for the conventional pull-off test was 27.5%, whereas the maximum value for modified method was 22.5% with fracture mode A. It was even

less with the virgin specimens, which had fracture mode B varying between 2% and 4.5%.

Table 6-6 Results of modified pull-off testing on a composite system

Surface preparation	Testing age (day)	Number of Samples	Bond strength (MPa)	COV (%)	Fracture mode
Non	1	3	0.18	4.5	B
	3	3	0.78	2.1	B
	7	3	1.13	2.9	B
	14	3	1.27	2	B
	28	3	1.31	2.9	B
sandblasted	28	5	0.52	22.5	A

It is widely known that the ASTM standard pull-off test is an appropriate method for examining the quality of the bond performance in existing or rehabilitated composite system of concretes, according to the fracture mode occurrences with the aforementioned challenges. However, the current modified pull-off test can be a proper and simple alternative, especially in case of concrete with lesser stiffness differences, compared to UHPC, such as high performance concretes. Through this method, the bond strength value for design and simulation purposes is attainable in addition to the quality, even though it did not work for the case of UHPC in this study because of the significant differences in the MOE of the NSC. The other crucial benefit of this modified test method is that it eliminates the drilling process, which can induce possible damages at the bond interface layer and in the underlying concrete. As mentioned earlier, the main problem with the drilling process is that when the core bit passes through the paste to the aggregate, or vice versa, it can induce stresses due to the stiffness differences between these textures which can damage the ITZ structure by making micro cracks.

6.5.4.4 Modified splitting tensile test. The mean bond strength of the five specimens tested with this method, associated with the corresponding COVs, are presented in Table 6-7. The observations during and after tests showed that the initial rack started at the interface layer between the two concretes; however, the crack went through the NSC, as presented in Figure 6-14, which means the achieved fracture mode

was type A for all of the tested specimens. This indicates that the bond strength between the UHPC and NSC was greater than that of the NSC itself. Thus, there was an acceptable bond at the interface layer indicating the excellent quality of the UHPC bond characterization with the NSC. However, the bond strength values at the interface layer were not achieved, which was one of the main goals of the modification for this test, even though the low COVs were still obtained.

6.5.4.5 Modified UHPC debonding test. In order to overcome the aforementioned limitations and challenges that are inherent in the conventional testing methods for UHPC cases, a modified debonding test method was introduced. This test was designed with the intention of concentrating the stress at the interface layer between the UHPC and the substrate where the fracture can occur. Additionally, this concentration can make it possible to obtain the bond strength values with reasonable COVs, which are suitable and reliable enough to use for simulation and/or designing purposes. Besides, it was attempted to ensure that the test condition matches the reality of the field as closely as possible.

Table 6-7 Results of UHPC debonding test on composite system

Samples	Bond strength (MPa)		COV (%)	Fracture mode
	Each sample	average		
1	2.5			A
2	3.2			A
3	2.9	3.0	2.1	A
4	3.8			A
5	2.5			A

In this method, the cone shape of the UHPC was designed in order to reduce the contact surface between the UHPC and NSC, as shown in Figure 6-15. First, the underlying concrete was cast into a cylindrical mold with a diameter of 130 mm and a height of 75 mm, and it was moist-cured for 28 days. The surface of the substrate was then sandblasted. Before casting the UHPC, the surface of specimens were carefully cleaned with pressurized air, and then a saturated surface dry condition was prepared. During casting process, a magnetic corner post levels, with a corner mount design that can read two sides for quicker and easier leveling, were used to prevent any possible

eccentricities and to maintain the molds in the exact vertical direction. After properly establishing the mold on the top surface of the substrate concrete, the UHPC was then cast and allowed to stay in the mold for 24 hr under wet burlap that was fully covered with a plastic sheet. The composite specimens were then demolded, after which they underwent moist curing with limed-saturated water for an additional 27 days. After the curing, the specimens were ready to test at the desired testing age. Therefore, both the top and bottom ends were sandblasted in order to provide a coarser surface to have the highest bond with the epoxy and the steel plate of the test set-up. Pressurized air was then used to clean and dry the sandblasted areas prior to bonding the top and bottom plates to the end surfaces of the composite system, using a fast-setting epoxy. Care was taken to ensure that the disk was accurately leveled, using a high-precision spirit bubble level, in order to prevent the potential loading eccentricities. Additionally, three pieces of angle irons were already attached to the disk to make sure the specimen was positioned at the center of the steel plate, as shown in Figure 6-16. The same procedure was applied for the opposite side after the epoxy hardened. To do the test, the prepared system was placed in the tension testing machine to ensure that it would have a full bite in the grips. The test was launched by applying the tension load to the specimen until it fractured. The ultimate load and the failure mode was recorded after the test was completed.

The results of the UHPC debonding tests are presented in Table 6-8. The results indicate that the fracture mode for all of the tests was mode B, indicating that the failure took place right at the interface layer between the UHPC and the underlying concret. Furthermore, the results of the bond strength signified that the performance of the bond between the UHPC and substrate concrete for all of the tests were successful, as the tensile bond strength exceeded the recommended 28-day minimum proposed by ACI 546-06. On the other hand, the results showed negligible variations, which resulted in very small COVs. This implied that the designed test method met the defined goals by leading the fracture location to the interface layer and decreasing the COV as much as possible.

Figure 6-14 Test set-up and fractures mode for modified splitting tensile test

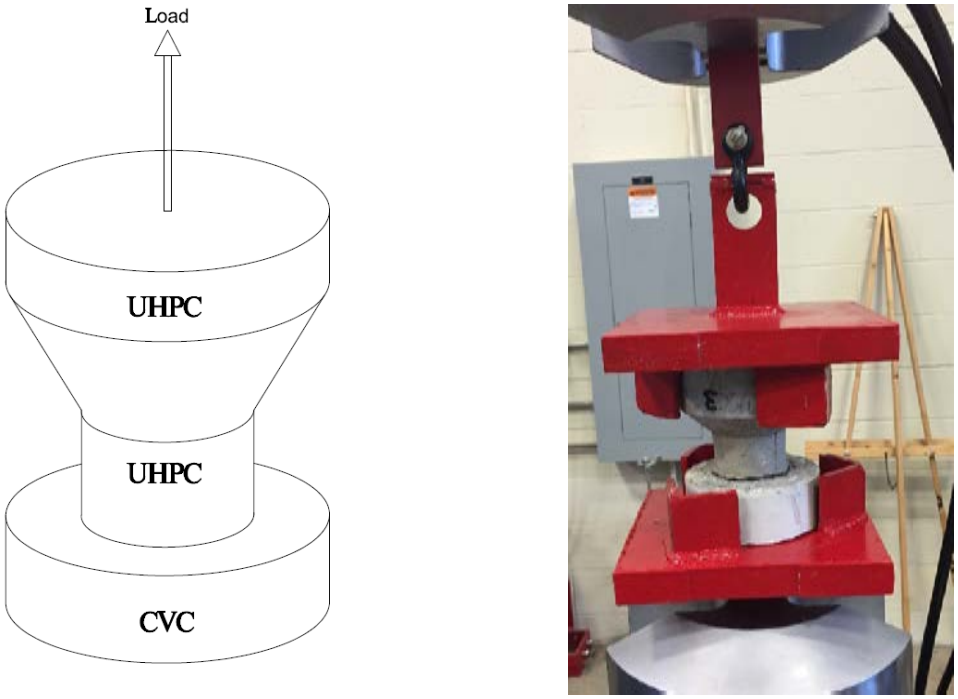

(a) (b)

Figure 6-15 Illustration of test set-up for UHPC debonding test

Table 6-8 Results of UHPC debonding test on composite system

Samples	Bond strength (MPa)		COV (%)	Fracture mode
	Each sample	Average		
1	2.3			B
2	2.2			B
3	2.2	2.22	1.39	B
4	2.1			B
5	2.3			B

Figure 6-16 Test set-up and fracture mode for UHPC debonding test

6.5.5. Summary. The results of shrinkage deformation were shown to be a function of UHPC mix design, location, and overlay thickness. The expansion rate decreased with increase in UHPC overlay thickness from 25 mm to 50 mm. For example, the EXC10LWS60 mixture with 25, 38, and 50 mm thicknesses exhibited maximum expansion of 820, 630 and 500 μm/m, respectively. After the EXC10LWS60 mixture, the EXC5LWS60 mixture showed the highest expansion values of 300 and 220 μm/m, respectively. Visual and microscopic inspections of UHPC overlays at the surface and interface layer showed no signs of cracking nor debonding after 150 days of casting. It should be noted that the variations of deformation are being monitored over time and the results will be updated.

UHPC is a different material compared to others due to its outstanding qualities in terms of durability and strength, which make it an interesting alternative as a fast-construction/rehabilitation material. In order to completely utilize these advantages,

distinctive knowledge is required for the production, construction and design of UHPC. In the current study, it was attempted to develop a fundamental understanding of the methodologies and the corresponding challenges that come with using UHPC as an overlay/repair material in terms of bond performance. The step-by-step experimental program not only highlighted the problems with determining the bond strength value of the UHPC, but also contributed to the development of a new test method as a solution for the discussed challenges. The investigation confirmed that the conventional standard test methods are not appropriate for UHPC applications, and that designing new test methods is inevitable. The results from this study indicated that outstanding bonding between UHPC and the underlying concrete can be reached by preparing the surface appropriately and by not using any bonding agents, such as epoxies or latex emulsions, which are commonly used in overlay/repair materials. The results also illustrated that the bond performance of UHPC appears to be adequate for overlay applications, and that the bond is not a limiting factor when considering the use of UHPC as an overlay. At the end of the study, the modified test method responded to the challenges related to characterizing the interfacial bond between the UHPC and the substrate concrete. The reliable bond strength of UHPC, with an acceptable coefficient of variance, is achievable by using this method for design and simulation purposes.

7. SUMMARY AND CONCLUSIONS

The research presented in this dissertation was developed in several directions to develop a cost-effective UHPC for bonded bridge deck overlays. Based on the test results from this research, the following conclusions can be drawn:

7.1. OPTIMIZATION AND PERFORMANCE OF COST-EFFECTIVE UHPC

A mix design methodology is presented for producing cost-effective UHPC with high-volume SCMs and conventional concrete sand. Based on the reported studies, the following conclusions can be drawn:

The MWC can first be used as an indicator of the packing density of binders in wet condition to narrow down binder systems and reduce the required number of experiments. The binder composition of UHPC can then be optimized with consideration on the HRWR demand, rheological properties, MWC, RWD, and compressive strength properties. A radar chart can be then employed for the analysis. Based on this approach the following binder combinations were selected: G50, G50SF5, FAC60, and FAC40SF5.

The second step is to determine the preliminary w/cm based on the 28-days compressive strength and HRWR demand value for paste mixtures prepared with the optimum binder combinations with w/cm values of 0.18-0.23. The optimum value for the selected binders was 0.20. The modified Andreasen and Andersen model can be used to optimize sand gradation. In this study, 70% river sand and 30% masonry sand were selected to achieve the highest packing density.

The next step involves the determination of the binder-to-sand volume ratio (V_b/V_s). Mortar mixtures made with the selected w/cm and G50SF5 binder were prepared with V_b/V_s values of 0.6, 0.7, 0.8, 0.9, 1.0 and 1.3. Based on flow properties and 28-days compressive strength, the optimum V_b/V_s was determined to be 1.0.

The optimum fiber content for the UHPC is experimentally determined given the flowability and flexural properties of UHPC made with various fiber contents. For the steel fibers considered in this study, 2% fiber volume was selected.

For the UHPC mixtures prepared with the various binder systems and optimized mixture proportioning, the UHPC mixtures were self-consolidating, stable, and had 28-

days compressive strengths of 120-125 MPa under standard curing condition. The strength can reach up to 178 MPa by applying heat curing at a maximum temperature of 90 °C for one day followed by 7-days moist curing. For the selected UHPC mixtures, the 28-days splitting tensile strength, modulus of elasticity, flexural strength, and toughness (T150) were 11.6-14.3 MPa, 48.8-51.6 MPa, 20.2-21.3 MPa and 50 ± 1.5 kN mm, respectively.

The designed UHPC mixtures exhibited relatively low autogenous shrinkage and drying shrinkage. The G50 mixture had the lowest autogenous and drying shrinkage of 255 lm/m at 28 days and 55 lm/m at 98 days, respectively. All tested UHPC mixtures exhibited a very high electrical resistivity and excellent frost durability.

The unit cost per compressive strength of the UHPC mixtures designed with high volume of SCMs and concrete sand can range between 4.1 and 4.7 $/m3/MPa. The mixture FAC60 was the most cost-effective mixture, which also developed better workability and lower unit cost per compressive strength of 3.7 ($/m3)/MPa than other mixtures.

7.2. ROBUSTNESS OF UHPC AT DIFFERENT CASTING AND CURING TEMPERATURES

The HRWRA demand increased regardless of the investigated UHPC mixture with the increase in temperature. UHPC made with FA required less HRWRA compared to that with GGBS and the reference mixture (25% SF). The FA60 mixture with 0.46% HRWRA at 10°C and G50SF5 mixture with 1.58% HRWRA at 30°C exhibited the lowest and highest HRWRA demands, respectively. Mini V-funnel flow time decreased by up to 45%, with the increase in temperature (10 to 30 ºC). Increasing the temperature accelerated the initial and final setting times by up to 4.5 and 5 hr, respectively.

Yield stress increased by up to 55% and plastic viscosity decreased by up to 45% with increasing the temperature from 10 to 30 ºC. UHPC made with GGBS exhibited the highest values of viscosity and the lowest yield stresses compared to the reference mixture and UHPC made with FA.

Temperature variation can significantly affect the development of mechanical properties of UHPC. Results indicated that mechanical properties of different UHPC improved with the increase in temperature. Increasing temperature from 10 to 30 ºC

improved the 28-d compressive strength of the G50, G50SF5, FA60, and FA40SF5 mixtures by 65%, 70%, 45%, and 40%, respectively. The flexural toughness (T150) enhanced by up to 65% with the increase in temperature where all mixtures had their minimum and maximum toughness at 10 and 30 ºC, respectively.

Increasing the temperature from 10 to 30 ºC led to increase in autogenous and drying shrinkage by up to 60% and 70%. UHPC made with GGBS or FA exhibited a reduction in autogenous and drying shrinkage by up to 300 and 350 μm/m, respectively, compared to the reference mixture at 56 d.

UHPC made with FAC and GGBS were more robust than the reference mixture made with 25% SF. In general, the FA60 and FA40SF5 mixtures resulted in greater robustness than other UHPC mixtures.

7.3. COUPLED EFFECT OF SATURATED LIGHTWEIGHT SAND AND SHRINKAGE-MITIGATING ADMIXTURES IN REDUCING SHRINKAGE OF UHPC

The incorporation of LWS at replacement levels of 25%, 40%, or 60% combined with 7.5% EXC resulted in drop in autogenous shrinkage compared to the G50 reference mixture. The expansion increased with increasing the LWS content where UHPC with LWS of 25%, 40%, and 60% led to 80 μm/m, 300 μm/m and 375 μm/m maximum expansion, respectively.

In combined system of LWS and EXC with different curing conditions, increasing LWS and EXC replacement levels along with extending moist curing significantly improved the expansion value during moist curing and shrinkage reduction during air-drying after. The EXC10LWS60 mixture had the best performance compared to other investigated UHPC mixtures, reaching the highest expansion of 900 μm/m, in the 7MC condition ending up with 105 μm/m after 91 d.

Moist-curing enhanced compressive strength. Regardless of the shrinkage-mitigating admixture, the highest compressive strength was obtained for the EXC7.5LW60 mixture (136 MPa) subjected to 7 d of moist-curing (7MC).

The combined incorporation of either EXC, EXM, or SRA with 60% LWS resulted in slightly decrease in compressive strength compared to the LWS60 mixture. The increase of the replacement level of EXC (5-10%), EXM (5-7%), and SRA (1.5-3%)

slightly decreased the strength from 140 to 130 MPa, 128 to 122 MPa, and 138 to 133 MPa, respectively, at 91 d of the 7MC condition.

The incorporation of LWS from 25% to 60 % resulted in considerable drop in HRWR demand from 1.23% to 1.05 % to ensure a fixed mini-slump flow. The HRWR demand of the investigated mixtures ranged between 0.97% and 2.37% with the lowest and highest values corresponding to the EXC5LW60 and EXC7.5 mixtures, respectively.

The coupled use of 60% LWS with different replacement values of EXC, EXM, and SRA showed a positive effect on reducing the mini-slump and mini-V-funnel loss compared to the G50 mixture. The use of LWS decreased loss in V-funnel time; 75% EXC with 25%, 40%, or 60% of LWS had the V-funnel flow time losses of 9, 7 and 4 sec, respectively.

The combined use of either EXC, EXM, or SRA with LWS is shown to significantly shorten the setting time. The initial and final setting times of the EXC7.5LW25 were 3.5 and 6 hr compared to 9 and 16 hr, respectively, for the EXC7.5 mixture.

7.4. UHPC PERFORMANCE AS BONDED OVERLAY

The findings of UHPC performance as bonded overlay are explained as followings.

7.4.1. UHPC Performance as Bridge Deck Overlay. The results of shrinkage deformation were shown to be a function of concrete mix design, location, and UHPC overlay thickness. As expected, slab made with 10% EXC10 combined with 60% LWS with 25 mm in thickness exhibited the highest expansion with 820 μm/m. On the other hand, UHPC overlay made with 50% GGBS without any LWS and EX ended up with total shrinkage of 100 μm/m after 130 days. Visual and microscopic inspections of the surface of UHPC overlays as well as interface layer at the edges of the slabs showed no signs of cracking nor debonding after 150 days of casting. It should be noted that the variations of deformation are being monitored over time and the results will be updated over time.

7.4.2. Bond Performance of UHPC Overlay. The results from this study indicated that outstanding bonding between UHPC and the underlying concrete can be

reached by preparing the surface appropriately and by not using any bonding agents, such as epoxies or latex emulsions, which are commonly used in overlay/repair materials. The results also illustrated that the bond performance of UHPC appears to be adequate for overlay applications, and that the bond is not a limiting factor when considering the use of UHPC as an overlay. At the end of the study, the new test method responded to the challenges related to characterizing the interfacial bond between the UHPC and the substrate concrete. The reliable bond strength of UHPC, with an acceptable coefficient of variance, is achievable by using this method for design and simulation purposes.

7.5. FUTURE RESEARCH

Based on the scope and derived conclusions and findings from the present research work, the following aspects are recommended for the potential future investigations:

- In this study, the performance of the developed UHPC mixtures for bonded bridge deck overlay were evaluated through laboratory scale investigation and validated on concrete pavement sections. However, for further validation, the performance (i.e., deformation and structural behavior) of such concretes should be verified under actual field conditions, such as pavement or bridge deck applications.
- As mentioned earlier, the performance of UHPC overlay were evaluated on pavement sections indoor without taking humidity and temperature variations caused by seasonal fluctuations into consideration. However, for further validation, the slabs can be exposed to a real outdoor environment in order to evaluate the performance under seasonal environmental variations.
- As an accelerated evaluation for aggressive environmental conditions, the fabricated slabs can be investigated under freeze/thaw cycling in order to monitor the performance of UHPC overlay in terms of debonding, delamination, and crack propagation.
- Pull-off test can be conducted on the slabs to assess the bond performance at the interface layer to compare with stresses.

- The structural performance of fabricated slabs can be evaluated under external loading.
- Numerical simulations (FEM) should be conducted based on experimental investigations. It is believed that such model can be quite useful for studying the effect of various parameters on the stress development and crack response.

APPENDIX: UHPC OVERLAY DELAMINATION DETECTION USING FIBER OPTIC SENSOR

This study develops a delamination detection system for smart UHPC overlays using a fully distributed fiber optic sensor. Three 450 mm (length) × 200 mm (width) × 25 mm (thickness) UHPC overlays were cast over an existing 200 mm thick concrete substrate. The initiation and propagation of delamination due to early-age shrinkage of the UHPC overlay were detected as sudden increases and their extension in spatial distribution of shrinkage-induced strains measured from the sensor based on pulse pre-pump Brillouin optical time domain analysis. The distributed sensor is demonstrated effective in detecting delamination openings from microns to hundreds of microns. A three-dimensional finite element model with experimental material properties is proposed to understand the complete delamination process measured from the distributed sensor. The model is validated using the distributed sensor data. The finite element model with cohesive elements for the overlay-substrate interface can predict the complete delamination process. It should be noted that this research was conducted in collaboration with Dr. Chen and his student Dr. Bao Yi published in the smart materials and structures journal (Bao et al., 2017).

1. DISTRIBUTED FIBER OPTIC SENSORS

1.1. Single Mode Optical Fibers

Light wave is guided in an optical fiber through total internal reflection. An optical fiber is typically packaged with protective coatings to prevent the fragile fiber from damage. In this study, two telecommunication-grade optical fibers are adopted. As illustrated in Figure 1, they are single mode optical fibers with dual-layer (2C) and three-layer (3C) coatings, respectively. The 2C fiber is a concentric cylindrical composite of a silica core of 8.2 μm in diameter, a silica cladding of 125 μm in outer diameter, an inner polymer coating of 190 μm in outer diameter, and an outer polymer coating of 242 μm in outer diameter. The inner coating is a soft, rubbery material that functions as a cushion of the optical fiber for mechanical loadings. The outer coating is a stiff material to protect the fiber from abrasion and environmental exposure (Chen at al. 2012). The inner and outer coatings are sequentially applied in a liquid form as the glass fiber was drawn, and

exposed to ultraviolet light for curing. The 2C fiber is small in cross section and particularly prone to shearing action. For this reason, the 3C fiber contains an additional protective polymer coating (buffer) of 880 μm in outer diameter outside the 2C fiber. The additional coating can significantly enhance the shear strength of the optical fiber (Chen at al. 2012), thus ensuring the survival of fiber sensors when deployed in field operations.

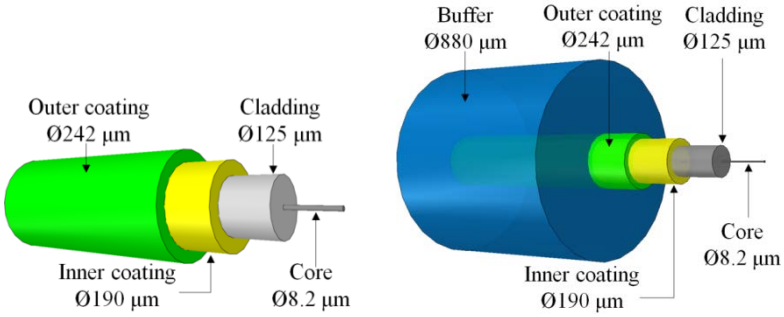

(a) (b)

Figure 1- Distributed fiber optic sensors: (a) 2C, (b) 3C.

1.2. Working Principle of PPP-BOTDA

Electromagnetic wave in an optical fiber generates acoustic waves through electrostriction effects, periodically altering the molecular structure and thus refractive index of silica glass. In analogy with FBG, the periodical modulation of refractive index that moves at acoustic velocity results in back-scattering of light, referred to as Brillouin scattering (Bao and Chen, 2016). The Brillouin scattering is nonlinear with a frequency shift in GHz or Brillouin shift. In the conventional BOTDA, a pump pulse and a probe continuous wave are injected from the two ends of an optical fiber and propagate in opposite directions. The Brillouin scattering process associated with the pump wave becomes stimulated when the intensity of the probe light exceeds a threshold value. If the frequency difference between the pump and probe waves matches the anti-Stokes frequency of the optical fiber, Brillouin gain takes place. In this case, energy is transferred from the acoustic waves to the probe signal.

In comparison with the conventional BOTDA, PPPBOTDA takes advantage of a pre-pump pulse, which greatly enhances the spatial resolution by stimulating acoustic waves before the narrow bandwidth pump signal arrives, as illustrated in Figure 2

(Kishida and Li, 2006). With a narrow pulse of 0.2 ns, a 20 mm spatial resolution can be achieved with 15 με and 0.75 °C accuracies for strain and temperature measurements, respectively (Kishida and Li, 2006). The Brillouin frequency shift, denoted by $\Delta\nu_b$, can be expressed as:

$$\Delta\nu_b = C_\varepsilon \Delta\varepsilon + C_T \Delta T \quad (1)$$

where C_ε and C_T denote the strain and temperature coefficients, respectively, evaluated at the reference strain and temperature; $\Delta\varepsilon$ and ΔT denote the strain and the temperature changes from their reference values, respectively.

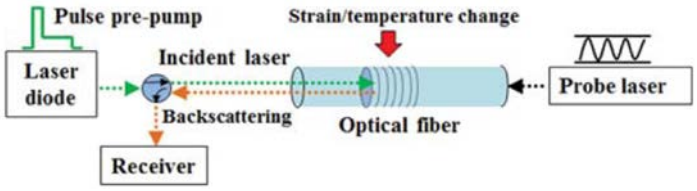

Figure 2- A typical PPP-BOTDA system (Kishida and Li, 2006)

1.3. Sensor Calibration

In this study, PPP-BOTDA measurements were taken using a Neubrescope (model: Neubrex NBX-7020). Data were sampled every 10 mm along the optical fiber so that the Brillouin frequency shifts between two points spaced at least 20 mm apart can be distinguished. The strain sensitivity coefficients of the 2C and 3C sensors were calibrated under uniaxial tension using a low-capacity load frame (load capacity: 100 N) at room temperature. The Brillouin frequency shift increased linearly with the applied strain with a slope of 0.0543 and 0.0466 MHz/με for the 2C and 3C sensors, respectively.

2. EXPERIMENTAL STUDIES

2.1. Materials

The substrate and overlay were cast with conventional concrete (CC) and UHPC, respectively, as specified in Table 1. For the CC, the water-to-cement ratio was set to 0.40 and coarse limestone aggregates with a maximum size of 21 mm were used (ASTM C136). For the UHPC, part of the cement was replaced by granulated blast slag to set an overall w/b of 0.20. During the mixing of UHPC, a polycarboxylate high range water

reducer was added to enhance the flowability of UHPC with a slump flow of 280 ± 10 mm measured in accordance with ASTM C230/C230M. Micro steel fibers, 13 mm in length and 0.2 mm in diameter, were used to enhance the tensile properties of UHPC.

Table 1- Mixture compositions

Materials	CC	UHPC
Type III cement (kg/m^3)	243	593
GGBS (kg/m^3)	-	546
Coarse aggregate (kg/m^3)	1046	-
River sand (0-5 mm) (kg/m^3)	792	704
Masonry sand (0-2 mm) (kg/m^3)	-	298
High-range water reducer (l/m^3)	0.8	54
Water (kg/m^3)	218	174
Steel fibers (kg/m^3)	-	156

2.2. Material Properties

The compressive and tensile properties of the CC were evaluated in accordance with ASTM C39 and ASTM C496, respectively. Five cylinders were prepared for each type of tests. The average compressive and splitting tensile strengths at 56 d (days) were 50.5 and 3.6 MPa, respectively. The average elastic modulus and Poisson's ratio at 56 d were 40.5 GPa and 0.20, respectively. The average density of the CC was 2500 kg m^{-3}.

Three UHPC prisms were prepared and their shrinkage was measured in accordance with ASTM C596. The final setting (time zero) of the UHPC was determined at 17 hr after casting by penetration needle tests in accordance with ASTM C403/C403M. Figure 3a presents the (average ± standard deviation) shrinkage strain as a function of elapsed time after the final setting. The average strain increased from 325 με at 1 d to 810 με at 21 d and then became stabilized afterwards. It should be noted the UHPC mixture used in this study was not optimized to minimize shrinkage, and efforts are underway by authors to reduce the shrinkage of UHPC for overlay application. The compressive and splitting tensile strengths were evaluated in accordance with ASTM C109/C109M and ASTM C307, respectively. As shown in Figure 3b, the average compressive strength increased from 64 MPa at 1 d to 124 MPa at 28 d. The average tensile strength increased from 3.1 MPa at 1 d to 11.0 MPa at 28 d. The elastic modulus and Poisson's ratio were

respectively determined to be 51 GPa and 0.18 in accordance with ACI 318. The density of the UHPC at 28 d was 2650 kg m^{-3}.

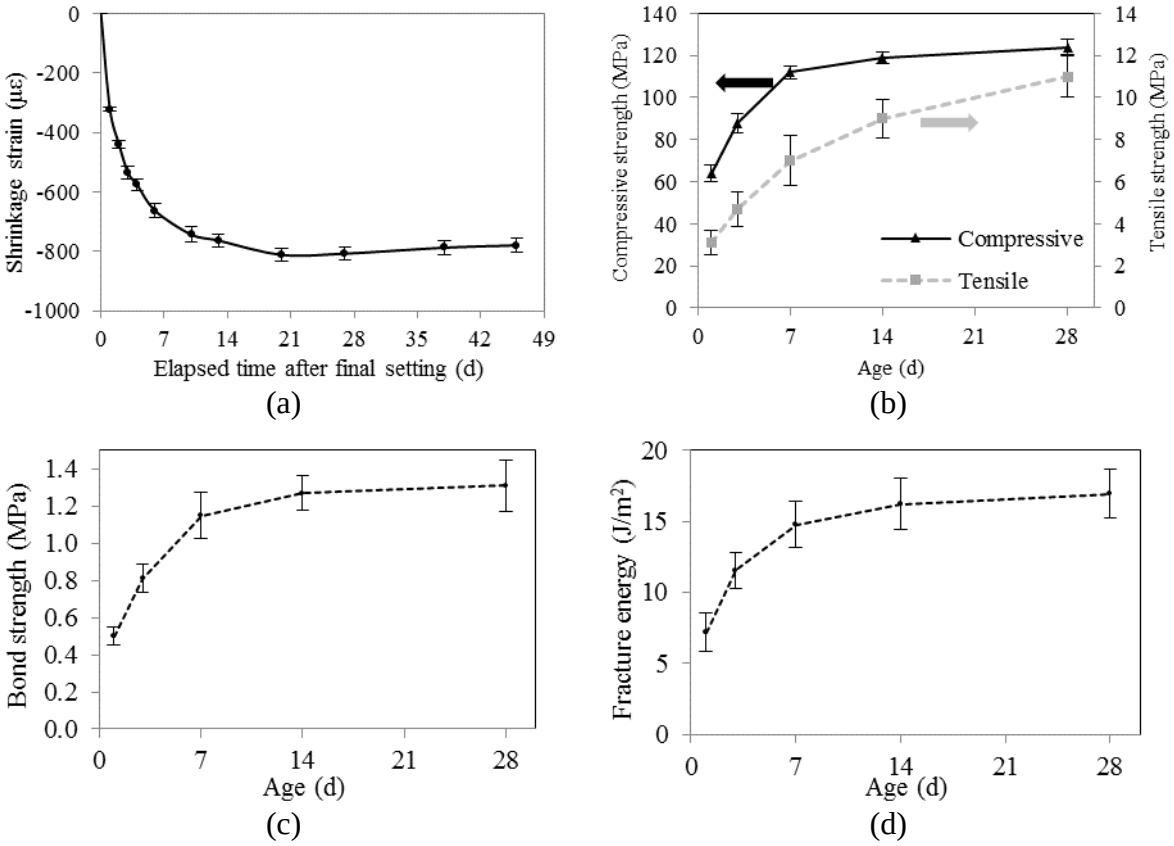

Figure 3 Material properties of UHPC: (a) total shrinkage, (b) compressive and tensile strengths, (c) bond strength, (d) fracture energy.

Three CC substrate prisms were prepared and cured for 60 d. A thin layer (approximately 25 mm thick) of UHPC was then cast on top of each CC substrate. In days of casting, hydrates such as calcium hydroxide (CH) and calcium silicate hydrate (C-S-H) were formed and bonded to both the substrate and overlay. The bond strength and fracture energy of the UHPC-CC interface were evaluated by pull-off tests at 1, 3, 7, 14, and 28 d (Al-attar, 2013; Seoa and Choi, 2014; Chan and Li, 1997). The fracture energy is defined as the work done by the pull-off force until debonding at the UHPC-CC interface. The average bond strength increased from 0.5 MPa at 1 d to 1.3 MPa at 28 d. The average fracture energy increased from 7.2 MPa at 1 d to 17 MPa at 28 d.

The microstructures of UHPC, CC, and their interface were examined using scanning electron microscopy (SEM). Figure 4a-d show the SEM images of an overall structure, the zoom-in interface, the UHPC overlay and the CC substrate. An interfacial transition zone of 10-30 μm thick (Li et al., 1995) has less hydration products (Bentz, 2000), higher porosity, and lower mechanical strength and elastic modulus than the UHPC overlay and the CC substrate (Wang et al., 2009; Akcaoglu et al., 2005). Compared with the UHPC, the CC contains more and larger capillary voids due to the higher water content.

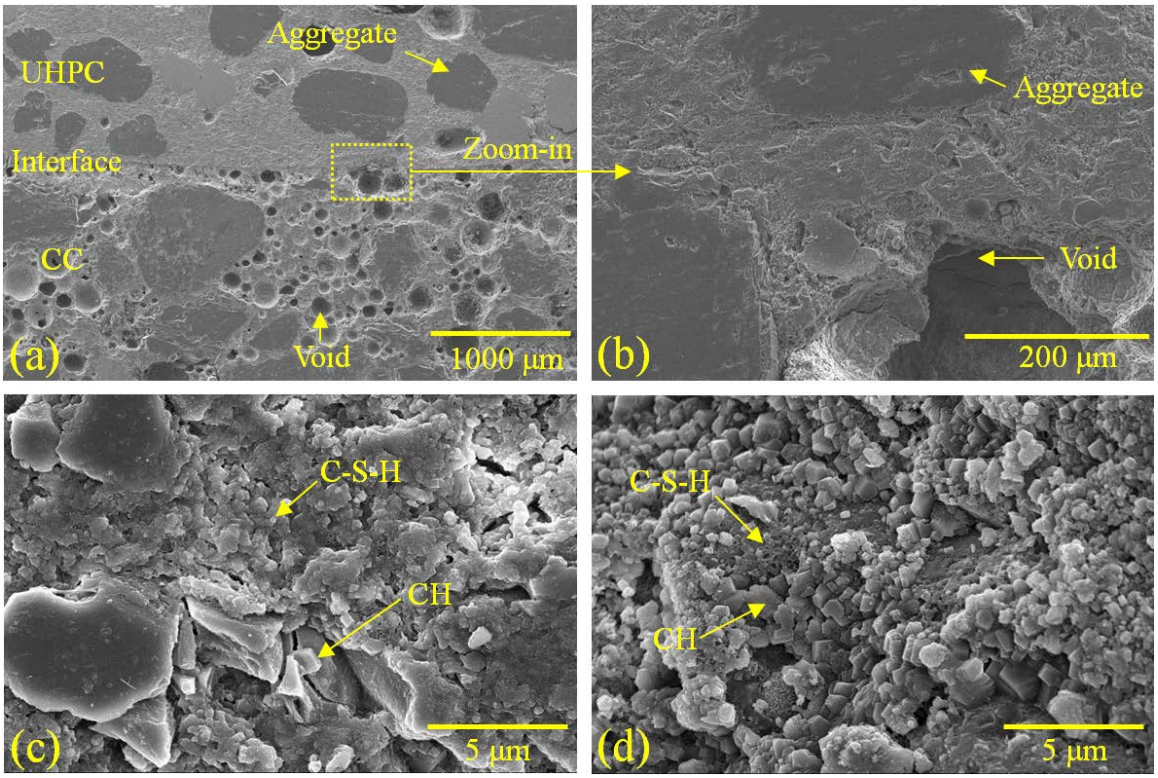

Figure 4 SEM images: (a) overall structure, (b) zoom-in interface, (c) UHPC, (d) CC

2.3. Preparation and Instrumentation of Specimens

Three concrete overlay specimens were prepared to understand the repeatability of measurements. As illustrated in Figure 5, each specimen was composed of a 200 mm thick CC substrate and a 25 mm thick UHPC overlay. The substrate concrete was cast in one lift and consolidated by hammer tapping at four sides for 20 times. After casting, the substrate concrete was covered with a wet burlap and plastic sheet for 7 d and then cured

in air under normal condition (room temperature: 22 ± 2 °C, relative humidity: 50 ± 2%) until 60 d when the shrinkage deformation became stabilized. Then, the UHPC overlay was cast on top of the substrate, cured under a wet burlap and plastic sheet for 24 h, and then air-cured under the same condition as the substrate. Immediately after the removal of formwork, two side faces along the longer side of the specimen were painted with three 1 mm thick layers of low-viscosity epoxy to prevent moisture exchange with the ambient environment, since there is little moisture transport between adjacent concrete in practice.

Each specimen was instrumented with three distributed fiber optic sensors: one 2C sensor and one 3C sensor in direct contact with the concrete for strain and temperature measurements, and one 2C sensor insulated by a thin polymer hose (0.5 and 0.7 mm in inner and outer diameters) for temperature compensation. The three distributed fiber optic sensors were closely deployed in a pattern as illustrated in Figure 5. The fibers were continuously passed back and forth through the overlay-substrate interface for 16 times, forming 16 intersection points at the interface zone: P1, P2,…, P16. In general, the spacing between two adjacent intersection points can vary in different applications, depending on where potential delamination needs to be monitored. In this study, the spacing between any two adjacent points was about 60 mm. The exact locations of the intersection points along the optical fiber were determined by applying a local thermal gradient using a hot tip prior to concrete casting. Two ends of each sensor were connected to the Neubrescope through transmission cables. Brillouin frequencies were measured along the length of the three distributed fiber optic sensors at 1, 3, 7, 14, 21, and 28 d after final setting of the UHPC.

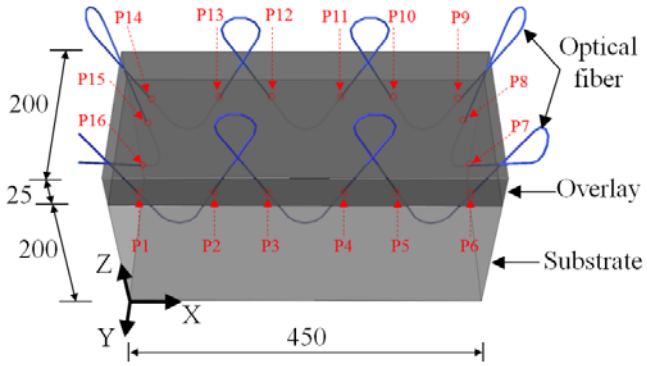

Figure 5- Illustration of test specimen (unit: mm)

3. STRAIN DISTRIBUTION AND DELAMINATION DETECTION

The measured Brillouin frequency distributions were converted into strain distributions based on the calibrated sensitivity coefficients. Figure 6a and b show the strain distributions in one specimen, which were measured from the 2C and 3C sensors, respectively. The horizontal and vertical axes represent the distance along the optical fibers and the measured strain values, respectively. Each figure contains four curves corresponding to 1, 2, 3, and 7 d measurements after concrete setting. Multiple peaks observed in each curve are indications and locations of the delamination that took place along the overlay-substrate interface.

Delamination along the overlay-substrate interface involves both separation and dislocation between the overlay and the substrate, which can be schematically represented by a combined opening-sliding movement as illustrated in Figure 7. Points ‘A’ and ‘B’, initially co-located, are displaced after delamination. The embedded optical fibers, which are perfectly bonded to the substrate and the overlay, are locally elongated in the vicinity of the overlay-substrate interface, resulting in sudden increases of strain as identified as sharp peaks in the strain distributions in Figure 6 (Feng et al., 2013). The peak strains increase with the opening width and sliding distance at the delamination surface, and their relationships can be represented by a bilinear equation (Bao et al., 2016). Therefore, once the peak strains are determined, their corresponding delamination can be quantified.

The peaks of strain distributions as shown in Figure 6 represent the locations of delamination in the specimen, specifically at the intersection points (P1, P2, P3,…, P16). Both visible and hidden cracks can be detected when they are intersected by the optical fibers. However, when two intersection points are close to each other, their corresponding peaks in the strain distribution can be too close to distinguish particularly at increasing strains/delamination. For example, the peaks corresponding to P11 and P12 in Figure 6a cannot be separated due to large delamination while the peaks corresponding to P4 and P3 can due to relatively small delamination. The contrast between the two areas symmetric to the centerline of the specimen along the long side indicates that the delamination pattern is asymmetric for the symmetric specimen. The onset and

propagation of delamination can also be monitored from the strain distribution. As indicated in Figure 6a, no delamination at P6 is detected within the 1st day but delamination is detected within the 3rd day. Therefore, the actual delamination at P6 happened between the 1st and 3rd days. Furthermore, the increase of each peak's magnitude depicts the growth of delamination. Overall, the measurements from two sensors are in good agreement. The small discrepancy is likely due to slightly different installation locations.

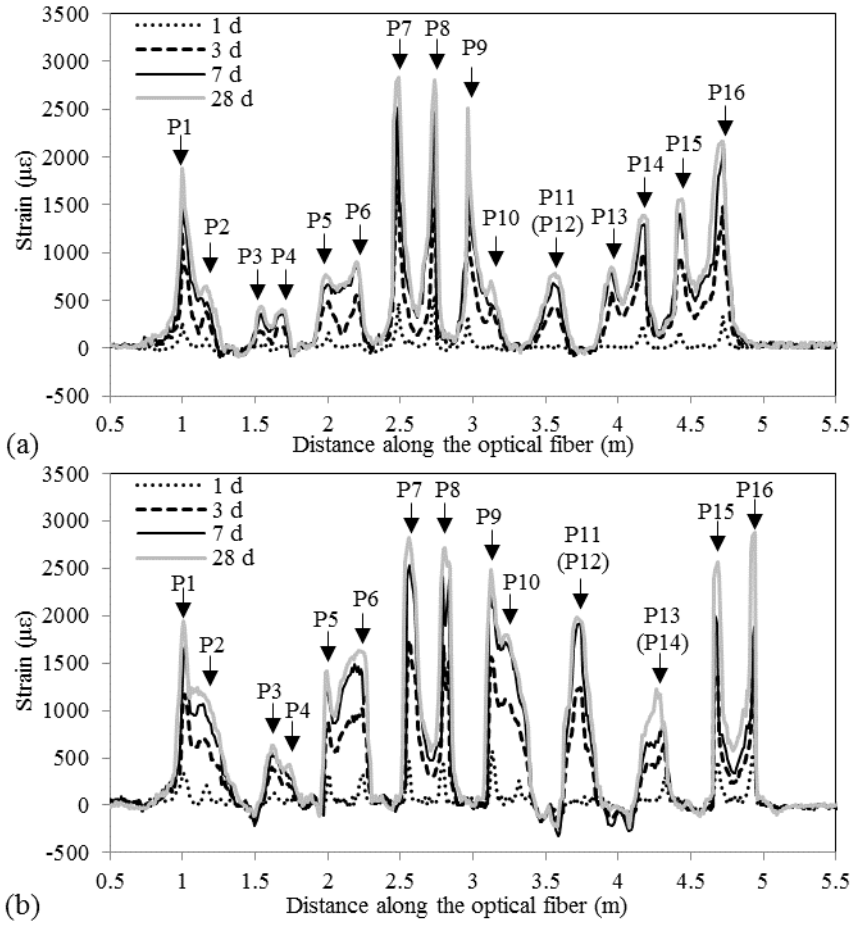

Figure 6- Strain distributions: (a) 2C sensor, (b) 3C sensor

The (average ± one standard deviation) peak strains of the three specimens are plotted at various intersection points in Figure 8. The peak strains and variations at all points increased over time from 1 to 28 d. The peak strains near the short-side edges of

the specimens were larger than those near the center since the short-side edges were subject to larger delamination due to symmetry of the specimens. The peak strains can be converted into delamination sliding distances based on the relation between the peak strain and sliding distance established previously (Bao et al., 2016). The 28 d average results from the three specimens are plotted at various locations of the intersection points along the overlay-substrate interface in Figure 9. The color bar represents the delamination distance in micron.

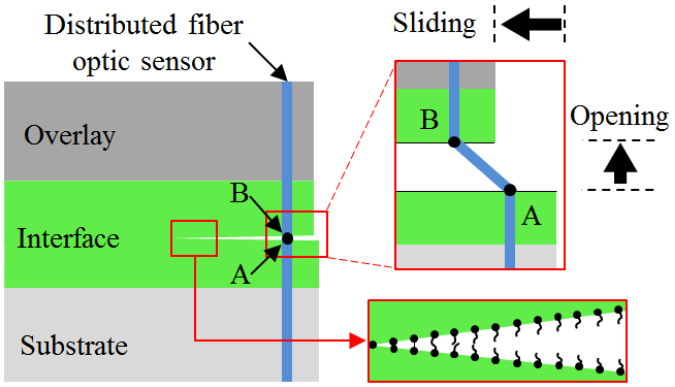

Figure 7- Combined opening-sliding movement

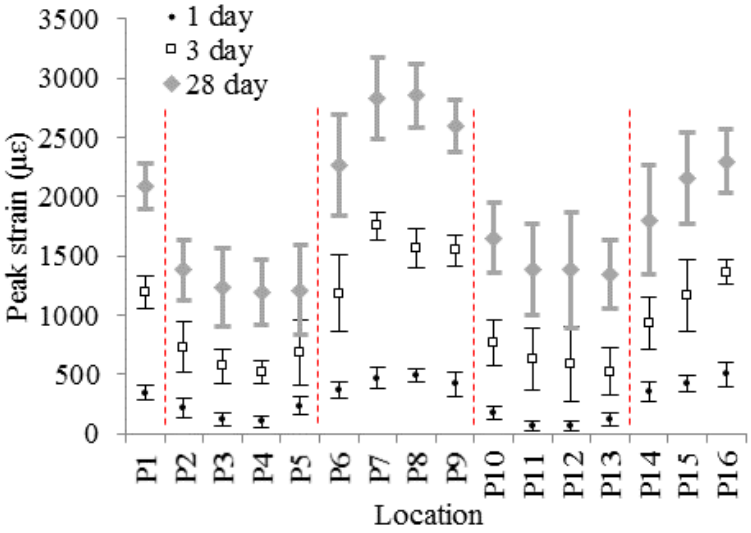

Figure 8- Peak strain vs. location

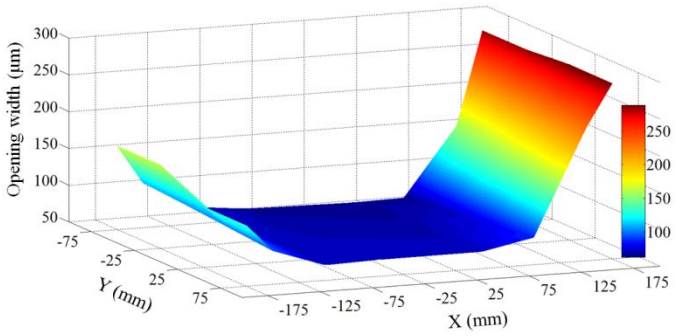

Figure 9- Visualization of delamination

After the completion of all measurements, the tested specimen corresponding to Figure 6 was submerged into a standard liquid dye diluted with water at a 1:1 volume ratio. The overlay was then removed for visual inspection as shown in Figure 10. The dark areas indicate the ingress of dye and thus represent the delaminated areas at the overlay-substrate interface. The light areas represent intact interface without delamination. Therefore, delamination at the interface occurs towards the two ends of the specimen and it is not symmetric about the centerline of the specimen along the long side, as indicated by the strain measurements in Figure 6. The distribution of delamination is in general agreement with the strain measurements as shown in Figure 9.

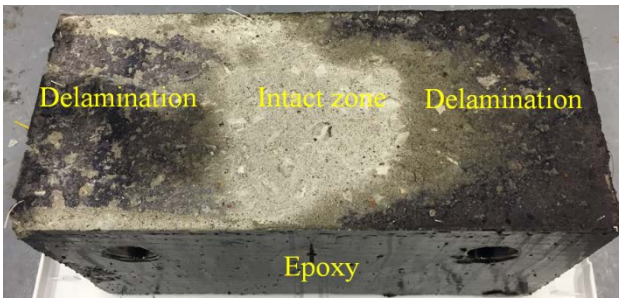

Figure 10- Photo of the overlay-substrate interface after the dye test

4. SUMMARY

Based on the experimental and numerical results, the following conclusions are drawn: (1) the distributed fiber optic sensor can be applied to monitor the initiation and propagation of delamination at the overlay-substrate interface. Delamination occurs at the

location of each sharp peak that appears on the strain distribution directly measured from the sensor. The degree of delamination is proportional to the peak strain. When the distributed sensor passes through the overlay-substrate interface at spatially distributed locations, delamination at the multiple locations enables the construction of a 3D delamination profile in space and its progression over time with continuous monitoring. Although both the 2C and 3C sensors perform satisfactorily, the 3C sensor is recommended for delamination detection due to its higher mechanical strength.

(2) The initiation and propagation of delamination at the overlay-substrate interface can be predicted using the finite element model with material properties obtained from standard tests and with cohesive elements used to represent delamination behavior. Prior to delamination, the overlay and substrate are slightly bent upwards and the substrate separates from its supporting floor.

Delamination takes place when the interfacial traction caused by shrinkage in the overlay exceeds the bond strength of the interface. Thus, delamination can be mitigated by controlling the shrinkage effect of the overlay material and enhancing the bond strength between the overlay and substrate. The predicted and experimental delamination values are in general agreement with 26% difference.

(3) Once initiated, delamination propagates along the interface and the bending curvature of the overlay and substrate is reduced. With an increase of shrinkage, the opening at the delaminated areas is reduced and the sliding distance is increased.

BIBLIOGRAPHY

ACI 318-14. (2014) “Building code requirements for structural concrete”, USA.

ACI Report. (2010). On early-age cracking: causes, measurement and mitigation.

American Concrete Institute-Committee 231: Farmington Hills, MI; 2010. p. 48.

ACI SP-256. (2008). Internal curing of high performance concrete: laboratory and field experiences. American Concrete Institute: Farmington Hills, MI. p. 110.

Ahlborn, T. M., Misson, D. L., Peuse, E. J., & Gilbertson, C. G. (2008). Durability and strength characterization of ultra-high performance concrete under variable curing regimes. In Proc. 2nd Int. Symp. on Ultra High Performance Concrete, Fehling, E., Schmidt, M., & Stürwald, S.(Eds.) Kassel, Germany (pp. 197-204).

Ahlborn, T. M., Peuse, E. J., & Misson, D. L. (2008). Ultra-high-performance-concrete for michigan bridges material performance–phase I (No. MDOT RC-1525).

Aïtcin, P. C. (2011). High performance concrete. CRC press.

Aitcin, P. C., Delagrave, Y., & Beck, R. (2000). A 100-m high prefabricated concrete pole: why not?. In Transmission and Distribution Construction, Operation and Live-Line Maintenance Proceedings. 2000 IEEE ESMO-2000 IEEE 9th International Conference on (pp. 365-374). IEEE.

Akçaoğlu, T., Tokyay, M., and Çelik, T. (2005) “Assessing the ITZ microcracking via scanning electron microscope and its effect on the failure behavior of concrete” Cem. Concr. Res. 35(3), 58-63

Al-Attar, T. S. (2013) “A quantitative evaluation of bond strength between coarse aggregate and cement mortar in concrete” Eur. Sci. J. 9 46-61.

Banfill, P. (1982). An experimental study of the effect of pfa on the rheology of fresh concrete and cement paste, In Proceedings, Intern. Symp. on the Use of pfa in Concrete, Leeds, eds. J.G. Cabrera and A.R. Cusens, University of Leeds, (1982) 161-171.

Bao, Y., and Chen, G. (2016) “Temperature-dependent strain and temperature sensitivities of fused silica single mode fiber sensors with pulse pre-pump Brillouin optical time domain analysis” Mes. Sci. Technol. 27 65101-11

Bao, Y., Meng, W., Chen, Y., Chen, G., & Khayat, K. H. (2015). “Measuring mortar shrinkage and cracking by pulse pre-pump Brillouin optical time domain analysis with a single optical fiber.” Materials Letters, 145, 344-346.

Bao, Y., Tang, F., Chen, Y., Meng, W., Huang, Y. and Chen, G. (2016) “Concrete pavement monitoring with PPP-BOTDA distributed strain and crack sensors” Smart Struct. Sys. (18) 405-23

Barrett, T. J., De la Varga, I., & Weiss, W. J. (2012). Reducing cracking in concrete structures by using internal curing with high volumes of fly ash. In Structures Congress 2012 (pp. 699-707).

Bentz, D. P. (2000) Fibers, percolation, and spalling of highperformance concrete ACI Mater. J. 97 (35),1-9

Bentz, D. P., & Peltz, M. A. (2008). Reducing thermal and autogenous shrinkage contributions to early-age cracking. ACI Materials Journal, 105(4), 414.

Bernardi S, Jacomo D., Boudry F. (2016). Overlay Ductal: a durable solution for bridges retrofitting. In proceeding of 1st International Conference on UHPC Materials and Structures, Changsha, China. pp. 626-631.

Beushausen, H., & Alexander, M. G. (2007). Localised strain and stress in bonded concrete overlays subjected to differential shrinkage. Materials and structures, 40(2), 189-199.

Blais, P. Y., & Couture, M. (1999). Precast, prestressed pedestrian bridge: World's first Reactive Powder Concrete structure. PCI journal, 44(5), 60-71.

Billberg, P., and Khayat, K. (2008). Use of Viscosity-Modifying Admixtures to Enhance Robustness, Proceedings of the Third North American Conference on the Design and Use of Self-Consolidating Concrete, Chicago, IL (2008).

Bonaldo, E., Barros, J. A., & Lourenço, P. B. (2005). Bond characterization between concrete substrate and repairing SFRC using pull-off testing. International journal of adhesion and adhesives, 25(6), 463-474.

Bonen, D., Deshpande, Y., Olek, J., Shen, L., Struble, L., Lange, D., and Khayat, K. (2007). Robustness of self-consolidating concrete, In Proceedings of the Fifth International RILEM Symposium on Self-Compacting Concrete, 33-42.

Bonneau, O., Poulin, C., Dugat, M., & Tcin, P. C. A. (1996). Reactive powder concretes: from theory to practice. Concrete International, 18(4), 47-49.

Broomfield, J. (2011). “Measuring concrete resistivity to assess corrosion rates.” Concrete Report from the Concrete Society/ Institute of Corrosion Liaison Committee, pp 37–39.

Bruhwiler, E., Denarié, E. (2008). “Rehabilitation of concrete structures using ultra-high performance fibre reinforced concrete.” In: Proceedings of the second international symposium on ultra high performance concrete, Kassel, pp 1–8.

Bruhwiler, E., Denarié, E. (2013). “Rehabilitation of concrete structures using ultra-high performance fibre reinforced concrete.” In: Proceedings of the second international symposium on ultra high performance concrete, Kassel, pp 1–8.

Castellote, M., Llorente, I., Andrade, C., & Alonso, C. (2003). Accelerated leaching of ultra high performance concretes by application of electrical fields to simulate their natural degradation. Materials and Structures, 36(2), 81-90.

Chan, Y. W., and Li, V. C. (1997) “Age effect on the characteristics of fibre/cement interfacial properties” J. Mater. Sci. 32. 5287-92.

Chen, G., Zhou, Z., Xiao, H., and Huang, Y. (2012) “Pilot Study on Rugged Fiber Optic Brillouin Sensors For Large-strain Measurements To Ensure The Safety Of Transportation Structures Report” MATC-25-1121-0001-114 and MATC- 25-1121-0001-242 Mid-America Transportation Center

Cusson, D., & Hoogeveen, T. (2007). An experimental approach for the analysis of early-age behaviour of high-performance concrete structures under restrained shrinkage. Cement and Concrete Research, 37(2), 200-209.

De Larrard, F. (2009). The High-Performance Cementitious Material (HPCM), a Cousin of UHPFRC for Long-Life Pavement. In BFUP (p. sp).

De Larrard, F., & Sedran, T. (1994). “Optimization of ultra-high-performance concrete by the use of a packing model.” Cement and Concrete Research, 24(6), 997-1009.

De Matteis, D., Novain, M., Marchand, P., Fabry, N., Petel, A., Chanut, S. (2008). A fifth French bridge including UHPFRC components, the widening of the Pinel bridge, in Rouen (France). Proceeding of the Second International Symposium on Ultra High Performance Concrete, Kassel, Germany. pp: 795-803.

Denarie, E., Bruhwiler, E., and Znidaric, A. (2005). Full Scale Application of UHPFRC for Rehabilitation of Bridges-from the Lab to the Field, in 5th FWP/ SAMARISSustainable and Advanced Material for Road Infrastructures.

Dils, J., Boel, V., & De Schutter, G. (2015). “Vacuum mixing technology to improve the mechanical properties of ultra-high performance concrete.” Materials and Structures, 48(11), 3485-3501.

Droll, K. (2004). Influence of additions on ultra high performance concretes–grain size optimisation. In Proceedings of the International Symposium on Ultra-High Performance Concrete, Kassel, Germany, Sept. 13(Vol. 15, pp. 285-301).

Dudziak, L., Mechtcherine, V. (2008). “Mitigation of volume changes of ultra-high performance concrete (UHPC) by using super absorbent polymers.” In: Proceedings of the second international symposium on ultra high performance concrete, Kassel, pp 425-432.

Dugat, J., Roux, N., & Bernier, G. (1996). Mechanical properties of reactive powder concretes. Materials and structures, 29(4), 233-240.

EFNARC. (2002). Specification and guidelines for self-compacting concrete, English edn. European Federation for Specialist Construction Chemicals and Concrete Systems, Norfolk

El-Dieb, A. S. (2009). “Mechanical, durability and microstructural characteristics of ultra-high-strength self-compacting concrete incorporating steel fibers.” Materials & Design, 30(10), 4286-4292.

Erdem, T. K., Khayat, K. H., & Yahia, A. (2009). Correlating rheology of self-consolidating concrete to corresponding concrete-equivalent mortar. ACI Materials Journal, 106(2), 154.

Feng, X., Zhou, J., Sun, C., Zhang, X., and Ansari, F. (2013) “Theoretical and experimental investigations into crack detection with BOTDR-Distributed fiber optic sensors” J. Eng. Mech. 139(1), 797-807

Ferraris, C. F., Obla, K. H., & Hill, R. (2001). “The influence of mineral admixtures on the rheology of cement paste and concrete.” Cement and concrete research, 31(2), 245-255.

Flatt, R. J., & Houst, Y. F. (2001). A simplified view on chemical effects perturbing the action of superplasticizers. Cement and concrete research, 31(8), 1169-1176.

Funk, J. E., Dinger, D. R. (1994). “Predictive process control of crowded particulate suspension.” Applied to ceramic manufacturing. Kluwer Academic Press, New York.

Gao, R., Liu, Z. M., Zhang, L. Q., & Stroeven, P. (2006). Static properties of plain reactive powder concrete beams. In Key Engineering Materials (Vol. 302, pp. 521-527). Trans Tech Publications.

Gettu, R., Nawaz Shareef, S., and Ernest, K. (2009). Evaluation of the Robustness of SCC, Indian Concrete Journal, 83 (6) 13-19.

Göller, F., Dikty, S., & Hamada, D. (2009). The relationship between retention stability and chemical structure of PCE. Special Publication, 262, 249-260.

Graybeal, B. (2011). “Ultra-high performance concrete.” FHWA-HRT-11-038. FHWA, U.S. Department of Transportation

Graybeal, B. A. (2006). Material property characterization of ultra-high performance concrete (No. FHWA-HRT-06-103).

Griffin, J. J., Harik, I. E., & Choo, C. C. (2006). Performance Evaluation of Bridges with Structural Bridge Deck Overlays (SBDO).

Habel, K., Charron, J. P., Denarié, E., & Brühwiler, E. (2006). Autogenous deformations and viscoelasticity of UHPFRC in structures. Part I: experimental results. Magazine of Concrete Research, 58(3), 135-145.

Habert, G., Denarié, E., Šajna, A., & Rossi, P. (2013). “Lowering the global warming impact of bridge rehabilitations by using Ultra High Performance Fibre Reinforced Concretes.” Cement and Concrete Composites, 38, 1-11.

Hassan, A. M. T., Jones, S. W., & Mahmud, G. H. (2012). “Experimental test methods to determine the uniaxial tensile and compressive behaviour of ultra high performance fibre reinforced concrete (UHPFRC).” Construction and building materials, 37, 874-882.

He, H. A., Dong, W., & Wu, Z. M. (2011). Study on long-term expansive deformation of self-stressing concrete with combined restrictions of steel fibers and steel bar. In Key Engineering Materials (Vol. 452, pp. 533-536). Trans Tech Publications.

Higuchi, T., Eguchi, M., Morioka, M., & Sakai, E. (2014). Hydration and properties of expansive additive treated high temperature carbonation. Cement and Concrete Research, 64, 11-16.

Houst, Y. F., Flatt, R. J., Bowen, P., Hofmann, H., Mäder, U., Widmer, J., ... & Sika, A. G. (1999, March). Influence of superplasticizer adsorption on the rheology of cement paste. In International symposium on: the role of admixtures in high performance concrete, Monterrey, Mexico (pp. 387-02).

Hwang, S. D., Khayat, K. H., & Youssef, D. (2013). Effect of moist curing and use of lightweight sand on characteristics of high-performance concrete. Materials and structures, 46(1-2), 35-46.

Hwang, S., & Khayat, K. H. (2005). “Effect of various admixture-binder combinations on workability of ready-mix self-consolidating concrete.” ACI Special Publications, 233, 25-44.

Iveson, S. M., Litster, J. D., Hapgood, K., & Ennis, B. J. (2001). “Nucleation, growth and breakage phenomena in agitated wet granulation processes: a review.” Powder technology, 117(1), 3-39.

Jolicoeur, C., Sharman, J., Otis, N., Lebel, A., Simard, M. A., & Page, M. (1997). The influence of temperature on the rheological properties of superplasticized cement pastes. Special Publication, 173, 379-406.

Khayat, K. H., Kassimi, F., & Ghoddousi, P. (2014). "Mixture Design and Testing of Fiber-Reinforced Self-Consolidating Concrete." ACI Materials Journal, 111(2), 143–152.

Khayat, K. H., Mitchell, D., Long, W. J., Lemieus, G., Hwang, S. D., Yahia, A., Cook, W. D., Baali, L. (2007). "Self-consolidating concrete for precast, prestressed concrete bridge elements." NCHRP Project 18-12. University of Sherbrooke, Quebec

Khayat, K. H., Petrov, N., Morin, R., Thibeault, M., Bissonnette, B. (2007). Comportement du béton autoplaçant fibré dans la réfection du passage inférieur du Viaduc Jarry- Querbes à Montréal. In: 8e Journées Scientifiques du (RF)2B, Montreal. p. 32-47.

Kim, D. H., Fowler, D. W., Ferron, R. P., Trevino, M. M., & Whitney, D. P. (2012). Materials selection for concrete overlays (No. FHWA/TX-11/0-6590-2).

Kishida, K., and Li, C. H. (2006) "Pulse pre-pump-BOTDA technology for new generation of distributed strain measuring system" Proc. Structural Health Monitoring and Intelligent Infrastructure (London, UK, 2006) pp 471–7

Knight, M., Wilson, G., Seger, W., & Mahadevan, S. (2004). Overlay types used as preventive maintenance on Tennessee bridge decks. Transportation Research Record: Journal of the Transportation Research Board, (1866), 79-84.

Koehler, E., Fowler, D. (2007). "Aggregate in self-consolidating concrete." In: ICAR project 108. The University of Texas at Austin: International Center for Aggregates Research

Krauss, P. D., Lawler, J. S., & Steiner, K. A. (2009). Guidelines for selection of bridge deck overlays, sealers and treatments. NCHRP Project, 20-07.

Krstulovic-Opara, N., Haghayeghi, A. R., Haidar, M., & Krauss, P. D. (1995). Use of conventional and high-performance steel-fiber reinforced concrete for bridge deck overlays. ACI materials journal, 92(6), 669-677.

Lange, D., & Shin, H. C. (2001). Early age stresses and debonding in bonded concrete overlays. Transportation Research Record: Journal of the Transportation Research Board, (1778), 174-181.

Le, H. T., Müller, M., Siewert, K., & Ludwig, H. M. (2015). “The mix design for self-compacting high performance concrete containing various mineral admixtures.” Materials & Design, 72, 51-62.

Li, L. G., & Kwan, A. K. (2011). “Mortar design based on water film thickness.” Construction and Building Materials, 25(5), 2381-2390.

Li, L. G., & Kwan, A. K. H. (2014). “Packing density of concrete mix under dry and wet conditions.” Powder Technology, 253, 514-521.

Li, V. C., Lim, Y. M., and Foremsky, D. J. (1995) Interfacial fracture toughness of concrete repair materials Fracture Mechanics of Concrete Structures, Proc. FRAMCOS-2 ed F H Wittmann pp 1329-44

Liu, J., Shi, C., Ma, X., Khayat, K. H., Zhang, J., & Wang, D. (2017). An overview on the effect of internal curing on shrinkage of high performance cement-based materials. Construction and Building Materials, 146, 702-712.

Lura, P., Pease, B., Mazzotta, G. B., Rajabipour, F., & Weiss, J. (2007). Influence of shrinkage-reducing admixtures on development of plastic shrinkage cracks. ACI Materials Journal, 104(2), 187.

Mechtcherine, V., Secrieru, E., & Schröfl, C. (2015). “Effect of superabsorbent polymers (SAPs) on rheological properties of fresh cement-based mortars-development of yield stress and plastic viscosity over time.” Cement and Concrete Research, 67, 52-65.

Meng, W., Khayat, K. H. (2017). Effects of saturated lightweight sand content on key characteristics of ultra-high-performance concrete. Cement and Concrete Research, Pending publication.

Meng, W., Valipour, M., & Khayat, K. H. (2017). Optimization and performance of cost-effective ultra-high performance concrete. Materials and Structures, 50(1), 29.

Misson D. L. 2008. Influence of Curing Regime on the Durability of an Ultra-High Performance Concrete Material, Thesis. Houghton, MI: Michigan Technological University.

Mo, L., Deng, M., & Tang, M. (2010). Effects of calcination condition on expansion property of MgO-type expansive agent used in cement-based materials. Cement and Concrete Research, 40(3), 437-446.

Mo, L., Deng, M., Tang, M., & Al-Tabbaa, A. (2014). MgO expansive cement and concrete in China: Past, present and future. Cement and Concrete Research, 57, 1-12.

Naaman, A. E., & Wille, K. (2012). The path to ultra-high performance fiber reinforced concrete (UHP-FRC): five decades of progress. In Proceeding of 3rd International Symposium on UHPC and Nanotechnology for High Performance Construction Materials. Kassel: Kassel University Press (pp. 3-13).

Nagataki, S., & Gomi, H. (1998). Expansive admixtures (mainly ettringite). Cement and concrete composites, 20(2-3), 163-170.

Nassif, A. Y., & Petrou, M. F. (2013). Influence of cold weather during casting and curing on the stiffness and strength of concrete. Construction and Building Materials, 44, 161-167.

Neville, A. M. (1999). Properties of Concrete, fourth edition, Pearson Education Limited, England.

Nunes, S., Figueiras, H., Oliveira, P. M., Coutinho, J. S., & Figueiras, J. (2006). A methodology to assess robustness of SCC mixtures. Cement and Concrete Research, 36(12), 2115-2122.

Orta, L., & Bartlett, F. M. (2014). Free Shrinkage Strains in Concrete Overlays. ACI Materials Journal, 111(3).

Ortiz, J., Aguado, A., Agulló, L., & García, T. (2005). Influence of environmental temperatures on the concrete compressive strength: Simulation of hot and cold weather conditions. Cement and concrete research, 35(10), 1970-1979.

Otsubo, Y., Miyai, S., & Umeya, K. (1980). "Time-dependent flow of cement pastes." Cement and Concrete Research, 10(5), 631-638.

Park, C. K., Noh, M. H., & Park, T. H. (2005). "Rheological properties of cementitious materials containing mineral admixtures." Cement and concrete research, 35(5), 842-849.

Park, S. H., Kim, D. J., Ryu, G. S., & Koh, K. T. (2012). "Tensile behavior of ultra high performance hybrid fiber reinforced concrete." Cement and Concrete Composites, 34(2), 172-184.

Plank, J., & Hirsch, C. (2007). Impact of zeta potential of early cement hydration phases on superplasticizer adsorption. Cement and Concrete Research, 37(4), 537-542.

Qi, M., Li, Z., & Ma, B. (2002). Shrinkage and cracking behavior of high performance concrete containing chemical admixtures. Journal of Zhejinag University: Science, 3(2), 188.

Rahman, M. K., Baluch, M. H., & Al-Gadhib, A. H. (2000). Simulation of shrinkage distress and creep relief in concrete repair. Composites Part B: Engineering, 31(6), 541-553.

Rajabipour, F., Sant, G., & Weiss, J. (2008). Interactions between shrinkage reducing admixtures (SRA) and cement paste's pore solution. Cement and Concrete Research, 38(5), 606-615.

Randl, N., Steiner, T., Ofner, S., Baumgartner, E., & Mészöly, T. (2014). Development of UHPC mixtures from an ecological point of view. Construction and Building Materials, 67, 373-378.

Resplendino, J. (2012). State of the Art of Design and Construction of UHPFRC Structures in France. Proceedings of Hipermat, 27-41.

Richard, P., & Cheyrezy, M. (1995). Composition of reactive powder concretes. Cement and concrete research, 25(7), 1501-1511.

Richard, P., & Cheyrezy, M. H. (1994). “Reactive powder concretes with high ductility and 200-800 MPa compressive strength.” Special Publication, 144, 507-518.

RILEM Report 41. (2007). Internal curing of concrete – state of the art. In: Kovler K, Jensen OM. editors. RILEM Publications S.A.R.L. p. 161.

Robins, P. J., & Austin, S. A. (1995). A unified failure envelope from the evaluation of concrete repair bond tests. Magazine of Concrete Research, 47(170).

Roy, D. M., & Asaga, K. (1979). Rheological properties of cement mixes: III. The effects of mixing procedures on viscometric properties of mixes containing superplasticizers. Cement and Concrete Research, 9(6), 731-739.

Russell, H.G., and Graybeal, B.A. (2013). Ultra-high performance concrete: A state-of-the-art report for the bridge community, No. FHWA-HRT-13-060.

Sakata, N., Marruyama, K., Minami, M. (1996). Basic properties and effects of welan gum on self-consolidating concrete, RILEM Proceedings 32, Production Methods and Workability of Concrete, Paisely, Ed. Bartos, P.J.M., Marrs, D.L. and Cleland, D.J. 237-253.

Schmidt, W., Brouwers, H. J. H., Kühne, H. C., & Meng, B. (2014). Influences of superplasticizer modification and mixture composition on the performance of self-compacting concrete at varied ambient temperatures. Cement and Concrete Composites, 49, 111-126.

Schober, I., & Flatt, R. J. (2006). Optimizing polycaboxylate polymers. Special Publication, 239, 169-184.

Seoa, D. S. and Choi, H. B. (2014) “Effects of the old cement mortar attached to the recycled aggregate surface on the bond characteristics between aggregate and cement mortar” Constr. Build. Mater. 59, 72-7.

Shann, S. V. (2012). Application of ultra high performance concrete (UHPC) as a thin-bonded overlay for concrete bridge decks. Michigan Technological University.

Shuguang, H., & Yue, L. (1999). Research on the hydration, hardening mechanism, and microstructure of high performance expansive concrete. Cement and concrete research, 29(7), 1013-1017.

Soudki, K. A., El-Salakawy, E. F., & Elkum, N. B. (2001). Full factorial optimization of concrete mix design for hot climates. Journal of materials in civil engineering, 13(6), 427-433.

Stovall, T., De Larrard, F., & Buil, M. (1986). Linear packing density model of grain mixtures. Powder Technology, 48(1), 1-12.

Sun, W., Chen, H., Luo, X., & Qian, H. (2001). The effect of hybrid fibers and expansive agent on the shrinkage and permeability of high-performance concrete. Cement and Concrete Research, 31(4), 595-601.

Tattersall GH, Banfill PFG (1983) Rheology of fresh concrete. Pitman, London

Tayeh, B. A., Bakar, B. A., & Johari, M. M. (2013). Characterization of the interfacial bond between old concrete substrate and ultra high performance fiber concrete repair composite. Materials and structures, 46(5), 743-753.

Tazawa, E. I. (Ed.). (1999). Autogenous shrinkage of concrete. CRC Press.

Termkhajornkit, P., Nawa, T., Ohnuma, H. (2001). “Effects of properties of fly ash on fluidity of paste.” Cem Sci Concr Technol 55:163–169.

Tomas, J. (2004). “Fundamentals of cohesive powder consolidation and flow.” Granular Matter, 6(2), 75-86.

Toutlemonde, F., Renaud, J. C., Lauvin, L., Brisard, S., & Resplendino, J. (2007). Local bending tests and punching failure of a ribbed UHPFRC bridge deck. In 6th International Conference on Fracture Mechanics of Concrete and Concrete Structures (Vol. 3, pp. 1481-1489).

Tran, Q. T., Toumi, A., & Turatsinze, A. (2007). Modelling of debonding between old concrete and overlay: fatigue loading and delayed effects. Materials and Structures, 40(10), 1045-1059.

Vande Voort, T. L., Suleiman, M. T., & Sritharan, S. (2008). Design and performance verification of ultra-high performance concrete piles for deep foundations (No. IHRB Project TR-558).

Walraven, J. C. (2002). From design of structures to design of materials. In Innovations and Developments In Concrete Materials And Construction: Proceedings of the International Conference held at the University of Dundee, Scotland, UK on 9–11 September 2002 (pp. 281-293). Thomas Telford Publishing.

Wang, C., Yang, C., Liu, F., Wan, C., & Pu, X. (2012). "Preparation of ultra-high performance concrete with common technology and materials." Cement and concrete composites, 34(4), 538-544.

Wang, X. H., Jacobsen, S., He, J. Y., Zhang, Z. L., Lee, S. F. and Lein, H. L. (2009) "Application of nanoindentation testing to study of the interfacial transition zone in steel fiber reinforced mortar" Cem. Concr. Res. 39 (70), 1-15

Weiss, J., Lura, P., Rajabipour, F., & Sant, G. (2008). Performance of shrinkage-reducing admixtures at different humidities and at early ages. ACI Materials Journal, 105(5), 478-486.

Wille, K., Graybeal, B. A. (2013). Development of Non-Proprietary Ultra-High Performance Concrete for Use in the Highway Bridge Sector, No.: FHWA-HRT-13-100.

Wille, K., Naaman, A. E., & El-Tawil, S. (2011). "Optimizing Ultra-High Performance Fiber-Reinforced Concrete." Concrete International, 33(9), 35-41.

Wille, K., Naaman, A. E., & Parra-Montesinos, G. J. (2011). "Ultra-High Performance Concrete with Compressive Strength Exceeding 150 MPa (22 ksi): A Simpler Way." ACI Materials Journal, 108(1).

Wong, H. H. C., & Kwan, A. K. H. (2008). "Rheology of cement paste: role of excess water to solid surface area ratio." Journal of materials in civil engineering, 20(2), 189-197.

Wu, Q., & An, X. (2014). "Development of a mix design method for SCC based on the rheological characteristics of paste." Construction and Building Materials, 53, 642-651.

Wyrzykowski, M., Trtik, P., Münch, B., Weiss, J., Vontobel, P., & Lura, P. (2015). Plastic shrinkage of mortars with shrinkage reducing admixture and lightweight aggregates studied by neutron tomography. Cement and Concrete Research, 73, 238-245.

Yang, S. L., Millard, S. G., Soutsos, M. N., Barnett, S. J., & Le, T. T. (2009). "Influence of aggregate and curing regime on the mechanical properties of ultra-high performance fibre reinforced concrete (UHPFRC)." Construction and Building Materials, 23(6), 2291-2298.

Yoshioka, K., Tazawa, E. I., Kawai, K., & Enohata, T. (2002). Adsorption characteristics of superplasticizers on cement component minerals. Cement and Concrete Research, 32(10), 1507-1513.

Yu, R., Spiesz, P., & Brouwers, H. J. H. (2014). "Mix design and properties assessment of ultra-high performance fibre reinforced concrete (UHPFRC)." Cement and concrete research, 56, 29-39.

Yu, R., Spiesz, P., & Brouwers, H. J. H. (2015). "Development of an eco-friendly Ultra-High Performance Concrete (UHPC) with efficient cement and mineral admixtures uses." Cement and Concrete Composites, 55, 383-394.

Yuguang, Y., Uijl, J. D., and Walraven, J. (2008). Study on Bending Behavior of an UHPC Overlay on a Steel Orthotropic Deck, in Second International Symposium on Ultra High performance Concrete. Kassel, Germany, p. 639-646.

Yurugi, M., Sakai G., and Sakata, N. (1995). Viscosity Agent and Mineral Admixtures for Highly Fluidized Concrete, Proceedings, Concrete under Severe Conditions, Environmental and Loading, K. Sakai, N. Banthia, and O. E. Gjørv, eds., Japan, 995-1004.

VITA

Mahdi Valipour was born in Khoy, Iran. He received his Master of Civil Engineering degree in 2010 from University of Tehran. He began his PhD at Missouri University of Science and Technology in August 2012. In December 2017, he received his Ph.D. in Civil Engineering from Missouri University of Science and Technology.